Mass Transport Studies In Membrane Filtration

Dimitri Mignard

Ph.D.

The University of Edinburgh

1998

DECLARATION:

I hereby declare that the following thesis is based on work carried out by me, that the thesis is my own composition, and that no part of it has been presented previously for a higher degree:

The research was conducted in the Department of Chemical Engineering under the direction of Dr. D.H. Glass and Dr. J.C. Christie.

ACKNOWLEDGEMENTS:

I wish to thank here the many people who helped me during the completion of this Ph.D. work.

Firstly, I would like to express how grateful I am to my Supervisor, Dr. D.H. Glass, who never failed in providing invaluable advice, support, and even material help when necessary. I would also like to thank very much Dr. Colin Prittchard for essential financial assistance while he was Head of the Department, and Dr. John Christie for his attention when presented with my work. I also owe much to my former Director of Studies at Birmingham University, Mr. Nick Emery, and to Dr. Kevin Wright for starting me up on much of my project.

At this stage, it seems that I should mention's everybody's name in the Department. There was vital and friendly technical support from Bobby, Rab, Ken, Tom, Debbie Sam and Matthiew, and also from other research students, research assistants and "computer people": Tom, Adam, Colm, Isabel, John, Steven, Owen, Christine, Bob, Geoff, Andy... zut alors, I MUST be forgetting somebody here! There also was a nice administrative staff to help with everything else: Joan, Margaret, Clare, and Sarah.

Special thanks should go to all my friends in Edinburgh - including the infamous "Dirty Weekenders" conservation society - , and also to my family.

Finally, I would especially like to dedicate this thesis to my Mum and my Granddad.

ABSTRACT

In ultrafiltration and microfiltration systems, fouling of the membrane restricts the permeate flux and the transmission of solutes. Development of a modular approach for modelling this complex problem has been discussed. The combination of concentration polarisation and "gel layer" deposition in tangential ultrafiltration was chosen as an example, because of its widespread occurrence and the fact that it had not been yet accurately modelled as a function of ionic strength and pH.

First, a programme to model concentration polarisation was written using the finite difference approach developed by Ilias and Govind. It was validated with experiments using Centrisystem C-300 and C-400 cartridges and BSA solutions (1-5 g/L), and experimental data from Yeh and Cheng with an H1P30-20 Amicon cartridge and Dextran T-500. The next step was to incorporate fouling into this model. To calculate the configurational Derjaguin-Landau-Vervey-Overbeek (DLVO) forces and the resulting osmotic pressures, large use was made of the work of Bowen *et al.* Concentration dependent diffusivities were calculated from the generalised Stokes-Einstein equation, and used in the transport equation to describe the concentration polarisation profile. It was shown that, when the transport equation did not have a solution at the membrane (or membrane + cake) surface, and that concentration was greater than the highest-concentration local maximum for the diffusivity, coagulation would occur. In this case, a monolayer of globular protein was assumed to deposit, and concentration polarisation was recalculated with this additional resistance.

Experiments with 1g/L BSA solutions and Amicon H1P30-20, for a range of transmembrane pressures, ionic strengths and pH, were compared with the model predictions. Both showed that fouling increased with ionic strength away from the Iso-Electric Point of BSA (IEP), and decreased with zeta potential. Simulation also showed that fouling could decrease with increased ionic strength around the IEP, in accordance with classical results. Total resistance to flux from experiments and simulation were in a similar range, although the lack of data relating zeta potentials and pH prevented further comparison. The model would also determine the critical pressure above which fouling occurred. However, observed values were significantly lower than predicted. Direct adsorption of the BSA onto the polysulfone membrane or the effect of high local pore velocities may both explain these discrepancies.

CONTENTS

2. MODELLING OF UF OF PROTEIN SOLUTIONS IN HOLLOW-FIBRE MODULES . 51

NOTATION:

The following notation was used in this work:

-Roman letters:

-a is the colloidal particle radius (m);

-A_m is the membrane surface area (m^2);

-c is the concentration (kg/m^3);

-c_0 is the inlet concentration (kg/m^3);

-c_g is the wall (gel) concentration (kg/m^3);

-C is the dimensionless concentration: $C = c / c_0$;

-C_g is the dimensionless concentration: $C_g = c_g / c_0$;

-C_m is the concentration at the membrane surface in Eq. (1.1) (kg/m^3);

-C_p is the concentration of the permeate in Eq. (1.1) (kg/m^3);

-C_r is the bulk concentration (retentate) in Eq. (1.1) (kg/m^3);

-d is the distance to the surface of the Outer Helmholtz-Plane (OHP);

-D is the solute Brownian diffusivity (m^2/s);

-D' is the solute effective diffusivity (with interactions between particles) (m^2/s);

-D_{ip} is the distance between the surface of two particles (m);

-e the elementary charge (1.6×10^{-19} C);

-f is the electrostatic repulsion force between two particles (N);

-F_{ATT} is the (attractive) London-Van der Waals force (N) between two particles;

-F_D is the disjoining force, exerted onto an area $A_e = 2\sqrt{3}(a + D/2)^2$ of monolayer of cake by the cake below (N);

-$F_{T\,(bottom)}$ is the force exerted onto a particle by the particles from the layer below;

-$F_{T(top)}$ is the force exerted onto a particle by the particles from the layer above (N);

-i is the index for the axial position along the fibre;

-I is the ionic strength of the solution;

-j is the index for the radial position to the centre of the fibre lumen;

-J_v is the permeate flux (m^3/s);

-k is the Boltzmann constant (1.38×10^{-23} J.K^{-1});

-K_H is the Happel permeability (m^2);

-l is the thickness of the boundary layer (m);

-L is the length of a hollow fibre (m);

-n^0 is the bulk ion number concentration (m^{-3});

-p is the pressure (Pa);

-p_0 is the inlet pressure (Pa);

-p_{per} is the pressure on the permeate side (Pa);

-P is the dimensionless pressure: $P = 2P / \rho u^2_{0,avg}$;

-P_1 is the operating (retentate side) pressure in dead-end filtration;

-P_2 is the pressure at the membrane-cake interface in dead-end filtration;

-P_3 is the pressure on the permeate side in dead-end filtration;

-P_{crit} is the critical pressure for membrane fouling (Pa);

-P_D is the disjoining pressure, equivalent to the osmotic pressure Π (Pa);

-Pe is the local Peclet number: $Pe = v r_i / D'$;

-$Pe_{0, wall}$ is the wall Peclet number: $Pe_{0, wall} = v_{0, wall} r_i / D$, at inlet;

-r is the radial position (m);

-r_{cell} is the Wigner-Seitz cell radius (m);

-r_1 is the inner radius of a hollow fibre (m);

-r_m is the intrinsic membrane resistance with a given buffer (m^{-1});

N.B.: r_m comes from the formula for the buffer flux:

$$v_{wall} = (p_{wall} - p_{per}) / (\mu_0 r_m)$$

-R is the dimensionless radial direction: $R = r/r_i$;

-Re is the local Reynolds number: $Re = v r_i \rho / \mu$;

-$Re_{0, wall}$ is the wall Reynolds number: $Re_{0, wall} = v_{0, wall} r_i \rho / \mu$, at inlet;

-R_m is the dimensionless membrane resistance: $R_m = 2 v_{0, wall} \mu_0 r_m / \rho u^2_{0,avg}$;

-T the absolute temperature (K).

-u is the axial velocity (m/s);

-u_0 is the inlet velocity (m/s) (depends on r)

-$u_{0, avg}$ is the average inlet velocity (m/s);

-U is the dimensionless axial velocity: $U = u / u_{0, avg}$;

-v is the radial velocity;

-v_{wall} is the permeate flux (m/s);

-$v_{0,\,wall}$ is the inlet permeate flux (m/s);

-V is the dimensionless radial velocity: $V = v / v_{0,\,wall}$;

-z is the axial position (m), unless specified as the valence number;

-Z is the dimensionless axial direction: $Z = v_{0,\,wall} z / u_{0,\,avg} r_i$;

Greek letters:

-ε is the cake voidage;

-ε_0 is the permittivity of vacuum (8.854×10^{-12} C.V^{-1}.m^{-1});

-ε_r is the relative permittivity of the buffer;

-ζ is the zeta potential (V);

-κ is the Debye parameter (see Eq. 2.18);

-μ is the solution viscosity, depending on local concentration (Pa.s);

-μ_0 is the buffer viscosity (Pa.s);

-π_{os} is the osmotic pressure (Pa);

-Π is the dimensionless osmotic pressure: $\Pi = 2\pi_{os} / \rho u^2_{0,avg}$;

-Π_e is the entropic pressure (Pa);

-ρ is the solution density (kg/m^3);

-σ is the solute rejection ratio;

-ξ is the dimensionless zeta potential: $\xi = ez\zeta/kT$

-ϕ is the particle volume fraction ($\phi = 1-\varepsilon$);

-ψ is the electrical potential (V);

-Ψ is the dimensionless potential: $\Psi = ez\phi/kT$;

GLOSSARY:

-**BSA** stands for Bovine Serum Albumin;

-**CF** stands for cross-flow;

-**DE** stands for dead-end;

-**DLVO** stands for Derjaguin-Landau-Vervey-Overbeek;

-**ECS** stands for Extra-Capillary Space;

-**MF** stands for Microfiltration

-**MWCO** stands for Molecular Weight Cut-Off;

-**PBE** stands for Poisson-Boltzmann Equation;

-**PBS** stands for Phosphate Buffer Saline;

-**TMP** stands for Transmembrane Pressure;

-**UF** stands for Ultrafiltration;

1. INTRODUCTION

1.1. OBJECTIVES OF THIS WORK

In the process industries, and especially in the food or pharmaceutical industries, membrane filtration offers huge potentials: Owing to their segregation power, polymeric or ceramic porous membranes offer the possibility to purify or concentrate interesting products in bulk quantities, especially in the mild operating conditions required by many biological products. However, and although they are now widely used, membranes often give results quite below these expectations: Main problems are:

-1) a lack of selectivity for the separation of compounds with molecular weights of the same order of magnitude;

-2) the need of an absolute reliability in some specific applications such as the removal of viral particles from blood products (Foster, 1995);

-3) fouling problems increasing costs in some industrial applications, or seriously restricting the scope of cell culture devices (Brotherton and Chau, 1995);

All those problems could be better dealt with if we had more understanding of mass-transfer phenomena in the vicinity of and at the membrane surface. Even though practical solutions can be found, such as air sparging (Cui and Wright, 1994) or standing vortex waves (Bellhouse *et al.*, 1996) to reduce fouling, the fundamentals themselves are not yet enough taken into account for predicting the behaviour of a given system when processed through a membrane, or for designing new solutions. The examples of microfiltration of protein solutions or cell culture broths, where a number of results are difficult to explain (Mercille *et al.*, 1994; Tracey and Davis, 1994), illustrate well this ignorance.

Bearing in mind this context, it was decided to look closer for the most inclusive and accurate modelling approach for ultrafiltration and microfiltration of macromolecular solutions. More specifically, it was decided to focus on the combined effects of concentration polarisation and surface deposition in tangential ultrafiltration of protein solutions in hollow-fibre modules, and to study the effects of ionic environment (pH and salinity).

1.2. CHARACTERISTICS OF MEMBRANE SYSTEMS

1.2.1. APPLICATIONS OF MEMBRANE SYSTEMS

A membrane is a porous material that provides a separation between two media, thus acting as a filter: it allows only some of the components in solution or suspension to pass from one side to the other. Applications dictate the characteristics that are chosen for the membrane, and in Biochemical Engineering they fall into two main categories:

- In **microfiltration**, porous membranes are used for the filtration of particles of a few microns in diameter: clarification of wine or juices, yeast filtration, sterile filtration, cells in immobilised cell cultures...

- In **ultrafiltration**, proteins are concentrated or fractionated through the membrane. Pore sizes are smaller than for microfiltration, and are defined in terms of Molecular Weight Cut-Off (MWCO) rather than diameter. Applications include dilute broth concentration (e.g. whey), protein separation, protein product integrated fractionation in immobilised cell cultures, immobilised enzyme reactors...

The following table sums up the applications of membranes according to the pore diameters or Molecular Weight Cut-Off:

Technique	Typical pore size, or Molecular Weight Cut-Off
Microfiltration	0.1-10 μm
Ultrafiltration	1-1000 kDa
Nanofiltration	< 5 nm

Table 1.1: *Filtration and pore size.*

This work mostly focussed on ultrafiltration. Microfiltration was also sometimes considered in this chapter, because of the frequent use of ultrafiltration membranes for microfiltration

purposes (e.g. cell separation, Marshall *et al.*, 1993), and vice-versa (e.g milk protein concentration with microfiltration membrane, Murkes and Carlsson, 1988). Nanofiltration was excluded from the scope of this work.

1.2.2. SOME GENERAL DEFINITIONS IN MEMBRANE SYSTEMS

1.2.2.1 Flows and pressure

In any mode of operation in a membrane system, the retained fluid is called the **retentate**, and the filtered fluid across the membrane is called the **permeate**, or **filtrate**.
When a back pressure is applied on the retentate side, the fluid is forced through the membrane and is recovered on the permeate side. The difference of pressure across the membrane is called the **Transmembrane Pressure (TMP)**.

1.2.2.2. Filtration characteristics

The performances of a filtration system are usually assessed with two essential figures:

- the permeate flux

The permeate flux, or filtration rate, is the flow rate of permeate generated per unit surface of membrane, under a given TMP. It usually is required to be as high as possible, to ensure short process time or high throughput. When the membrane is damaged or too dirty, the filtration rate is affected.

- the rejection ratio

For a given solute or suspended material, under a given TMP, the permeability of the membrane could be evaluated measuring the ratio C_p/C_r, where C_p is the concentration in the permeate, and C_r is the concentration in the retentate. The complementary quantity, which expresses the ability of the membrane to retain the product, is referred to as the rejection ratio (σ):

$$\sigma = 1 - C_p/C_r$$

1.2.2.3. Modes of operation

Two basic modes of operation can be distinguished. To some extent, most design can be reduced to a combination of the two.

-Dead-end filtration

In Dead-End mode (DE), the feed is directly forced through the membrane, and a cake forms on top of the membrane (*Fig. 1.1*). This cake causes severe deterioration of the flux, and is usually periodically removed by back-flushing from the permeate side during the filtration.

-Cross-flow filtration

In Cross-Flow filtration mode (CF), also called tangential filtration, the fluid is circulated parallel to the membrane. Its pressure forces out the permeate, while shear forces limit the accumulation of retained product on the membrane. However, the decrease of the tangential velocity at the vicinity of the membrane, and the boundary layer associated with it, can cause some Dead-End filtration and a cake to form. The particular case of tubular or Hollow-Fibre devices, in which the fluid is circulated inside the cylindrical membrane, is illustrated in *Fig. 1.2*: this diagram shows the accumulation of solute ("concentration polarisation") and the formation of a thin cake ("tightly-bound deposit").

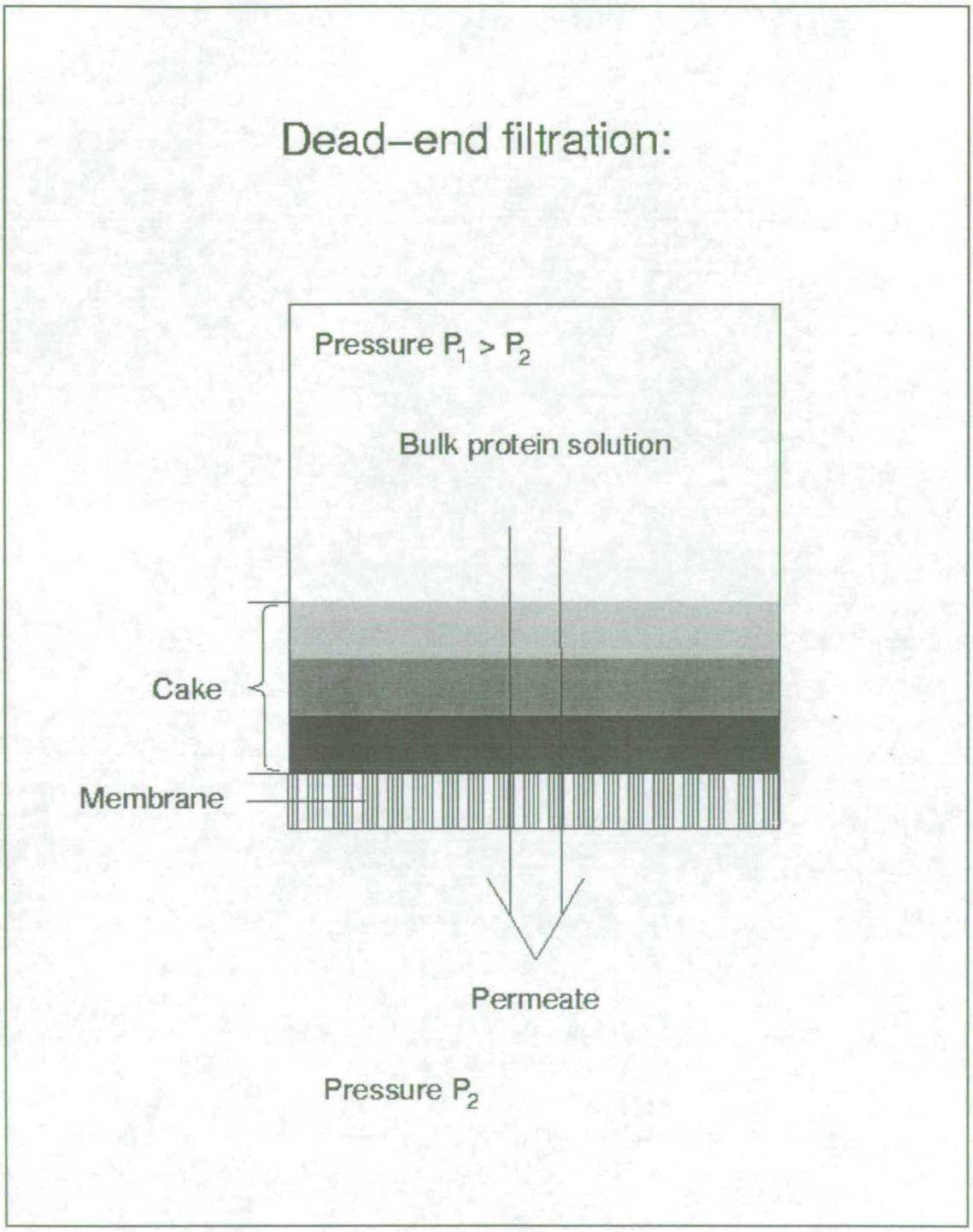

Fig. 1.1: Dead-End filtration and cake formation.

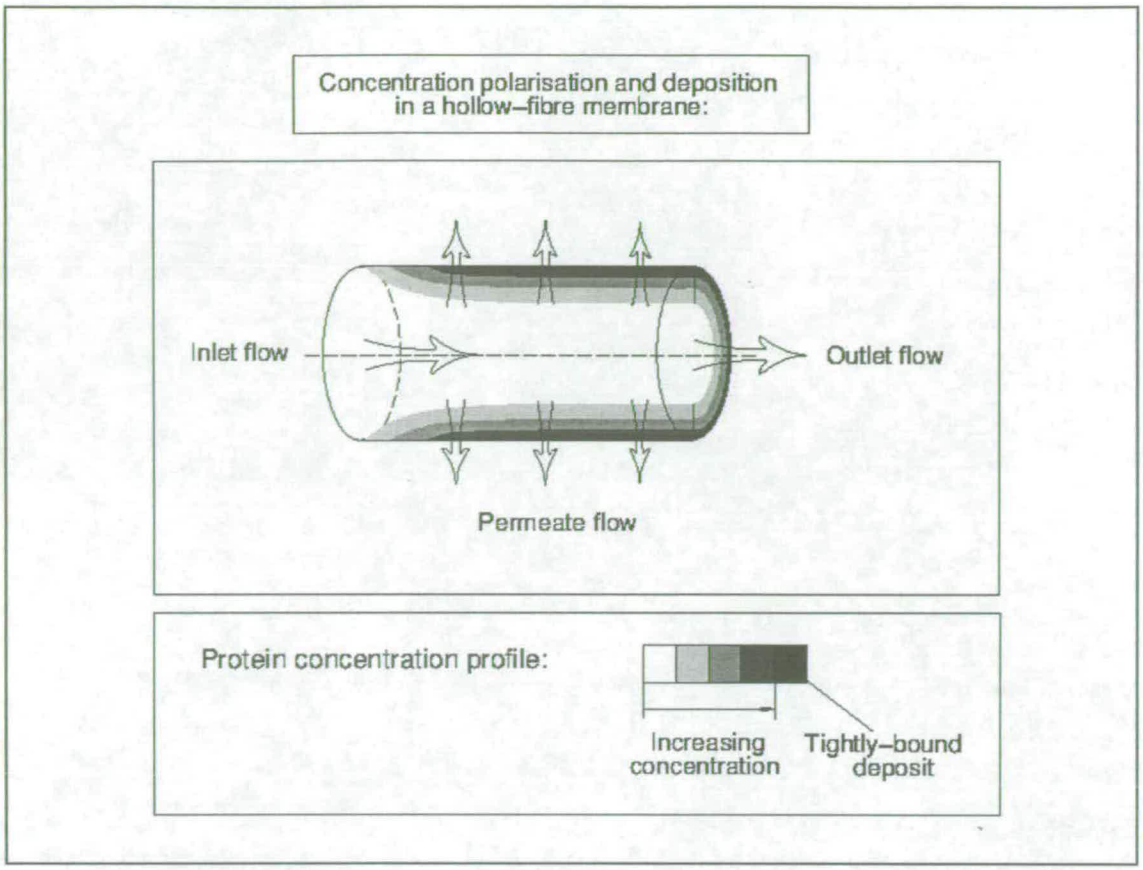

Fig. 1.2: *Cross-Flow filtration in a tubular or an Hollow-Fibre membrane: The protein concentration profile shows concentration polarisation and thin cake ("tightly-bound") deposition*

1.2.3. CHARACTERISTICS OF THE MEMBRANE

The performance of a membrane device is primarily determined by the material, structure and pore characteristics of the membrane, and surface properties.

1.2.3.1. Material

The choice of the material for a membrane is based upon:

-the porosity of the material, and the requirements on the pore size and density;

-mechanical strength and chemical stability;

-the surface properties of the material: Charges and chemical groups in the membrane affect the behaviour of the filtered elements, and can be modified by the solvent

or the ionic strength of the environment, or by deposition. Hydrophobic and hydrophilic membranes surface may also differ in their performance or fouling properties.

-biocompatibility for biomedical and biochemical engineering applications (toxicity or ability to withstand steam sterilisation).

1.2.3.2. Pore size, distribution and shape

Pore size for ultrafiltration and microfiltration membranes was introduced in section 1.2.1. Very often, the size of the pores is not uniform, and a distribution must be considered. For instance, in systems studied by Ko *et al.* (1993), the polycarbonate membrane PC015 had a closely controlled pore size distribution within a range of ± 15%, whereas regenerated cellulose membranes (RC membranes) had a wide distribution. It has been shown that large pores, representing only a fraction of the total number of pores, accounted for most of the flow through clean UF and MF membranes. For instance with UF membranes, *Fane et al.* predicted that 50 % of the solvent flow went through 20-25% of the pores (Marshall *et al.*, 1993), and *Munari et al.* (1987) showed on a PC300 membrane that the largest 10 % of the pores drained 70% of the flow.

1.2.3.3. Asymmetric membranes

Very often as well, the pore mouths on the retentate side do not have the same shape as those on the filtrate side. Again, in the study by Ko *et al.* that was mentioned earlier, the PC015 membranes were homoporous - i.e. with symmetric pores. However, the RC membranes had an asymmetric structure, with presumably pore mouth sizes corresponding to the MWCO on the retentate side, but larger (and presumably uncontrolled) on the filtrate side. The side that is meant to be the retentate side is usually referred to as the Tight Side (TS), whereas the other side that has enlarged pore mouths is the Open Side (OS). The Tight Side controls the filtration, whereas the matrix ensures mechanical support.

1.2.4. MEMBRANE MODULE GEOMETRY

When flat sheets of membranes are used, this configuration is called "plate and frame". In cross-flow mode, channels for the fluid covering all the membrane surface can be obtained by the use of suitably shaped seals, which are inserted between the plate and frame and the membrane.

Industrial devices often consist of tubes (or bundles of tubes), as illustrated in *Fig. 1.2*. For cell culture, small-scale separations or haemodialysis, very fine tubes can be used in hollow-fibre devices (between 200 and 500 μm in diameter): This allows a compact presentation of large surface areas, and low shear rates for sensitive products such as a patient's blood. However, operating pressures are usually limited to 10 kPa (Kirk and Othmer, 1995).

Spiral-wound modules consist of one or several membrane sheets, each covered by a non-permeable spacer sheet, that is wound around a central, perforated collector tube (*Fig. 1.3*). Again, the advantage here is a high surface-to-volume ratio, with also the possibility of high pressures. However, the limitation here is the pressure drop encountered by the permeate as it spirals towards the central tube, with a path up to a few meters long. In commercial modules, with typical dimensions of 100-150 cm long and 10-30 cm in diameter, this problem is solved by winding together up to 30 membrane envelopes about $2m^2$ each in area (Kirk and Othmer, 1995).

1.2.5. PREPARATION OF POLYMERIC MEMBRANES

The way the membrane is prepared conditions its properties: pore size and thickness (and hence permeability and mechanical properties), chemical or surface properties, etc. Membranes are usually made of ceramic or polymeric material. Taking polymeric membranes as an example, the main processes of manufacture are briefly reviewed below (from (Yoshihito and Tsutomu, 1991):

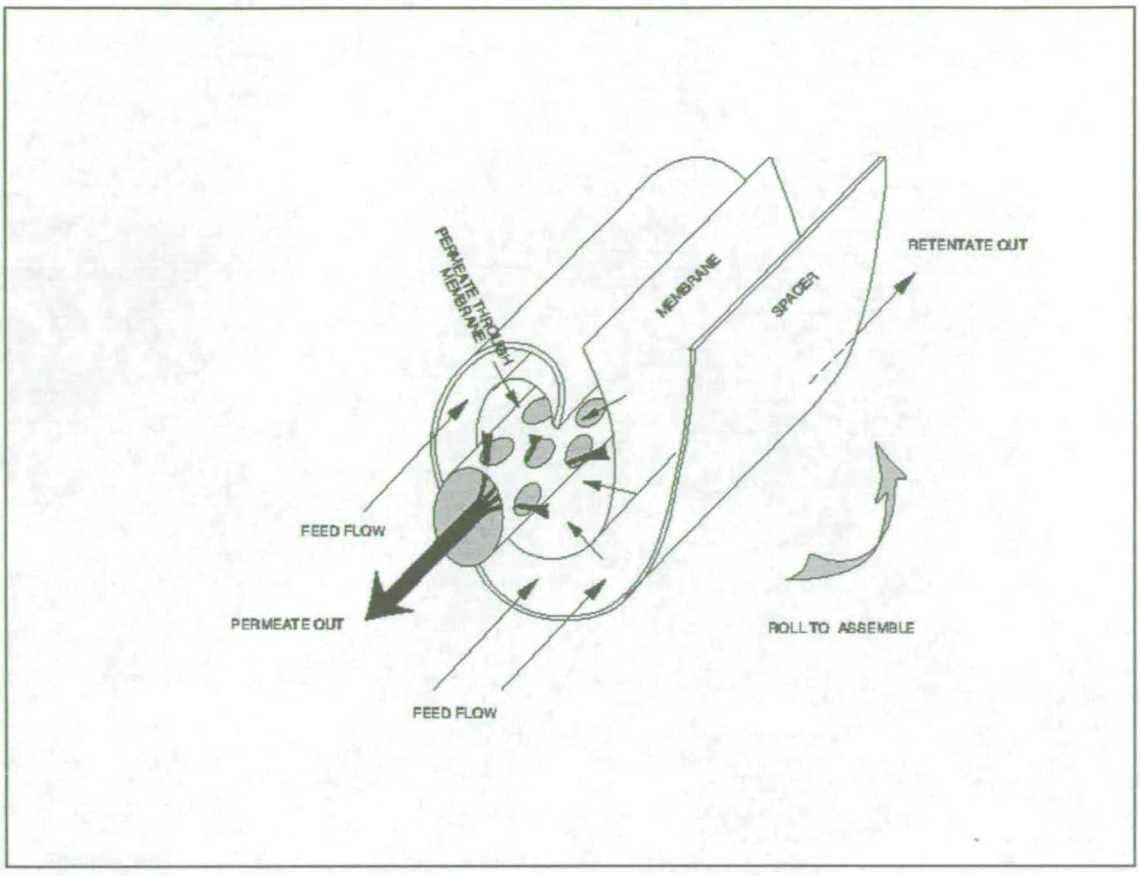

Fig. 1.3: Spiral-wound module construction.

1.2.5.1. Extrusion and stretching (MF membranes)

MF membranes can be manufactured out of thermoplastic polymers: the polymer is melted and extruded through a die, giving thus a porous membrane. Stretching that hot membrane causes the pores to enlarge, and the final membrane has rectangular shaped pores (e.g. 0.2x0.02 μm). Examples of such products are the Celgard membranes, made of polypropylene.

1.2.5.2. Phase inversion method (UF and some MF membranes)

-Method

This method is used to prepare UF or MF membranes out of polymers: A casting solution, containing a polymer in solution, is cast onto a glass plate, expanded (spread) to a given thickness. After some of the solvent has evaporated, the resulting film is

immersed into a nonsolvent bath (usually water), where it gels and forms the porous membrane.

-Properties of the membranes

The resulting properties or the membranes are then influenced by a number of process parameters, including: the polymer and the solvent that was used, the thickness of the film, the different temperatures (solvent, bath, ambient, glass), and timing. The phase inversion method usually results in asymmetric membranes: The gelation being more sudden at the interface film-water, the pores that form are much narrower there than near the glass surface. That interface forms then the tight, controlling side of the membrane.

-MF membranes

For MF membranes, the restriction in the phase inversion process is that the polymer must be a crystallite (e.g. polyethylene), that is to say presenting many crystals inside the amorphous bulk: the crystals ensure the mechanical strength of the membrane, holding together the large pores without deformations.

-Hollow fibres

The phase inversion process is used for the preparation of hollow fibres: The casting solution is first injected into a spinneret, and contacted with an inside coagulation agent on the surface of a cylinder, which creates a lumen space. The hollow fibre is then extruded and passed through a gelling bath to complete its solidification.

1.2.5.3. Track etching method (MF membranes)

In the track etching method, radiations from a radioactive substance form tracks of damaged material within the membrane. Etching with an alkali solution then enlarges these tracks. The striking features of the membranes obtained from this process are the cylindrical shapes and narrow size distribution of the pores.

1.3. MASS TRANSFER PROBLEMS IN ULTRAFILTRATION

1.3.1. CONCENTRATION POLARISATION AND FOULING

We already mentioned (1.2.2.3) the advantages of cross-flow over dead-end filtration. However, even in cross-flow mode, two phenomena still contribute to reducing the permeate flux, and therefore the performance of the membrane: the first one is concentration polarisation, i.e. accumulation of the solute in the vicinity of the membrane surface. It opposes increasing osmotic pressure to the operating pressure, as well as increasing viscosity. Concentration polarisation is essentially reversible: decreasing the operating pressure, or temporarily flushing the membrane with buffer, will restore the flux. The other flux-limiting phenomenon is the deposition of a gel that the macromolecule may form, and is refered to as "fouling". In particular, fouling forms a layer at the surface of the membrane if the protein is rejected. Particles and solutes smaller than the pores may deposit within the pores, and internal fouling occurs then by a narrowing of the pores. Particles and solutes of a size within the pore size distribution may block the pores, maybe at the rate of one pore plugged for every molecule entering it. Internal fouling occurs then by decrease in the number of pores available. Contrary to concentration polarisation, the reduction in flux caused by fouling cannot usually be reversed by a decrease in pressure or a simple rinsing of the membrane: cleaning the system is required. In bioseparation, compounds involved in fouling are proteins and lipids. Fouling by proteins is usually reckoned to be of major importance, and has mostly been studied.

1.3.2. FLUX DECLINE AND TRANSMISSION DURING CROSS-FLOW UF

1.3.2.1. Filtration of a protein solution at a given TMP

The cross-flow filtration of a solution through a UF or MF membrane at constant TMP does not usually lead to a permeate flux constant with time, at least at the beginning. Even with **pure solvent**, a slight initial decline is often observed. It is attributed to the swelling of

the membrane when it absorbs the solvent. Another possible cause is the compression of the membrane material under the applied TMP, which narrows the pores.

When measuring the flux of a **protein solution** through a membrane in C.F. mode, and when the TMP is maintained constant, three periods of decline can be identified:

- a first sharp decrease in flux over the first seconds or minutes of the filtration, usually attributed to the build-up of a so-called concentration polarisation layer (see next section);

- a slower decline in flux during the following hour, due to the adsorption of a protein layer onto or into the membrane, followed by further deposition on that layer (see section 1.3.4.);

- a quasi-steady-state, with a slow decline of the flux, due either to deposition of further protein onto the adsorbed layer or to consolidation of the deposit.

A typical plot of the permeate flux versus time is presented below:

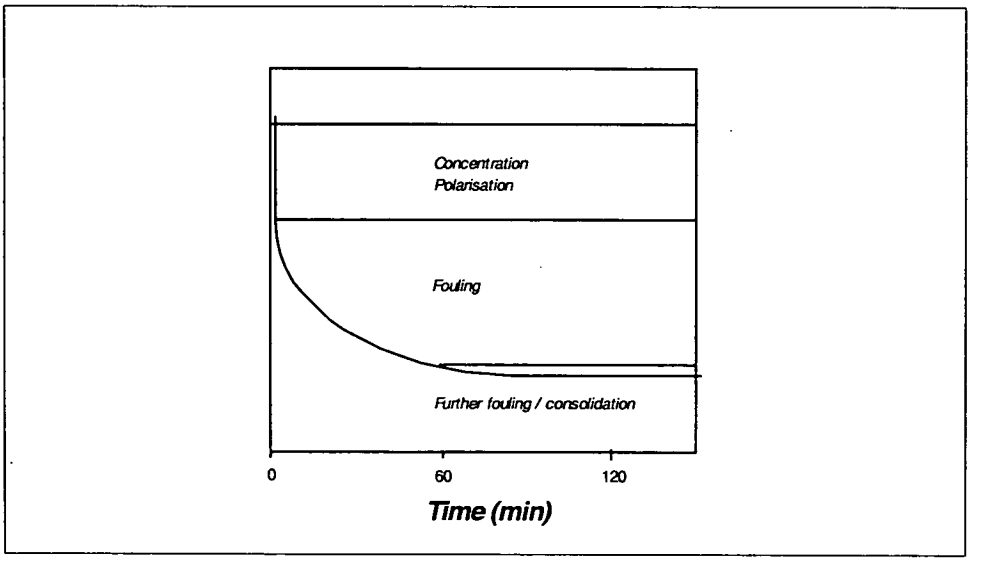

Fig. 1. 4: *Three main stages of fouling.*

1.3.2. 2. Limiting fluxes at high TMP's

Considering the tangential filtration of a pure solvent (usually water or a buffer solution) through the membrane, it is usually found that the permeate flux varies linearly with the applied TMP, or at least always increases with TMP.
However (as observed, for instance, by Jonsson (1984) on a UF system, and Bowen and Gan (1991) on a MF system), filtering a protein solution leads to:

-higher initial fluxes at higher TMP's

-a linear relationship between the steady-state flux and the TMP at low TMP's;

-a steady-state flux that does not vary with the applied TMP at higher TMP's; this, flux independent from the pressure, is called the limiting flux.

The value of the limiting flux decreases with increasing concentration and decreasing cross-flow velocity.

1.3.2.3. Critical pressure and critical flux

If the membrane module is operated at constant pressure, a critical pressure P_{crit} can be found below which fouling is absent, and above which it occurs. A critcal permeate flux can similarly be defined when operating at constant permeate flux (e.g. Harmant and Aimar (1996), on latex particles in an UF stirred cell).

1.3.2.4. The increase in rejection of solutes

Another phenomenon coupled with the reduction in flux is the increase of the rejection ratio. It suggests a narrowing of the average pore size. It is sometimes an inconvenience in UF when selectivity is required for fractionation, and in MF when solute proteins are the desired product to be separated from cells or debris. It is often an advantage in UF when concentrating a protein broth is required.

1.3.3. FIRST APPROACHES ON MASS TRANSFER IN ULTRAFILTRATION

In the 60's, the first attempts to elucidate the mechanisms of fouling were based on chemical engineering approaches. These led to the study of concentration polarisation, as well as the gel polarisation theory:

1.3.3.1. Concentration polarisation

When a protein retentate, of bulk concentration C_r, is processed through a UF membrane, or in many cases a fouled MF membrane, its concentration increases near the membrane within a so-called polarisation layer (*Fig. 1.5*): This phenomenon is called concentration polarisation. It results in a locally high osmotic pressure, that can be expressed in terms of a resistance to the flux, and which causes the initial drop of flux in filtration experiments with a clean membrane. The thickness l of the polarisation layer for a given solution mostly depends upon the hydrodynamic conditions - transmembrane pressure, cross flow velocity, viscosity - rather than upon the membrane or the ionic strength and pH.

A material balance over layer elements of the polarisation layer, combined with Fick's law of diffusion, leads to the equation

$$J_v = \frac{D}{l} * \ln \frac{C_m - C_p}{C_r - C_p} = k * \ln \frac{C_m - C_p}{C_r - C_p} \qquad \textbf{(1.1)}$$

where J_v is the solvent permeate flux ($m^3/m^2/s$);

C_m is the concentration at the membrane surface;

C_p is the permeate concentration;

D is the macrosolute diffusivity (m^2/s);

l is the boundary layer thickness (m);

k is the mass transfer coefficient (m/s).

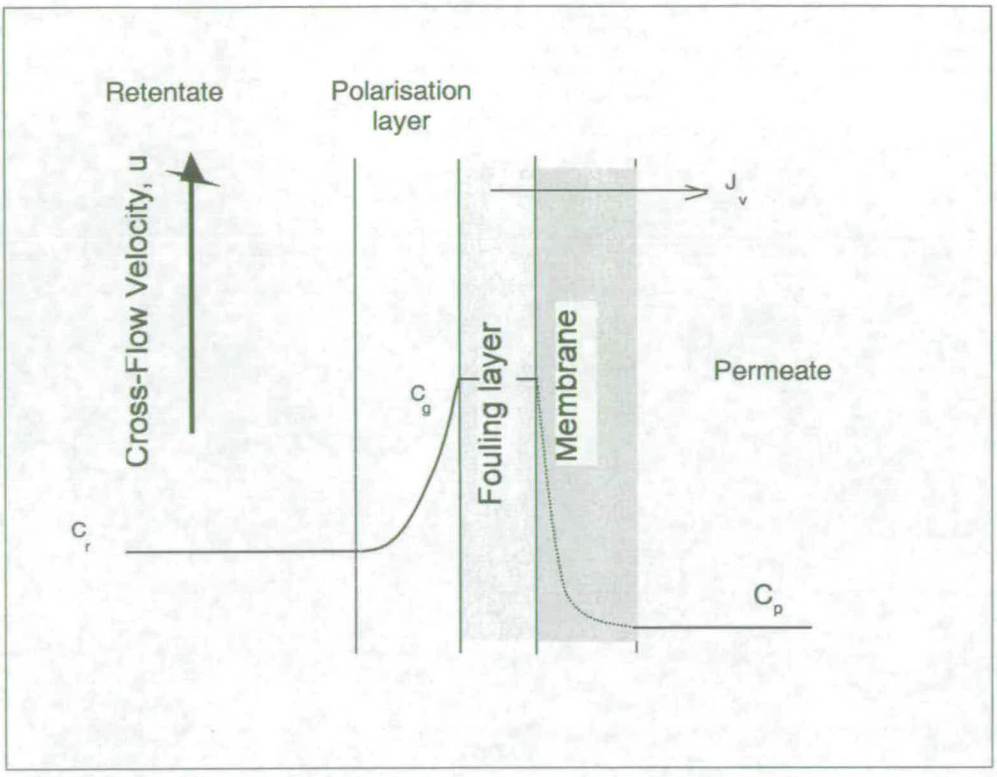

Fig. 1.5: *concentrations and fluxes around the membrane.*

1.3.3.2. Gel polarisation theory

At some stage during the concentration polarisation, the protein concentration at the membrane surface may reach a concentration C_g above which a gel forms (*see Fig. 1.5*). A fouling layer of protein is thus formed, resulting in an additional resistance to the flux across the membrane. This model sometimes fit well with experimental data. It also explains the limiting flux (see 1.3.2.2.), as well as the linear relationship often observed between J_v and $-ln(C_r)$ in equation (1.1): the plot of J_v against $ln(C_r)$, at constant pressure, leads to a straight line, and this line meets the x-axis at a value considered as C_g, for which the flux becomes zero. Therefore, one may assume that the gel layer is the cause of the limiting flux.

However, several shortcomings needed to be alleviated: first, the value of C_g depended on the solution, and on the membrane, and could only be inferred from the filtration experiment. Moreover, the fact that filtrations of solutions concentrated above C_g were feasible denied the model. More thorough investigations, involving the study of the membrane structures and of the interactions of the solution components, were required.

1.3.4. EXPERIMENTAL FINDINGS

Comparisons between experiments where operating conditions were varied, or systems where different kinds of membranes and proteins were used, led to a few general conclusions, drawn by Marshall, Munro and Trägårdh (1993) in their literature review on fouling. This section owes much to these authors, and a number of the articles they mentioned were consulted whenever it was possible, and especially all of those essential for understanding the phenomena, or just important evidences. More recent papers on the subject were also consulted.

1.3.4.1. Influence of operating conditions

a) Transmembrane pressure:

The constant, limiting flux at high TMP's has already been mentioned (see section 1.3.2.2.). In MF, however, compaction of the cake sometimes causes the permeate flux to decline with increased TMP (see, for instance, Murkes and Carlsson, 1988). Therefore in MF, there is an optimum TMP for the maximum flux that provides enough driving force without too much fouling. That optimum was found to decrease with increasing pore size (Marshall *et al.*, 1993). To a lesser extent, this can be found in UF as well, for highly concentrated retentates (e.g. Jonsson, 1994).

The rejection ratio was found sometimes to decrease with increased TMP at the beginning of an UF, but always later it increased due to fouling. The temporary decrease in retention was probably due to concentration polarisation: since the solute is concentrated in the vicinity of the membrane, more protein than expected from the bulk retentate concentration can reach the permeate side.

b) cross-flow velocity:

When considering highly retentive systems in UF, it has been found that with increased flow velocities the permeate flux increased, because the fouling and the polarisation layer were reduced (see, for instance, Meireles *et al.*, 1991). In addition, the recovery of the initial flux was greater with a high velocity rinsing of the fouled membrane. Nakanishi and Kessler studied the fouling and rinsing of an UF membrane for processing skim milk. They found that the recovery of the flux after rinsing was the highest when both the UF velocity and the rinsing velocity were increased. Still in these highly retentive UF systems, protein retention has often been found to decrease with cross-flow velocity (Marshall *et al.*, 1993).
In cases, such as MF, where low retention was expected, i.e. when the size of the pores was larger than the size of the proteins, only a limited effect of cross-flow velocity on permeate flux was found (Bowen and Gan, 1991).

c) temperature:

Increasing the temperature should increase the permeate flux, because of a decrease in viscosity and an increase in diffusion coefficients. This is often confirmed in practice, in MF and UF, at least for the initial flux (e.g. Meireles *et al.*, 1991).

However, temperature increases denaturation and aggregation of the proteins, which in turn often causes greater fouling: Meireles *et al.* (1991), using turbidity measurements and size exclusion HPLC, found that BSA solutions were undergoing spontaneous denaturation above 8 °C, and that the rate of denaturation increased with temperature. UF fluxes for a 100 kDa polysulfone membrane were initially increasing with temperature, but at 22 °C, decreased below the steady state value reached at 8 °C. They could correlate the fouling of the membrane with the protein aggregation, and hence with the increased temperature.

Campbell *et al.* (1993) ultrafiltered an α-amylase (50-55 kDa MW) through a 60 kDa polysulfone membrane. In the range of 12 °C to 60 °C, they found for the permeate flux an optimum temperature of 25 °C. This can be interpreted again as an initial decrease in viscosity and increase of diffusivity with temperature, but which cannot compensate for

increased denaturation and subsequent fouling above 25 °C. In addition, Campbell *et al.* observed that the rejection ratio decreased with temperature, but the activity of the enzyme in the permeate decreased too. In addition, the activity of the permeate decreased also with time, although control solutions at the same concentration and temperature remained stable over the same duration. Campbell *et al.* concluded that temperature was not by its own the main factor of fouling, and that it did not increase adsorption of the enzyme enough to compensate for a better transmission; however, the filtration caused denaturation of the enzyme, and this phenomenon was enhanced by the temperature.

1.3.4.2. Feed characteristics and fouling

a) The influence of the feed concentration, and/or viscosity:

In UF, the gel polarisation theory predicts a decrease of permeate flux proportional to the logarithm of the bulk concentration in protein (see eq. (1.1) in section 1.3.3.), as well as a lesser influence of concentration when cross-flow velocity is increased. This is actually often observed (Cheryan, 1986; Kessler, 1981). However, this is not necessarily true with a highly concentrated feed as reported sometimes (e.g. Le et al., 1984; Pritchard, 1990).

The influence of an increase in concentration depends as well on the way fouling occurs. If fouling affects only the surface of the membranes rather than the inside of the pores, then it has been found (Marshall *et al.*, 1993) that an increase in concentration causes an increase in the total membrane resistance. In this case, Daufin *et al.* and Sun and Ouyang showed that the irreversible fouling (adsorbed layer) did not vary much, whereas the reversible fouling, attributed to concentration polarisation and removed by water flushing, increased with concentration (Marshall *et al.*, 1993). The retention characteristics of the membrane are usually not affected when only surface fouling occurs. If on the contrary the fouling occurs inside the very pores (internal fouling), then the permeate flux decreases faster with increased concentrations (Bowen and Gan, 1991), and presumably the rejection ratio increases quicker.

b) The influence of aggregates:

Protein aggregates can strongly increase fouling of MF and UF membranes (e.g. Tracey and Davis (1994) on the microfiltration of BSA, and Kim *et al.* (1993) on the ultrafiltration and microfiltration of BSA). Prefiltration can remove aggregates, and it improves both UF and MF permeate fluxes of protein solutions. For instance, Kelly *et al.* (1993) filtered BSA solutions through 0.16 μm Filtron membranes. They found that the fluxes depended upon the technique of manufacture of the BSA, and that prefiltering with a 100kDa membrane of a badly fouling fraction could vastly improve the flux. Aggregates seemed to be responsible for the fouling that can be avoided by prefiltration. Examining their membrane with scanning electron microscopy, Kelly *et al.* found that, without prefiltration, the badly fouled membranes were coated with a thick layer of protein and large protein aggregates, whereas when the membranes were used with prefiltered feed, the protein deposit was not formed. Gel filtration analysis enabled them to correlate the increased rate of fouling with an increased number of large molecular weight compounds. They suggested that aggregates deposit onto the membrane, and may in addition act as "seeds" for further deposition. Aggregates are also reckoned to block the larger pores that ensure most of the flux circulation (see section 1.2.3.2.) and thus cause significant loss in flux.

c) The influence of pH:

The pH has indeed an influence on permeate flux, rejection ratio, and fouling rate of a given membrane, but the mechanisms are unclear.

A protein usually contains a number of chemical groups (mainly amine and carboxyl) whose charges vary with the pH. The following table sums up the qualitative change in global charge of a protein with the pH:

pH	< IEP	IEP (IsoElectric Point)	> IEP
group amine	NH_2^+	NH	NH
group carboxyl	COOH	COOH	COO^-
net charge	+	0	-

Table 1.2: *pH and net protein electrical charge.*

The membrane may in addition behave in a similar way. For instance aluminium oxide membranes are amphoteric too, and polysulphone membranes have an acidic behaviour due to their SO_3H groups.

Permeate flux, for protein solutions such as BSA or casein, has often been reported to vary with pH, and to pass through a minimum around the IsoElectric Point (IEP) (e.g. Fane, Fell and Waters, 1983). This is usually attributed to an easier adsorption or deposition of the protein (Bowen and Hughes, 1990; Clark *et al.*, 1991; Fane, Fell and Suki, 1983; Reihanian *et al.*, 1983) when it has no net charge and is therefore less sensitive to electrostatic repulsion forces. Bowen and Hugues (1990) studied the filtration of BSA with aluminium oxide membranes: These authors found that at a pH below 4, i.e. below the IEP's of both the membrane and the protein, adsorption decreased rapidly. However, there are some indications that the minimum flux at the IEP may be only due to the charge of the protein itself: Nyström (1989) worked on UF of ovalbumin through GR61PP and GS61PP polysulphone membranes. He found again that permeate flux was at its minimum at the IEP of the protein, but in addition he observed that the GS61PP membrane was negatively charged at a pH below this IEP. Therefore, in spite of having the protein and the membrane of opposite charge, adsorption is not enhanced enough to cause a further decrease of flux below the IEP. According to Nyström, when the protein is charged, either negatively or positively, its stability in solution is enhanced, and it tends to adsorb or deposit less; if it is positively charged, it may adsorb initially as a thin layer, neutralising thus the membrane charge and helping to prevent further deposition. Fane, Fell and Suki (1983) gave another interpretation for the minimum flux at the IEP of BSA: they suggested that when the

protein had no net charge, its shape in solution was more compact and it tended to form a less permeable deposited layer.

Some observations contradicted this general rule of a minimum flux around the IEP. For instance, Matthiasson (1983) found that in static cell membranes, adsorption increased as pH decreased. However, at least 10 times less deposit is formed in static experiments when compared with a dynamic one (e.g. Fane, Fell and Suki, 1983): the contribution of this phenomenon in dynamic studies may be negligible, and possibly the nature of the deposit is very different (McDonough *et al.*, 1990).

The influence of pH on retention has been studied to (Fane, Fell and Waters, 1983; Hanemaaijer, 1985; Hanemaaijer et al., 1988-1989, Renner and Abd-El-Salam, 1991), but no general trend has been found so far.

d) The influence of the ionic strength

The concentration of mineral ions in solution may have a marked effect on the performances of a filtration, affecting both the amount of protein deposited and the permeate flux. For instance, Fane, Fell and Suki (1983) ultrafiltered 0.1% BSA solutions with retentive PM30 and GR61PP polysulphone membranes. When the solution did not contain any salt, they observed a minimum flux at a pH equal to the IEP, as usually observed (see section above). By contrast, the addition of 0.2M sodium chloride resulted in the permeate flux increasing from pH = 2 to 10, and when compared with unsalted conditions, lower fluxes away from the IEP and higher fluxes around the IEP. Fane *et al.* suggested that ions would reduce the compactness of the BSA proteins around the IEP by binding to the protein, and thus increase the permeability of the deposited layer. Away from the IEP, the ions would bind to the proteins again, but this time it would cause shielding of the protein charges; under these conditions, the stability of the protein in solution would decrease, and the contracted molecules would form a deposited layer less permeable than if no salt was added.

Minerals in solution can also contribute directly to the structure or the composition of the fouling layer: For instance, calcium is known to decrease permeate flux in whey filtration (Marshall *et al.*, 1993). Its phosphate salt in milk and whey has been shown to be an essential component of the fouling layer. For instance, Vetier *et al.* showed that increased calcium content in milk caused increased fouling due to calcium phosphate precipitation, and that increasing or decreasing the soluble calcium content respectively increased or decreased the amount of deposited nitrogen compounds (protein) (Marshall *et al.*, 1993). They concluded that the calcium and phosphate solutes in milk played their most important role as a "cement", between micelles and the membranes, as well as between the micelles themselves.

e) Multicomponent mixtures

As a general rule, the addition of a larger component to a protein solution increases the retention of the smaller components, as much work shows (Blatt et *al.*, 1970; Bottino *et al.*, 1984). Porter (1988) suggested that the larger components could form a secondary membrane of reduced porosity that can be more retentive than the actual membrane. Tam and Tremblay (1991) filtered mixtures of five different polyethylene glycols (PEG) through a PTGC Millipore 10 kDa membrane. Comparison of the data on the filtration of individual PEG's with data on mixtures enabled them to calculate the apparent MWCO of the membrane for the mixtures. They showed that the apparent MWCO curves shifted to lower values when a mixture was used. They suggested that a differential solute lag accounts for this shift towards a higher retention, because the larger molecules encounter more friction in the pores and slow down the smaller ones, and may even block the pores.

Specific component interactions in the solution could also in some cases produce more complex effects: Papamichael and Kula (1987) filtered PEG in the presence of BSA. They showed that the retention of PEG first increased from 0.3 to 0.58 when up to 0.2% BSA was added to a pure solution, but then the retention decreased with increased concentration of BSA, until it reaches a stable value of 0.18 above 4% BSA. Although the initial increase of retention can be interpreted with the mechanisms suggested by Porter or Tam and Tremblay, the decreasing retention stage is not clearly

understood. Papamichael and Kula suggested that PEG, which is known to carry a large "cocoon" of water molecules held by hydrogen bonds, sees its size reduced in the presence of large numbers of BSA molecules competing for water.

1.3.4.3. Fouling and pore size

Gatenholm *et al.* (1988) showed that the final permeate flux was in fact proportional to the intrinsic membrane resistance (clean membrane) with a range of UF and MF membranes. In some traditional MF applications, such as cell and cell debris removal, or cell washing and recycling, it has been usually found that fluxes, in the long term, were better with high cut-off UF membrane (MWCO > 100 kD) than with MF membranes (Marshall *et al.*, 1993). A possible explanation for this is the internal fouling of MF membranes by debris and protein aggregates, while UF membranes are mostly affected by surface fouling.

In a more general way, it is reckoned that the steady-state flux in UF increases with decreasing pore size, owing to a lower fouling resistance for small pore membranes (Marshall *et al.*, 1993). Fane, Fell and Waters (1983) showed that the relevant parameter to consider was in fact the ratio of the protein size to the pore size: Using a PM30 ultrafiltration membrane (30 kD MWCO), and comparing the filtration of BSA (69kD) and lysozyme (14.2 kD) solutions, they found that

- the initial flux was higher for the lysozyme solution. This was to be expected, since BSA should be totally retained due to its size;

- the flux declined sharply for the lysozyme solution, and its steady state value was lower than for the BSA solution;

- however, the final rejection ratio of lysozyme was still 45% at steady state.

1.3.4.4. Influence of the membrane composition

Hydrophobicity and electrical charges of the membrane have a significant impact on the performances of the membrane.

a) Hydrophobicity of the membrane results in more severe fouling

Static adsorption of protein is more important on hydrophobic membranes: Reihanian *et al.* (1983) studied the static adsorption of BSA onto UF membranes. They found that onto the hydrophobic XM 200, XM 50 and PM 30 polysulphone membranes, adsorption caused losses of permeability, and increased with increased concentration of protein. On the contrary, onto the hydrophilic YM 30 and UM 10 it led to no reduction of permeability and was therefore negligible.

However, commercially available hydrophilic membranes have not so far outperformed the hydrophobic membranes. This is because concentration polarisation is also a flux-reducing factor, and a decreased fouling may allow a higher concentration polarisation to effectively cancel out any improvement in flux. This was reported for instance by Rolchigo *et al.* (Marshall *et al.*, 1993) who experimented on a 100kDa hydrophilic Ultrafilic membrane, and its hydrophobic precursor. It was assumed that the only difference between the two membranes was in their hydrophobicity. On processing a protein mixture through these membranes arranged in a cross-flow system, Rolchigo *et al.* found similar permeate fluxes for both membranes, and a higher rejection ratio for some proteins with the hydrophobic precursor. However, when instead of a crossflow they used a rotary system (spinning filter) with a high Taylor number, the hydrophilic membrane outperformed the hydrophobic one, with a higher protein transmission, and a much higher permeate flux. In cross-flow filtration, concentration polarisation and protein loosely bound onto the membrane probably account for most of the flux reduction, whereas with rotary system, they are minimized by the shear forces and only the tightly adsorbed protein can affect the membrane performances.

Direct analysis of fouled membranes confirms that hydrophobic membranes foul differently and worse: Sheldon *et al.* (1991) filtered BSA solutions through

polysulphone (hydrophobic) and regenerated cellulose (hydrophilic) membranes. Flux data showed that not only more protein adsorbed per unit surface onto the hydrophobic membrane, but also that the specific resistance per unit mass of adsorbed protein was higher for the hydrophobic membrane. Moreover, freeze fracture and deep etching techniques showed that, in solution as well as at the surface of the fouled hydrophilic membrane, BSA molecules were more or less globular and with normal dimensions, as expected. However, the molecules appeared long and filamentous at the surface of the fouled hydrophobic membranes. This difference is well explained by the structure of the BSA molecules, which normally presents a hydrophilic outer layer: the hydrophobic membranes contribute in some ways to denature BSA molecules and bind to their internal hydrophobic sites.

b) An hydrophilic surface may not compensate for the hydrophobicity of the matrix - Possible mechanism for the fouling of an hydrophobic membrane

Coating of the hydrophobic membranes with an hydrophilic material is sometimes practiced as a way to overcome their bad fouling behaviour. However, this may not solve the problem. Ko *et al.* (1993) studied the adsorption of BSA and β-Lactoglobulin (βLG), onto hydrophilic regenerated cellulose membranes (RC), and onto a hydrophobic polycarbonate PC015 membrane coated with polyvinylpyrrolidone (PVP). The PVP coating confers hydrophilic properties to the surface of the PC015 membrane, and provides a steric hindrance preventing proteins adsorbing directly onto the membrane. Ko *et al.* showed that, in spite of a lower protein load under either static or dynamic conditions, the PC015 membrane formed a higher fouling resistance, most of which was due to adsorption. With RC membranes, the mass-transfer resistance was mostly due to concentration polarisation. To quantify better the effect of adorption and its different nature in both cases, the notion of specific relative resistance was introduced. This is defined as

$$SR_a=(r_a/r_m)/g_a$$

where r_a= resistance of the adsorbed layer (m^{-1}),

r_m= resistance of the clean membrane (m^{-1}),

g_a= adsorbed protein load (mg/m^2).

It was found that SR_a was greater for the PC015 membrane than for the RC membranes. This indicated that the adsorbed layers on the RC membranes were more loosely packed or more hydrated than the one on the PC015. A model was proposed, in which the adsorbed layers on the RC membranes were constantly supplied with water coming from the permeate side through the hydrophilic matrices, whereas the adsorbed layer on the PC015 membrane could not be provided with water through the hydrophobic matrix and became dehydrated. This study showed clearly that the matrix properties are at least as important as the surface properties.

c) Charge effects

The membrane charge, the pH and the ionic strength of the solution have combined effects on the membrane performances, some of which have been previously discussed in section 1.3.4.2. Generally, a similar charge for the membrane and the protein gives better permeate fluxes. This can be exploited to enhance the separation of similar sized proteins, as showed for instance Nakao *et al.* (1988).

1.3.5. MECHANISMS AND MODELS FOR THE FOULING OF UF AND MF MEMBRANES

1.3.5.1. Advances in concentration polarisation models

A better understanding of concentration polarisation, and of the physical properties of the fluid in the boundary layer, has allowed modeling ultrafiltration without necessarily the need to hypothesize on the formation of a gel above a limit concentration.

Jonsson (1984) studied the cross-flow ultrafiltration of whey proteins and dextrans through a totally retentive membrane. Before doing so, however, the viscosity and osmotic pressure of the solutions were measured for concentrations up to 50%. The permeability l_p of the membrane was then measured for pure water. Only then, the permeate flux of the macromolecular solutions was measured. As can be seen on the graphs, the typical flux-pressure profile was observed (see section 1.3.2.2.). From the osmotic pressure model

$$J_v = l_p(\Delta P - \pi_{os}) \tag{1.2}$$

it was possible to estimate π_{os}, the osmotic pressure at the membrane surface, from which the wall concentration C_m could be found. This allowed calculation of the mass transfer coefficient k (see equation (1.1)) for dextran T20 solutions. At any given cross-flow velocity, k was found fairly constant for all pressure and concentrations, although slightly decreasing for high values of these parameters. The relationship between k and the crossflow velocity u was in good agreement with the usually accepted correlations in laminar and turbulent regime:

$$[\frac{k\,d_h}{D}]_{lam} = 1.86 \cdot [Re \cdot Sc \cdot \frac{d_h}{L}]^{1/3} \tag{1.3}$$

and

$$[\frac{k\,d_h}{D}]_{turb} = 0.023 \cdot Re^{0.8} \cdot Sc^{1/3} \tag{1.4}$$

where

d_h= hydraulic diameter of flow channel;

L= length of flow channel;

Re= Reynolds number = $(d_h u \rho)/\mu$;

Sc= Schmidt number = $\mu/(\rho D)$.

Using then typical values of k and l_p from the experiments, and equations (1.1) and (1.2) from the boundary layer model, a graph of the permeate flux J_v versus the logarithm of the bulk concentration C_r at constant TMP can then be plotted. This

graph shows a linear relationship between J_v and $ln(C_r)$ at high concentrations, and that no flux is possible for concentrations corresponding to $\pi_{os}= TMP$. Therefore, there is not need to assume that a gel forms at high concentration near the membrane, it is just that the osmotic pressure stops the flux.

Jonsson's approach gave a good fit with experimental data for the variations in concentration and cross-flow velocity, but rather less good for the variations in pressure. As the author pointed out, this may have been due to increases in viscosity at high pressure. Another possibility is that gel formation does actually occur, but depends in fact of a complex set of conditions: Concentration, pressure, pH, etc.

Aimar and Field (1991) also interpreted the limiting flux without citing gel formation, but conducted a thorough hydrodynamic study, including viscosity, concentration and velocity profiles within the boundary layer. They found that the plot of the flux against the logarithm of the bulk concentration was in agreement with the gel theory on its linear part, but then before reaching the value zero, an upward curvature of the plot allowed non zero-fluxes above the "gel" concentration.

Aimar *et al.* (1989) were interested in assessing the development of the boundary layer along the length of UF channels. To do so, they used an osmotic model in which they introduced a concentration profile within the boundary layer, a relationship between viscosity and the local concentration, and a relationship between the boundary layer thickness l and the solution properties, wall concentration and cross-flows at a distance x from the inlet.

Interestingly, they confirmed an idea that has often been expressed: although a common practice is to work at constant pressure in protein filtration experiments, this leads to a complete change in wall concentration profile during an experiment. Their graphs showed decreases in flux of one order of magnitude. This is due to the change in resistance of the membrane during the experiment. On the other hand, working at constant permeate flux should not change the concentration profile, as shown by their simulation. This is therefore a far better approach for studying fouling.

Another interesting finding of that team is the possibility of observing the effects of protein deposition onto (or into) the membrane independently from the effects due to concentration polarisation: concentration polarisation causes a limit flux at high TMP, whereas for lower values of the TMP, it does not influence the flux. Only actual protein deposition decreases the slope of the flux *vs* TMP characteristics in its linear part, for lower values of the TMP (see 1.3.2.2.). Trying to explain why they could not find a limit flux in an experiment, Aimar *et al.* ran a simulation in which the length of the channel as well as the resistance of the membrane was changed. They found that a minimum channel length, as well as a high enough permeate flux, was necessary in order to observe a fully developed boundary layer. Therefore, concentration polarisation must be studied on channels of enough length (up to 500 mm in the simulation), and when estimating this length, allowance must be made for the increase in resistance due to fouling.

Aimar *et al.* suggested the use of short channels for the study of fouling independently from concentration polarisation, however we must state here that the fouling mechanism studied by this method must not be concentration dependent. For instance, gel formation is expected to take place when concentration at the membrane surface is high enough, making this phenomenon possible only if concentration polarisation occurs. Internal fouling, on the other hand, may be more easily studied in these conditions.

1.3.5.2. Models derived from classical filtration theory apply for some colloids, but not for proteins

For DE filtration, as well as for CF filtration, a general expression for the resistance of the cake forming is the well-known **D'Arcy's law**:

$$J_v = \frac{1}{A_m}\frac{dV}{dt} = \frac{\Delta P}{\mu_0(r_m + r_a)} \qquad \textbf{(1.5)}$$

where t is the time of ultrafiltration (s);

V is the permeate volume (m^3);

ΔP is the pressure drop across the membrane (Pa);

A_m is the membrane area (m^2);

μ_0 is the solution viscosity (Pa.s).

r_m is the membrane resistance (m^{-1});

r_a is the cake resistance (m^{-1});

For the dead-end filtration of particles suspended in a fluid, the integration of D'Arcy's law leads to the **classical constant-pressure filtration equation**:

$$\frac{t}{V} = \frac{r_m . \mu_0}{\Delta P . A_m} + \frac{c_0 . r_g . \mu_0}{2 . \Delta P . A_m^2} . V \qquad \textbf{(1.6)}$$

where μ_0 is the viscosity of the permeate (Pa.s);

c_0 is the concentration of particles in the feed solution (kg/m^3);

r_g is the specific resistance of the gel layer (m/kg).

This equation can as well be recast in terms of total resistance, r_{tot}, as a function of time:

$$r_{tot} = \frac{\mu_0 \Delta P}{J_v} = r_m (1 + 4 K_{CFM} A_m^2 J_0^2 . t)^{0.5} \qquad \textbf{(1.7)}$$

where

$$K_{CFM} = \frac{r_g \mu_0}{2 A_m^2 \Delta P} \qquad \textbf{(1.8)}$$

and J_0 is the initial permeate flux (buffer on clean membrane). In these equations, it is assumed first that all the particles from the permeate volume stay in the cake. In addition, the intrinsic membrane properties are not modified, the fouling layer is made-up of rigid spheres piled-up onto each other, and fouling is restricted to the membrane

surface. This model fits with experimental data for some colloids, as shown for instance by Bodzek *et al.* (1993) for the ultrafiltration of latex emulsion waste water.

However, when filtering colloids through membranes with pores of dimensions similar to those of the particles, severe fouling occur due to deposition within the pores. This was shown by Kim *et al.* (1994), who filtered very dilute silver colloids through 30, 100, 300 kDa and 0.22 µm membranes. The 30 kDa membrane had pores smaller than the colloid particles. The retention was high, a cake formed onto its surface, and the flux reached a steady state value. With the 100 and 300 kDa membranes, the pore size was only slightly larger than the particles, severe **internal fouling** occurred. With the 0.22 µm membrane, retention was low and only a small reduction in flux was observed, which was expected given the larger size of the pores compared to the particles (5.7-10.9 nm). A model describing internal fouling is therefore required for some systems.

In addition, with proteins, it seems that fouling can occur and plug the pores even when those are much larger than the protein molecules: we mentioned already in 1.3.4.2 that more severe fouling occurred with broths containing proteins when they were processed through large pore membranes rather than small pore membranes, and that an optimal pore size could be found to maximize the permeate flux.

Another problem is that the **protein cake** formed may be **compressible**: for instance, Grund *et al.* (1992) processed BSA solutions through UF membranes. In a first phase of the experiment, the steady-state permeate flux was measured at a given TMP, and the TMP was increased for each new reading: the permeate flux was then plotted against the TMP. However, in the second phase, the fluxes were then measured for decreased TMP's, and were found lower than that observed for the same TMP's during the first phase. It is usually reckoned that this **hysteresis** is due to a partially irreversible compression of the protein cake. We may see it also as a heavier deposition of tightly-bound protein at higher TMP's which does not redissolve at lower TMP.

For these reasons, models designed for uncompressible cake filtration are not enough, and mechanisms of protein fouling must be investigated.

1.3.5.3. The location of fouling - surface fouling and internal fouling

a) Surface fouling

Many observations show the occurrence of surface fouling with proteins during RO and UF, and with milk during MF. In such a case, a resistance-in-series model can describe the flux reductions: a resistance for the deposited layer, r_a, is added to the intrinsic resistance r_m. To account for concentration polarisation, an additional resistance r_{cp} may also be used, unless it is already allowed for with an osmotic pressure effect ($\Delta\pi_{os}$). In this latter case, ΔP - $\Delta\pi_{os}$ is used instead of the applied transmembrane pressure ΔP. Equations similar to those leading to the classical constant pressure model (Eq. (1.6) can then be derived.

However, this approach has its limits even when only surface fouling occurs, because the cake may not have a uniform nor constant structure. For instance, Glover and Brooker studied the RO filtration of milk, and showed that the density of the deposited casein layer on the surface of the membrane increased with proximity to the membrane (Marshall *et al.*, 1993). Moreover, Vetier *et al.* filtered milk through a 0.2 μm membrane, and found that the deposited layer was, in fact, made of two parts: an upper layer with a protein composition similar to that of milk, and a lower layer richer in BSA, indicating there a progressive internal plugging of the micellar casein deposit (Marshall *et al.*, 1993).

b) Internal fouling:

Another mechanism of fouling affecting UF and MF membranes is internal fouling, i.e. the deposition of protein inside the bulk or the pores of the membrane.

In UF, fouling affects usually the surface of the membrane, but evidence was found that some protein was trapped within the membrane itself too. Among others, Sheldon *et al.* (1991) using staining techniques together with transmission electron microscopy,

gave evidences of internal fouling with BSA on 10 kDa polysulfone and RC membranes. Kim *et al.* (1992) ultrafiltered BSA solutions through various membranes. Using the Hagen-Poiseuille equation for capillary flows:

$$J_{pore} = \frac{\pi d_p^4 \Delta P}{128 \mu h_p} \tag{1.9}$$

where J_{pore} is the flux through a pore, d_p the pore diameter, and h_p the pore length, they showed that the adsorption of one or two layer of BSA molecules inside the pores was enough to account for the observed reduction in flux.

In MF as well, protein deposits can be found inside the pores. For example, Attia *et al.* showed that the casein of milk could both form a layer at the surface, and deposit within the pores of a 0.2 µm membrane. However, they previously found that deposit within the pores did not occur with a 0.8 µm membrane (Marshall *et al.*, 1993).

The modelling of this phenomenon often involves an estimate of the reduction in permeate flux, due either to a narrowing or a blocking of the pores. Two examples of model, both of which assume a single pore diameter and cylindrical pore shape, are presented below.

In the **Standard Blocking Model**, it is assumed that pores are progressively restricted, that the foulant deposits evenly, and that the decrease in pore volume is proportional to the volume of spent permeate. Integrating then D'Arcy's law with these assumptions gives:

$$r_{m(i)} = r_m.(1 + K_{SBM}\, A_m J_0 t\,)^2 \tag{1.10}$$

with

$$K_{SBM} = \frac{4.C_{SBM}}{A_m N_0 \pi h_p d_p^2} \tag{1.11}$$

where

$r_{m(i)}$ is the fouled membrane resistance;

r_m is the membrane intrinsic resistance;

A_m is the membrane area;

d_p is the initial pore diameter;

J_0 is the flux through a clean membrane;

C_{SBM} the protein volume deposited per unit filtrate volume;

t is the time.

The exponent in (Eq. 1.10) is 2, whereas it is only 0.5 in the rather similar (Eq. 1.7).

In the **Complete Blocking Model**, on the other hand, it is assumed that a given pore is either plugged, or retains its initial diameter. The number of pores that become plugged increases proportionally with the filtrate volume:

$$r_m = r_{m0} \cdot e^{K_{PBM} t} \tag{1.12}$$

in which

$$K_{PBM} = C_{PBM}\, \pi\, d_p^4 \frac{A_m \Delta P}{128\, \mu_0 h_p} \tag{1.13}$$

where C_{PBM} is the number of pores per unit membrane surface area that become plugged per unit filtrate volume.

The Hagen-Poiseuille equation for the flow inside a capillary is widely used, to relate the changing diameter of the pores with a decrease in flux or an increase in TMP.

1.3.4.4. Structure of the fouling material

In order to model either the pore or the surface fouling, one must have an idea of the structure of its forming material, with its porosity and permeability to water and solutes. We listed below the various structures that are encountered:

-Fouling by sheet and fouling by stacked micelles or granules

Fouling by sheet is often observed with BSA (for instance, see Ko *et al.* (1993), or Kim *et al.*, 1992 and 1993). This kind of deposit is called so because under the electron microscope it appears as a compact pile of very thin layers. It is different from fouling by micelles (for example, see Vetier *et al.* on combined effect of micellar deposition and fouling of BSA in the voidages (Marshall *et al.*, 1993)), and different from fouling by granules. For instance, Lee and Merson ultrafiltered (PM10) and dead-end filtered (0.4 μm Nuclepore membrane) various whey protein solutions, and found that BSA and β-Lactoglobulin formed sheets on the surface, especially near the pore entrance, whereas γ-globulin formed granules. The granules were roughly spherical bodies of irregular sizes, and were randomly agglomerated. When concentration of γ-globulin increased, the granules stacked into layers, and the permeability of that deposit was not so reduced as that of the BSA and β-Lactoglobulin sheets (Marshall *et al.*, 1993).

As a general rule, micelle and granule deposits allow fluids to flow through their voidages, whereas sheets hardly do. Sheldon *et al.* (1991) filtered BSA solutions through polysulfone (hydrophobic) and regenerated cellulose (hydrophilic) membranes. Flux data showed that not only more protein adsorbed per unit surface onto the hydrophobic membrane, but also that the specific resistance per unit mass of adsorbed protein was higher for the hydrophobic membrane. Using freeze fracture and deep etching techniques, the same authors found that, in solution as well as at the surface of the fouled hydrophilic membrane, BSA molecules were more or less globular and with normal dimensions, as expected. However, the molecules appeared long and filamentous at the surface of the fouled hydrophobic membranes. This difference is well explained by the structure of the BSA molecules, which normally presents a hydrophilic outer layer: the hydrophobic membranes contribute in some ways to denature BSA molecules and bind to their internal hydrophobic sites.

-Fouling by aggregates forming before the membrane

We already mentioned the role of aggregates in fouling: fouling can be reduced if they are removed from the solution prior to filtration. However, Kim *et al.* (1993), filtering BSA solutions through various UF and MF membranes in a stirred cell, found that they do form at the vicinity of the membrane. They used in their experiments nitrogen pressure to provide the driving force, for it had been found that peristaltic pumps caused aggregates to form, and they did not recycle the feed. In spite of this, aggregates appeared when both the concentration and the transmembrane pressure were high enough. For a given concentration, the pressure above which aggregates would appear was dependent on the membrane, and would decrease with increased membrane permeability to water. Duration of the experiment, as well as speed of stirring, caused aggregation too. Kim *et al.* concluded that rapid supersaturation of protein molecules and high shear rates (either from an impeller or at the entrance of a pore), as well as prolonged exposure to shear, determined aggregation, which in turn should significantly affect membrane performances.

1.3.6. CONCLUSIONS ON MEMBRANE FOULING

Fouling has been found to be a complex phenomenon, depending much on the system studied and on the operating conditions. General features are summed-up below:

-Concentration polarisation accounts for some noticeable features associated with fouling, such as the limit flux at high TMP, and very high concentration, viscosity and osmotic pressure at the membrane wall. It is sensitive to the geometric and hydrodynamic characteristics of the system, and it can probably influence at least surface fouling.

-The effects of the feed characteristics (pH, ionic strength) and handling (pumping and shear causing aggregate formation, prefiltration...) are crucial in

determining the extent of fouling. Fouling seems to be more important when the pH is close to the protein IEP. Fouling increases with ionic strength when the pH is away from the IEP, but has been reported to decrease with ionic strength when pH is near the IEP.

-Fouling often increases with pore size, and a UF membrane may be found more convenient for MF applications.

-It is still unclear whether internal fouling happens by initial adsorption and further deposition inside the pores, or whether aggregates form at the entrance or within the pores, and whether shear rates inside the pores can affect conformation and stability of the solute proteins, causing them to deposit or aggregate.

-There are several possible mechanisms and locations for the proteins to deposit. Occurrence, possibly simultaneous, of these mechanisms according to the conditions and characteristics of the system, may explain why it is so difficult to predict the fouling behaviour of a membrane.

-The aim of this PhD thesis was therefore to develop a general approach allowing to model and predict mass-transfer in a variety of systems and conditions. As an example of combination of different mechanisms leading to fouling, the simultaneous effects of concentration polarisation and cake build-up in cross-flow filtration were modelled and checked experimentally for hollow-fibre geometry (case that was illustrated in *Fig. 1.3*).

2.

MODELLING ULTRAFILTRATION IN HOLLOW-FIBRE MODULES

2.1. MODEL DEVELOPMENT

2.1.1. PARAMETERS AFFECTING THE MEMBRANE PERFORMANCE

Many different designs exist in micro- and ultra-filtration. In any mode of operation however, two basic mechanisms remain: either Dead-End or Cross-Flow filtration, or a combination of the two, occurs in the vicinity of the membrane. Being able to model these two phenomena would enable us to check fundamental mechanisms with experiments. In addition, these fundamental models could be incorporated in more specific ones for more complex situations, e.g. with air sparging or standing vortex waves. Therefore, the modelling of these two situations was addressed in this work.

The following points should be paid special attention when modelling a system or carrying out experiments to validate it:

- Presence of particulates and debris:

We believe that their unwanted presence in some situations is simply ignored, although they might explain some failures. For instance, it has been reported that serum supplemented medium for cell-culture had the ability to foul MF hollow-fibre membranes so much that the flux was stopped (Brotherton and Chau, 1995). However, we often observed debris visible to the naked eye in Foetal Calf Serum. In some cases, this can be even aggravated by clumping of the debris (Mercille *et al.*, 1994).

When debris is present, we need at least an idea of its size distribution, and what kind of cake it could form. For instance, a compressible cake will lead to greater reductions in flux, whereas a cake formed with rigid particles may have large voids between these particles, resulting in a low resistance to the flow.

In some particular cases, e.g. some mycelial fermentations, flocs may be present. If these flocs are frail, they may break-up at the entrance of a pore, resulting in some impurity in the permeate product, or some unexpected fouling.

- Aggregates:

Thermodynamics could enable us to predict the composition of a solution containing monomers and aggregates of a given solute species. The basic rule is that the chemical potential of all molecules of a given species, including monomers and those in aggregates, is the same.

This works only for systems at equilibrium, though. During filtration, changes in concentration near the membrane or in the retentate affect the chemical potential, hence the degree of aggregation. So do the shear rates, too, either at the entrance or within the pores, or at the surface of the membrane. It is therefore necessary to know the values of the kinetic constants for aggregation, and compare them with the filtration rate and, if relevant, with the recycle rate.

- Surface properties of the system:

Data on the protein and membrane surface charges as a function of pH and ionic strength should be known.

- Specific properties of some components:

These could include, for instance, different kinds of deposit forming for different pH's, such as in the case of casein.

- Pore size distribution and solute size distribution

It is of special interest when they overlap, and internal fouling may compete with surface fouling (*e.g.* Tracey and Davis, 1994).

2.1.2 PHYSICAL MODEL

The model presented here was designed to predict surface fouling and critical fluxes in crossflow ultrafiltration of protein solutions through hollow-fibre modules. It also included ionic strength and pH effects.

A protein solution at a concentration c_0 is tangentially cross-filtered through a hollow- fibre UF membrane of lumen radius r_i and intrinsic resistance r_m. The inlet pressure is p_0, the permeate-side pressure p_{per}, the average inlet velocity $u_{0,avg}$. Total rejection of the protein is assumed. The model aims to predict the axial velocity profile $u(r, z)$, the radial velocity profile $v(r,z)$, the pressure $p(z)$ and the concentration profile $c(r,z)$ at steady-state, for all radial coordinates r and axial coordinates z (with r=0 on the centerline and z=0 at the inlet). It also aims to predict the local thickness of the fouling layer τ_{cake}, hence the total fouling resistance r_a and the critical value of the permeate flux (or pressure) for which it appears.

2.1.3 TWO STEP APPROACH

Ilias and Govind's model (1993) for concentration polarisation in UF tubular modules was adapted for this purpose by including dynamic effects on the macromolecules. This was achieved by using the Stokes-Einstein generalised equation presented by Phillies *et al.* (1976) which expresses the diffusivity coefficient as a function of the osmotic pressure and the drag force. Osmotic pressure included electrostatic and London-Van der Waals forces plus entropic pressure, and was calculated according to Bowen and Jenner's model (1995). Interactions between the protein and the membrane were neglected. Therefore, fouling was due to coagulation of the protein, which was predicted when the mass-transport equation diverged to values higher than that of the maximum osmotic pressure.

The present PhD research work developed this approach, by focussing on concentration polarisation, on cake modelling, and on the combination of the two for real operation. The following three sections describe the models used to simulate each of these situations.

2.2. MODELLING OF CONCENTRATION POLARISATION

2.2.1. INTRODUCTION

2.2.1.1. Preliminary assumptions

Here, we are interested only in reported work where the properties of the boundary layer were considered to be dependent on the axial position. An assumption that is usually made is that the boundary layer presents radial symmetry and its thickness depends only of the distance downstream of the cross-section considered.

2.2.1.2. Principles

Our goal is to model concentration polarisation in hollow fibres, but with a specific interest in finding concentration and velocity profiles both radially and lengthwise. It seems there are only few studies on this subject in the literature, and this section reviews them while justifying our choice for adapting the model developed by Ilias and Govind (1993).

a) Equations of continuity, motion and mass transport:

In most published works, the starting point for modelling concentration polarisation is either to write down the equations of continuity, of momentum and of mass transport of the solute, or in a equivalent fashion to apply mass and momentum balances over defined control volumes (e.g. an infinitesimal section across the boundary layer).

b) Boundary conditions:

Then, boundary conditions of the system must be defined, with reasonable assumptions. For instance, in the model of Yeh and Cheng for hollow-fibres (1994), it is assumed that at the outlet of the fibres the permeate flux gradient in the axial direction is nil. This condition is

equivalent, however, to assuming that the concentration polarisation layer is fully developed at the outlet. We have seen in section 1.3.5.1 that this may actually not be always the case. Moreover, Yeh and Cheng's model predicts fluxes lower than those their authors experimentally observed, which could be explained by this hypothesis being wrong.

c) Physical properties of the solution:

As the concentration increases in the boundary layer on approaching the membrane surface, the viscosity of the solution is bound to increase and, as a consequence, the convective flux is slowed. At the same time, the osmotic pressure increases, causing an additional resistance to flow. The diffusivity of the solute may also vary with concentration. Therefore, one needs to assume or to compute a concentration profile within the boundary layer. Then, one may assume or get from experimental data, either a viscosity-concentration relationship, or a similar relationship for the osmotic pressure, or the diffusivity. A perfectly rigorous model would take into account these three relationships at the same time.

2.2.1.3. Solving the equations

a) Analytical solution:

Fluid velocity profiles and concentration profiles in hollow-fibre systems are functions of the following parameters:

-Pressure decreases downstream; radial variations can be neglected.

-Axial velocity decreases near the wall (momentum flux) and downstream (losses from permeation).

-Concentration increases downstream and near the wall. Axial diffusion is usually neglected.

Therefore, only few simplifications can be made in the equations. As a consequence, analytical solutions will not be possible, unless assumptions are made on the concentration profile and on the velocity profiles. Thus, Aimar, Howell and Turner (1989) in their model

assumed a concentration profile. They also remarked that the shear stress in the boundary layer was constant, and they found a simple relationship between the local axial velocity u, the local viscosity μ, and the local permeation rate Q. However, this approach implicitly assumes that the radial velocity v is constant throughout the boundary layer and equals the permeation velocity. In addition, the concentration profile they asumed could not satisfy all of the boundary conditions.

b) Numerical solutions:

Numerical methods can still however solve the problems. In fact, they might give better results with less assumptions, provided not only that convergence occurs during the computations, but also approximation and machine errors are controlled. Ilias and Govind (1993) developed a model based on finite difference approximations that was flexible enough to allow for introducing variable viscosities and diffusivities. This work will use this model to simulate ultrafiltration in hollow-fibre modules.

2.2.2. ILIAS AND GOVIND'S MODEL

2.2.2.1. Ilias and Govind's paper

In their paper "*A Study on Concentration polarization in Ultrafiltration*", published in 1993 in *Separation Science and Technology*, Ilias and Govind presented a numerical method to solve the coupled transport equations for momentum and solute in tubular ultrafiltration. Their work showed good enough agreement with experimental data even though some improvement seemed necessary. Although the measured fluxes were lower than the predicted fluxes, the difference might have been accounted for due to deposition of material (*e.g.*: measured fluxes were less than half the predicted flux of 4.10^{-4} cm/s at a cross-flow velocity of 35 cm/s). More of concern perhaps is that an estimate of both the approximation and machine errors should be made too.

2.2.2.2. Flexibility of the model

a) Geometry:

Although the geometry chosen by Ilias and Govind is tubular, it can certainly be transposed to other systems such as flat sheet channels, just by rewriting and discretizing the equations and boundary conditions for the new geometry.

b) Physical parameters:

The model can be adapted easily to take into account various parameters to describe the system more accurately:

-influence of osmotic pressure;

-dependency of the diffusivity on the local concentration;

-dependency of the viscosity on the local concentration;

-local resistance to the permeate flux of the membrane or a cake;

c) Microfiltration:

In Ilias and Govind's model, the diffusivity of solutes in the transport equation may include not only a Brownian motion effect, but also mutual solute interactions and dragging forces. It should be possible to apply the model to microfiltration of particles by using an effective diffusivity worked out from a dynamic balance on the suspended particles. The main difficulties there would be to obtain values for the drag coefficients (from correlations or experiments), and to check the assumptions stated in the next section are still valid.

2.2.2.3. Assumptions

The model is quite flexible, making the sole assumption that the permeate flux is small. This has two consequences when considering the transport equations:

-1) the membrane wall radial velocity is negligible compared with the average cross-flow velocity;

-2) the gradient of the cross-flow velocity along the membrane is small;

These assumptions result in one single simplification in the transport equations (see next section). However, they may not be true in Microfiltration where permeate fluxes are higher, and the complete, non simplified equations might then have to be considered.

2.2.2.4. Description of the tubular system and nomenclature

The following notation is used in this section:

-z is for the axial position, and r for the radial position;

-at the entrance of a tube, $z=0$; at the end, $z=L$;

-on the centerline of the tube, $r=0$; on the membrane surface, inside, $r=r_i$;

-p is the pressure, p_0 the inlet pressure, p_{per} the pressure on the permeate side;

-π_{os} is the osmotic pressure;

-c is the concentration, c_0 the inlet concentration and c_g the wall (gel) concentration;

-u is the axial velocity, and v the radial velocity;

-u_0 is the inlet velocity (depends on r), and $u_{0,avg}$ is the average inlet velocity;

-v_{wall} is the permeate flux, and $v_{0,wall}$ is the inlet permeate flux;

-r_m is the intrinsic membrane resistance, and A_m the membrane surface area;

-σ is the solute rejection ratio;

-ρ is the solution density, and μ its viscosity;

-D is the solute diffusivity;

N.B.: the intrinsic membrane resistance comes from the formula giving the buffer flux:

$$v_{wall} = (p_{wall} - p_{per}) / (\mu r_m),$$

We summed-up some of these notations on the following diagram:

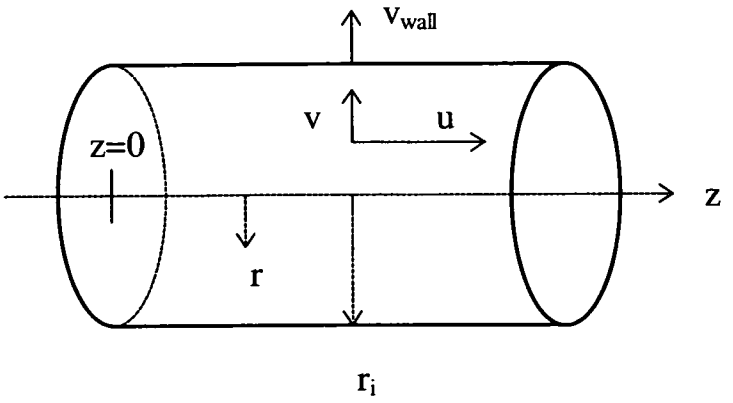

Fig. 2.1: A section of fibre with notation for geometry and flow.

The following dimensionless parameters were also introduced:

-radial direction $R = r/r_i$;

-axial direction $Z = v_{0,wall} z / u_{0,avg} r_i$;

-radial velocity $V = v / v_{0,wall}$;

-axial velocity $U = u / u_{0,avg}$;

-pressure $P = 2p / \rho u^2_{0,avg}$;

-osmotic pressure $\Pi = 2\pi_{os} / \rho u^2_{0,avg}$;

-wall Reynolds number $Re_{0,wall} = v_{0,wall} r_i \rho / \mu$, at inlet;

-wall Peclet number $Pe_{0,wall} = v_{0,wall} r_i / D$, at inlet;

-concentrations $C = c / c_0$ and $C_g = c_g / c_0$;

-membrane resistance $R_m = 2v_{0,wall} \mu . r_m / \rho . u^2_{0,avg}$;

2.2.2.5. Governing equations and boundary conditions

In a cylindrical geometry, at steady state, and taking into account the assumptions made in 2.2.2.3, we get

-for the continuity equation,

$$\frac{\partial U}{\partial Z} + \frac{1}{R}\frac{\partial}{\partial R}(RV) = 0\,; \qquad \textbf{(2.1)}$$

-for the momentum transport equation, at constant viscosity:

$$U\frac{\partial U}{\partial Z} + V\frac{\partial U}{\partial R} = -\frac{1}{2}\frac{dP}{dZ} + \frac{1}{Re_{0,wall}}\left(\frac{\partial^2 U}{\partial R^2} + \frac{1}{R}\frac{\partial U}{\partial R}\right); \qquad \textbf{(2.2)}$$

-and for the solute transport equation, at constant diffusivity:

$$U\frac{\partial C}{\partial Z} + V\frac{\partial C}{\partial R} = \frac{1}{Pe_{0,wall}}\left(\frac{\partial^2 C}{\partial R^2} + \frac{1}{R}\frac{\partial C}{\partial R}\right). \qquad \textbf{(2.3)}$$

The following boundary conditions apply:

-at the inlet (**Z**=0),

$U_0(R) = 2(1-R^2)$ assuming parabolic profile (Poiseuille flow);

$V_0 = 0$;

$C_0 = 1$;

-at the membrane wall (***R***=1),

$U_{wall}(Z) = 0$ (no slip condition);

$V_{wall}(Z) = \dfrac{(P_{wall} - P_{per}) - (\Pi_{wall} - \Pi_{per})}{R_m}$ (membrane flux);

$\left.\dfrac{\partial C}{\partial R}\right|_{R=1} = Pe_{0,wall}\sigma V_{wall}(Z)C_g(Z)$;

(from diffusion flux = convective flux at steady state);

(2.4 - 2.6)

-at the centerline (R=0),

$$\left.\frac{\partial U}{\partial R}\right|_{R=0} = 0 \quad \text{and} \quad \left.\frac{\partial C}{\partial R}\right|_{R=0} = 0. \qquad \textbf{(2.7 and 2.8)}$$

In the membrane flux condition, the osmotic pressure Π depends on the concentration: hence, $\Pi_{wall}(C_g)$.

2.5.4.6. Discretization and resulting finite-difference equations

The space within the tubular membrane is divided up into small elements:

- in the z direction , the elementary step is constant and called ***dZ***; successive positions are indexed i, with i=1 at the inlet (Z=0) and i=m at the outlet;

-in the R direction, the positions are indexed j, starting from j=1 at R=0 to j=n at R=1; the step may vary for increased accuracy, i.e. the step is noted DR1 between j-*1* and j, and DR2 between j and j+*1*.

The following diagram summarizes this:

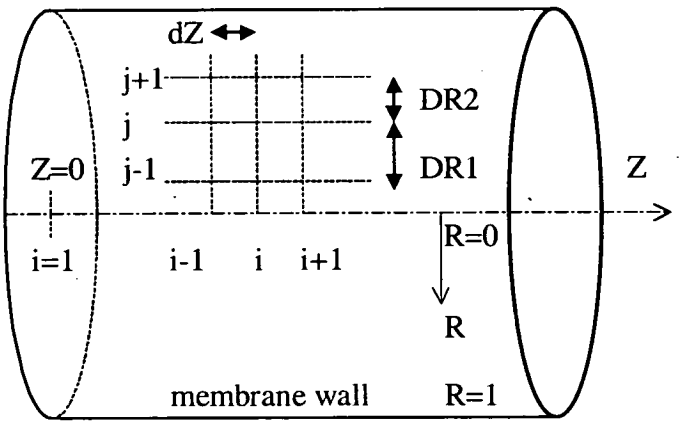

Fig. 2.2: Discretization.

The suitability of the choice for the grid (especially in the radial direction) was assessed checking the global mass balance on the solute at steady state:

Flow-rate of solute at inlet = Flow-rate of solute at outlet + Flow-rate of solute in permeate,

with the following values:

$$\text{Flow - rate of solute at inlet} = \sum_{j=1}^{n-1} \pi (R_{j+1} - R_j).(U_{1,j} C_{1,j} R_j + U_{1,j+1} C_{1,j+1} R_{j+1})$$

$$\text{Flow - rate of solute at outlet} = \sum_{j=1}^{n-1} \pi (R_{j+1} - R_j).(U_{m,j} C_{m,j} R_j + U_{m,j+1} C_{m,j+1} R_{j+1})$$

$$\text{Flow - rate of solute in permeate} = \sum_{i=1}^{m-1} \pi \times 1 \times (Z_{i+1} - Z_i).(C_{i,n-1} V_{i,n-1} + C_{i+1,n-1} V_{i+1,n-1}).$$

Using these notations for the discretization, Taylor's expansions for U, V and C and their first and second derivatives could be found. The equations from the previous section were then rewritten so that each of their terms was converted to an expression at least of the second order. We found results differing from those published by Ilias and Govind:

- after a discretisation scheme centered on (i, j-*1/2*), and then a few transformations, the continuity equation gave*

$$V_{i,j} = -\frac{1}{R_j} \sum_{k=2}^{j} \frac{(R_k - R_{k-1})(R_k + R_{k-1})}{4dZ} (U_{i,k} - U_{i-1,k} + U_{i,k-1} - U_{i-1,k-1}); \qquad \textbf{(2.9)}$$

* This result differs from that published by Ilias and Govind, which was

$$V_{i,j} = -\sum_{k=2}^{j} \frac{1}{R_k} \frac{(R_k - R_{k-1})(R_k + R_{k-1})}{4dZ} (U_{i,k} - U_{i-1,k} + U_{i,k-1} - U_{i-1,k-1});$$

- assuming the factors U and V in the left hand-side to remain constant enough from i-1 to i, and expressing all derivatives of U at i as functions of U_{i-1}, U_i and U_{i+1} (three point-centered difference scheme), the momentum transport equation gave**

$$A_j U_{i,j-1} + B_j U_{i,j} + D_j U_{i,j+1} = E_j \quad \text{for} \quad 2 \le j \le n-1,$$

with

$$A_j = \frac{-1}{(DR1+DR2).DR2}\left\{DR1.V_{i-1,j} + \frac{2}{Re_{0,wall}} - \frac{DR1}{R_j.Re_{0,wall}}\right\};$$

$$B_j = \frac{U_{i-1,j}}{dZ} + \frac{1}{DR1.DR2}\left\{(DR1-DR2).V_{i-1,j} + \frac{2}{Re_{0,wall}} - \frac{DR1-DR2}{R_j.Re_{0,wall}}\right\};$$

$$D_j = \frac{1}{(DR1+DR2).DR1}\left\{DR2.V_{i-1,j} - \frac{2}{Re_{0,wall}} - \frac{DR2}{R_j.Re_{0,wall}}\right\};$$

$$E_j = \frac{U_{i-1,j}^2}{dZ} - \frac{1}{2}\frac{dP}{dZ}.$$

(2.10)

Assuming that values of $U_{i-1,j}$ and $V_{i-1,j}$ are known for all j's, and that $U_{i,1}$ and $U_{i,n}$ are known, the above equation written for all j's in between 2 and n-1 allow us to find all $U_{i-1,j}$ for all j's, using an algorithm specific to tridiagonal matrixes.

** Again, these results differ from those published. Ilias and Govind found

$$A_j = \frac{-1}{(DR1+DR2).DR2}\left\{DR1.V_{i-1,j} - \frac{2}{Re_{0,wall}} - \frac{DR1}{R_j.Re_{0,wall}}\right\};$$

$$B_j = \frac{U_{i-1,j}}{dZ} + \frac{1}{(DR1+DR2).DR2}\left\{(DR1-DR2).V_{i-1,j} + \frac{2(DR1+DR2)}{DR1\cdot Re_{0,wall}} - \frac{DR1-DR2}{R_j.Re_{0,wall}}\right\};$$

$$D_j = \frac{-1}{(DR1+DR2).DR1}\left\{DR2.V_{i-1,j} - \frac{2}{Re_{0,wall}} - \frac{DR2}{R_j.Re_{0,wall}}\right\}.$$

- in an almost identical fashion, the solute transport equation may be written as:

$$F_j C_{i,j-1} + G_j C_{i,j} + H_j C_{i,j+1} = I_j \quad \text{for} \quad 2 \le j \le n-1,$$

with

$$F_j = \frac{-1}{(DR1+DR2).DR2}\left\{DR1.V_{i-1,j} + \frac{2}{Pe_{0,wall}} - \frac{DR1}{R_j.Pe_{0,wall}}\right\};$$

$$G_j = \frac{U_{i-1,j}}{dZ} + \frac{1}{DR1.DR2}\left\{(DR1-DR2).V_{i-1,j} + \frac{2}{Pe_{0,wall}} - \frac{DR1-DR2}{R_j.Pe_{0,wall}}\right\};$$

$$H_j = \frac{1}{(DR1+DR2).DR1}\left\{DR2.V_{i-1,j} - \frac{2}{Pe_{0,wall}} - \frac{DR2}{R_j.Pe_{0,wall}}\right\};$$

$$I_j = U_{i-1,j}\frac{C_{i-1,j}}{dZ}.$$

(2.11)

The same method as for eq. (2.10) applies therefore here: all values at the line *i* are found knowing the values at the previous line by solving the system of equations from *j*=2 to *n*-1.

- the derivative boundary conditions at the wall and at the centre of the tube were written using respectively a three-point backward difference scheme and a three-point forward difference scheme:

$$C_{i,n} = \frac{(R_n - R_{n-2})^2 C_{i,n-1} - (R_n - R_{n-1})^2 C_{i,n-2}}{(R_{n-1} - R_{n-2})[2R_n - R_{n-1} - R_{n-2} - Pe_{0,wall}\sigma V_{i,n}(R_n - R_{n-1})(R_{n-1} - R_{n-2})]};$$

$$U_{i,1} = \frac{U_{i,2}(R_1 - R_3)^2 - U_{i,3}(R_1 - R_2)^2}{(R_2 - R_3)(2R_1 - R_2 - R_3)};$$

$$C_{i,1} = \frac{C_{i,2}(R_1 - R_3)^2 - C_{i,3}(R_1 - R_2)^2}{(R_2 - R_3)(2R_1 - R_2 - R_3)}.$$

(2.12 - 2.14)

2.2.2.7. Algorithm

-1) Assume all values for U, V, and C at i=1 (boundary conditions);

-2) i =2;

-3) Assume dP/dZ (Poiseuille equation), and therefore P at i =2;

Assume $C_{2,n}$, and C_g at i=2 different from $C_{2,n}$ (taking an arbitrary large value);

-4) Work out $V_{2,wall}$ using the membrane flux boundary condition; assume $V_{2,n} \neq V_{2,wall}$;

-5) While i <m+1:

{

-6) While $C_g \neq C_{i,n}$:

{

-7) While $V_{i,n} \neq V_{i,wall}$:

{

-8) Solve momentum transport equations (written for $2 \leq j \leq$ n-1) and find all $U_{i,j}$ at i ;

-9) Solve continuity equation to find all $V_{i,j}$ at i ;

-10) If $V_{i,j} > V_{i,wall}$, increase dP/dZ;

else if $V_{i,j} > V_{i,wall}$, decrease dP/dZ;

-11) Work out P_i ;

-12) Work out $V_{i,wall}$ using the membrane flux boundary condition;

}

-13) With the converged flow field, solve the solute transport equations (for $2 \leq j \leq$ n-1);

-14) Change the value of C_g to $(C_g + C_{i,n})/2$;

}

-15) i=i+1;

}

-16) Check the overall mass balance.

2.2.3. MODEL VALIDATION

Ilias and Govind's simulations with tubular membranes (diameter 12.5 cm) were reproduced and compared with the results published by these authors. Crossflow velocity varied between 0.35 and 0.95 m/s, concentration between 1 and 10 g/L, and pressure between 20000 and 100000 Pa. Intrinsic membrane resistances were given by inlet permeate fluxes (see figures below), and resistance to flux due to concentration polarisation was given by

$$r_{cp} = 2 \cdot 10^9 \cdot exp(0.17 \cdot c_g)$$

in which c_g is in g/L and r_{cp} in m^{-1} (Nakao *et al.*, 1979).

The graphs show that there was some discrepancy between the results obtained with the formula given in this section and the results given by Ilias and Govind. Checks were made difficult due to several factors: Firstly, when using the formulae published by the original authors, the programme would diverge. It may well be that the formulae published were not correct - for instance, one may expect the factors B_j in equation (2.10) to be symmetrical with respect to *DR1* and *DR2*, since (2.10) is obtained from a three-point centered scheme, but this was not the case in their paper. (The same remark applies for G_j in equation (2.11)). Another problem was that the values for the membrane intrinsic resistance were omitted, and had to be estimated from near-inlet fluxes ($z=10^{-7}$ m) in published graphs. Finally, no indication was given about the grid used, and no mention of mass-balance consistency check made in the method section.

Perhaps due to any of these factors, the permeate fluxes found in this study were consistently lower that those published, and this was related to higher wall concentrations (typically twice higher than that published).

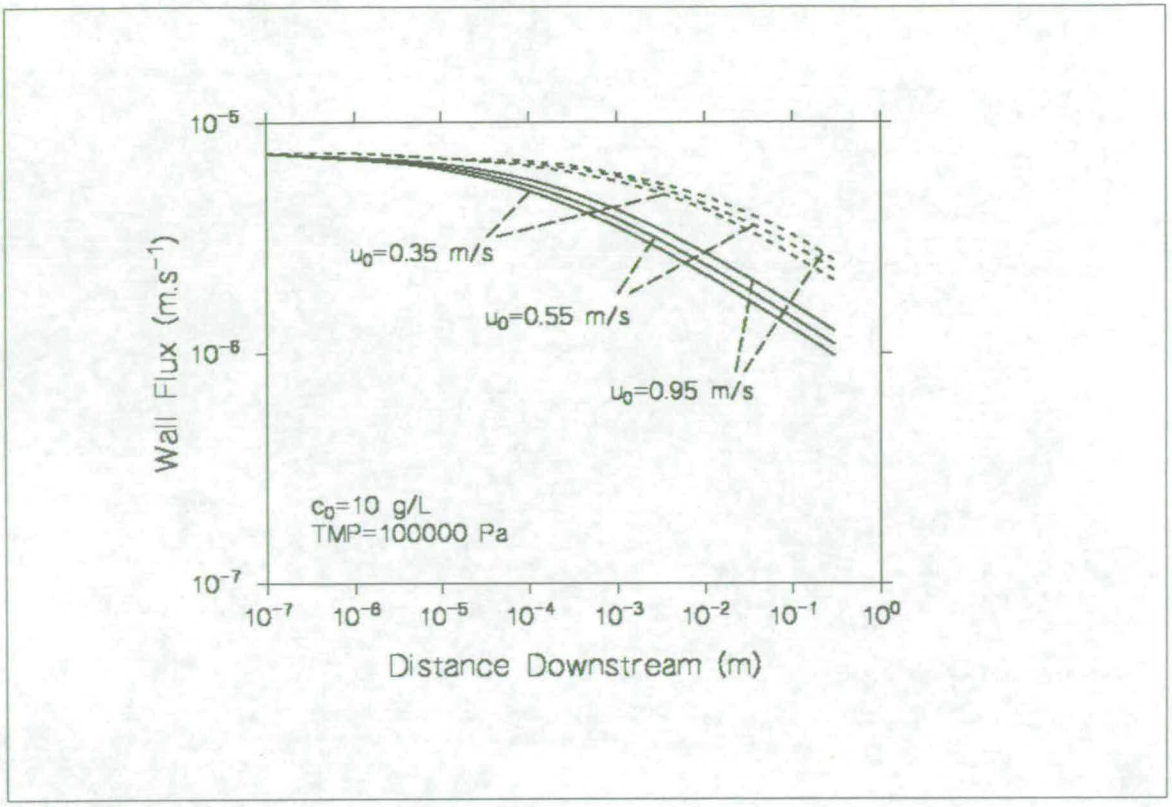

Fig. 2.3 a)

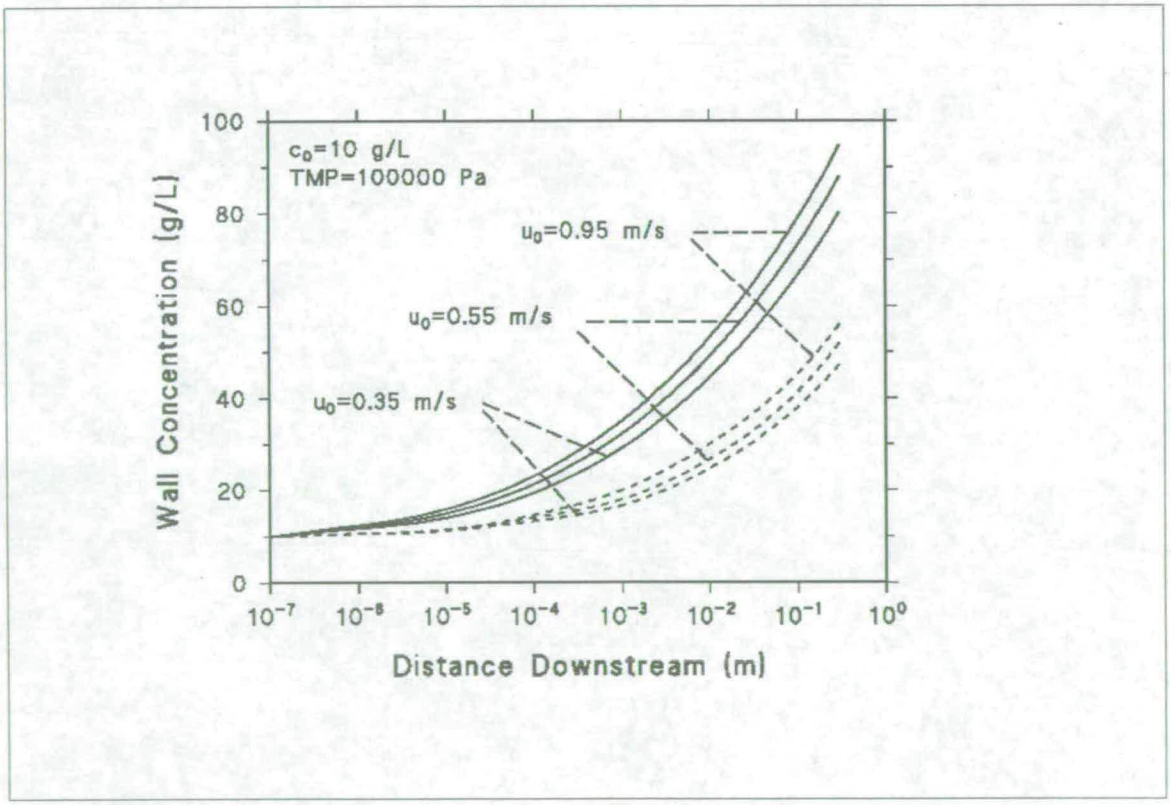

Fig. 2.3 b)

Fig. 2.3: *Crossflow filtration of PVA 224 on T4/A membranes: influence of the crossflow velocity on* ***a):*** *permeate flux, and* ***b):*** *wall concentration.*

- - - -: Ilias and Govind's simulations; —— : simulations obtained from this Ph.D. work.

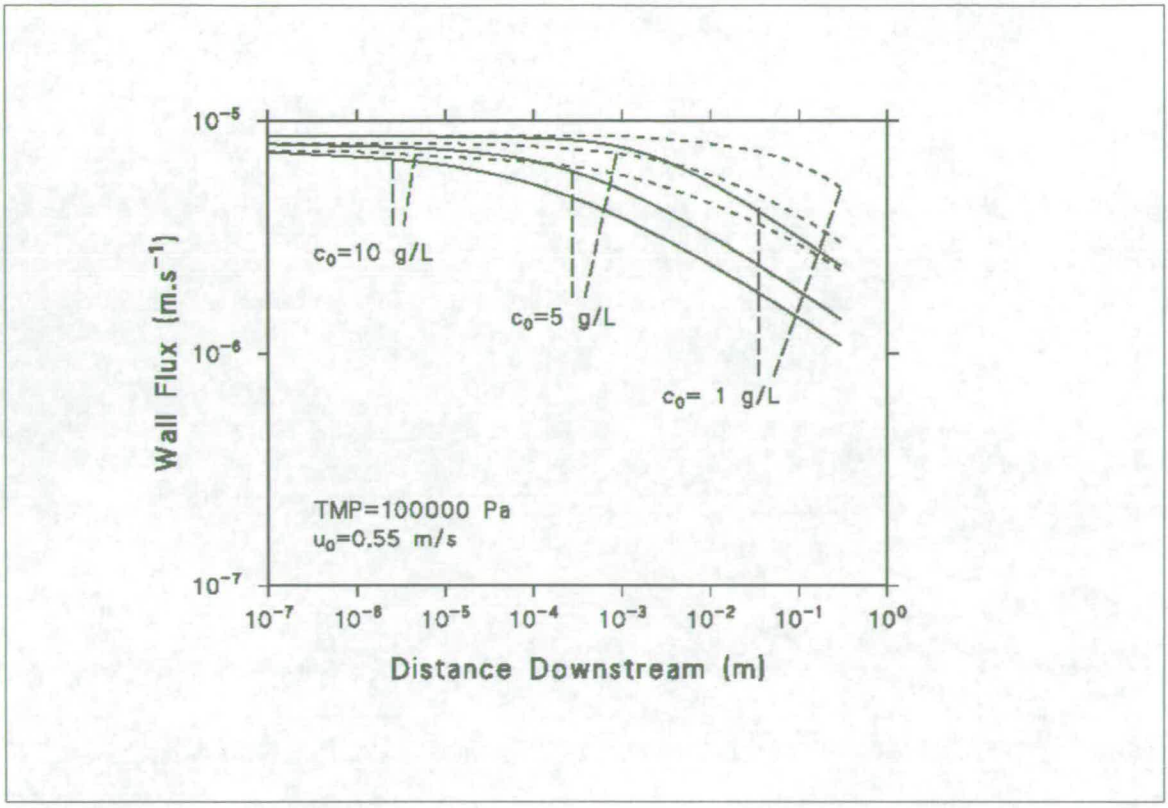

Fig. 2.4 a)

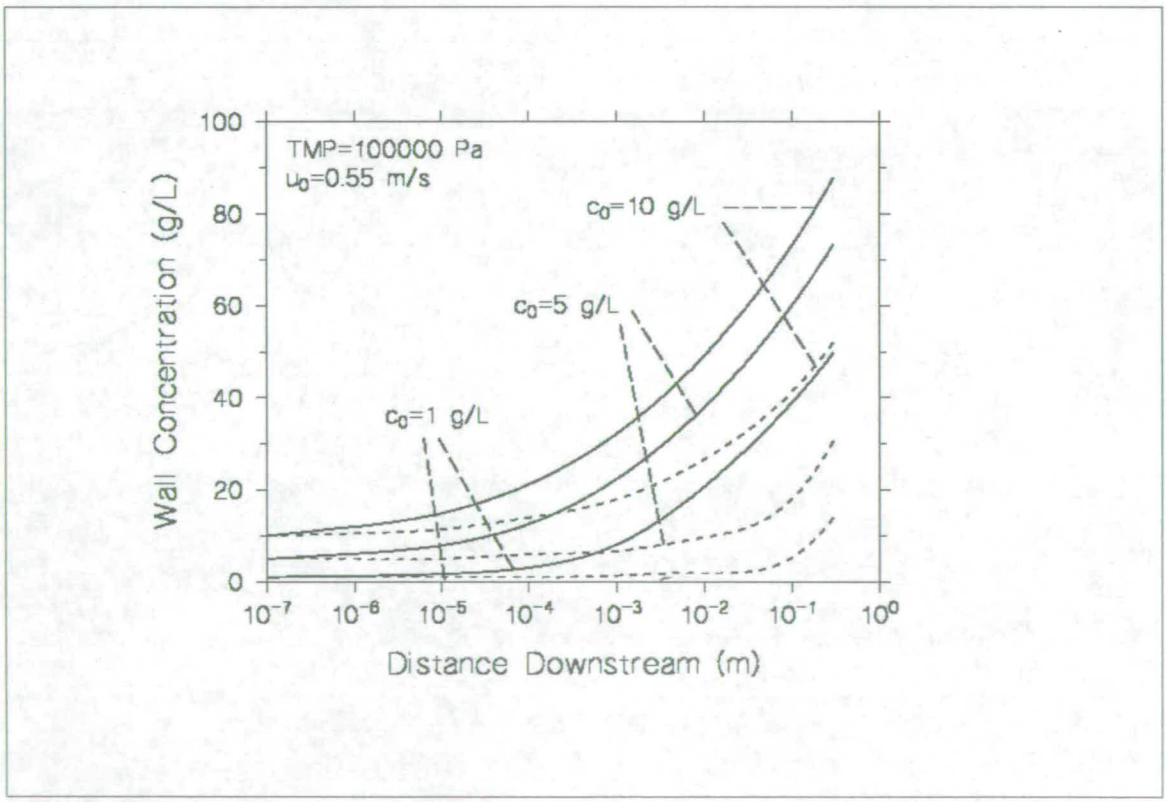

Fig. 2.4 b)

Fig. 2.4: *Crossflow filtration of PVA 224 on T4/A membranes: influence of the inlet concentration on* ***a):*** *permeate flux, and* ***b):*** *wall concentration.*

- - - -: Ilias and Govind's simulations; —— : simulations obtained from this Ph.D. work.

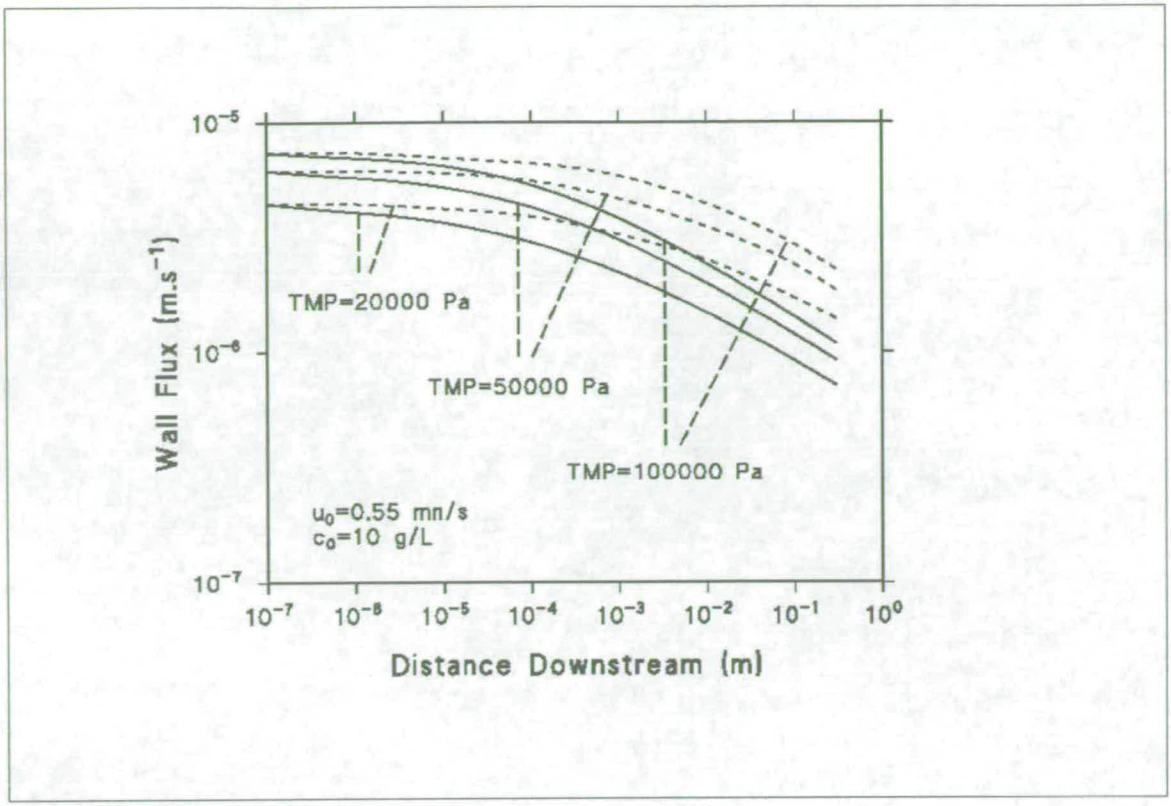

Fig. 2.5 a)

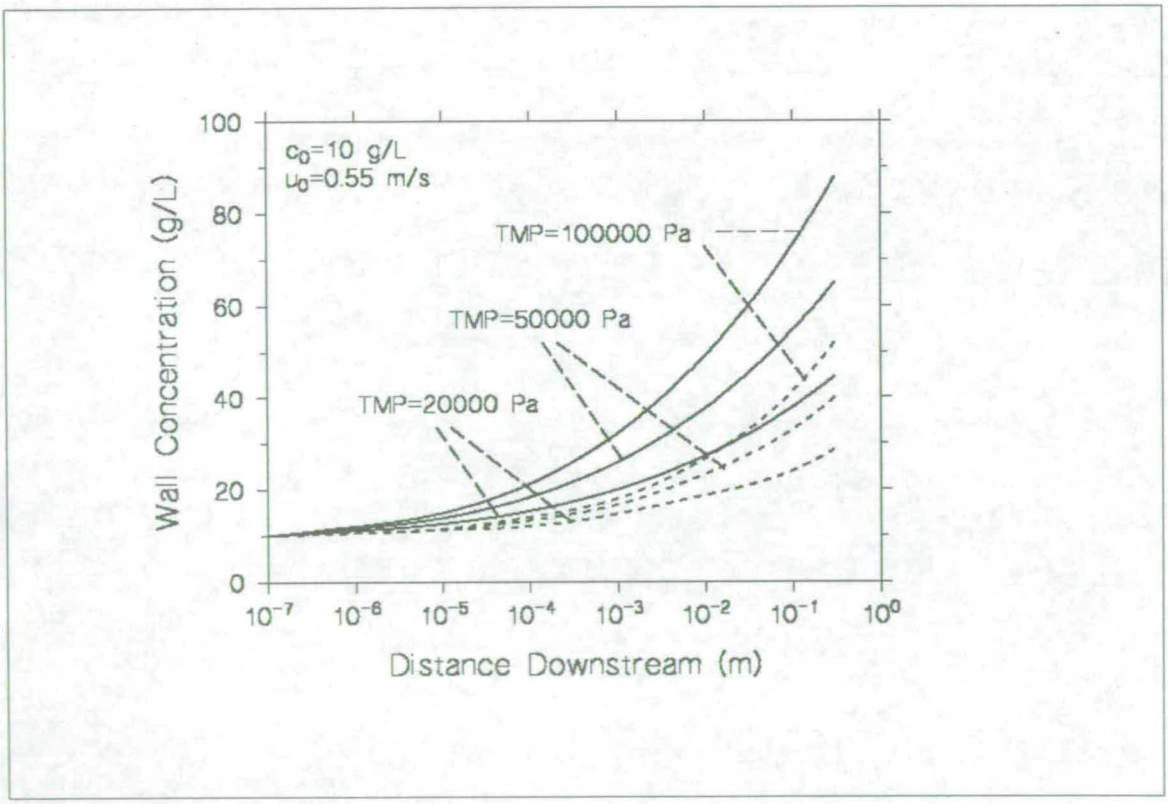

Fig. 2.5 b)

Fig. 2.5: *Crossflow filtration of PVA 224 on T4/A membranes: influence of the transmembrane pressure (TMP) on* ***a):*** *permeate flux, and* ***b):*** *wall concentration.*

- - - -: Ilias and Govind's simulations; —— : simulations obtained from this Ph.D. work.

2.3. SURFACE FOULING IN DEAD-END MODE

2.3.1. BOWEN AND JENNER'S MODEL (1995)

This model was chosen for three reasons:

-Bowen and Jenner found it to predict accurately enough the results of Dead-End filtration with total rejection in two cases: first, with silica suspensions, then with BSA solutions.

-It takes into account a number of parameters: concentrations, compressibility of the cake, pH (through zeta potential), ionic strength, London-Van der Waals forces, electroviscous effects, etc.; as far as we know, it is the only model to do so.

-It requires very little empirical data specific to the system: provided that the appropriate physical data on the different species in solution are available, there is no need to obtain system-dependant parameters, such as a gel concentration or a specific cake resistance.

2.3.2. PRINCIPLE

This model relies on the knowledge of interparticle interactions, and how they balance the pressure at any point within a filtration cake. This allows calculating local cake voidages at a time t knowing flow rates and pressures at that time. A suitable filtration law gives then the permeate flux z and the total permeate volume collected V as a function of time and cake properties, which enables us to find flow rates and pressures at a time $t+dt$.

2.3.3. FORCES and PRESSURES

The physics of charged colloidal interactions helps understand how a cake forms during filtration of protein solutions.

2.3.3.1. DLVO theory

The widely used Derjaguin-Landau-Verwey-Overbeek (DLVO) theory describes colloidal interaction by assuming the colloid particles exert onto each other at least two kinds of forces of opposite effects: a repulsive force, which is usually electrostatic, and an attractive force, usually of the London-Van der Waals type. Subsequent development of the theory included other additional forces, such as steric forces, hydration or hydrophobic forces.

One of the weaknesses of the theory is that it fails to describe the behaviour of a concentrated dispersion. First, it considers only pairwise interactions of particles, whereas at high concentrations each particle is under the simultaneous influence of several of its neighbours. In addition, the bulk of the solution is considered to act as a constant concentration sink: it supplies or absorbs the electrolyte ions that are concentrated or depleted around the charged particles. Again, such a bulk area does not exist at high concentration.

2.3.3.2. Wigner-Seitz cell approach

For those reasons, Bowen and Jenner applied a more accurate approach. They considered a Wigner-Seitz cell approach to describe the interparticle interactions within a filter cake: by perpendicularly bisecting the lines to the nearest neighbours of an atom, they divide the cake into regular polyhedra centred on each particle. Each polyhedron was then approximated by a sphere of equal volume, and of radius r_{cell}. By describing the cake as locally being a regular lattice, this simplification allows to take into account the influence of

all closest neighbours onto every particle. If a **hexagonal close-packed configuration** is chosen (*Fig. 2.6*), the cell radius r_{cell} is

$$r_{cell} = (2a + D_{ip})\left(\frac{3}{4\pi\sqrt{2}}\right)^{1/3}, \qquad \textbf{(2.15)}$$

where D_{ip} is the interparticle distance and a the particle radius.

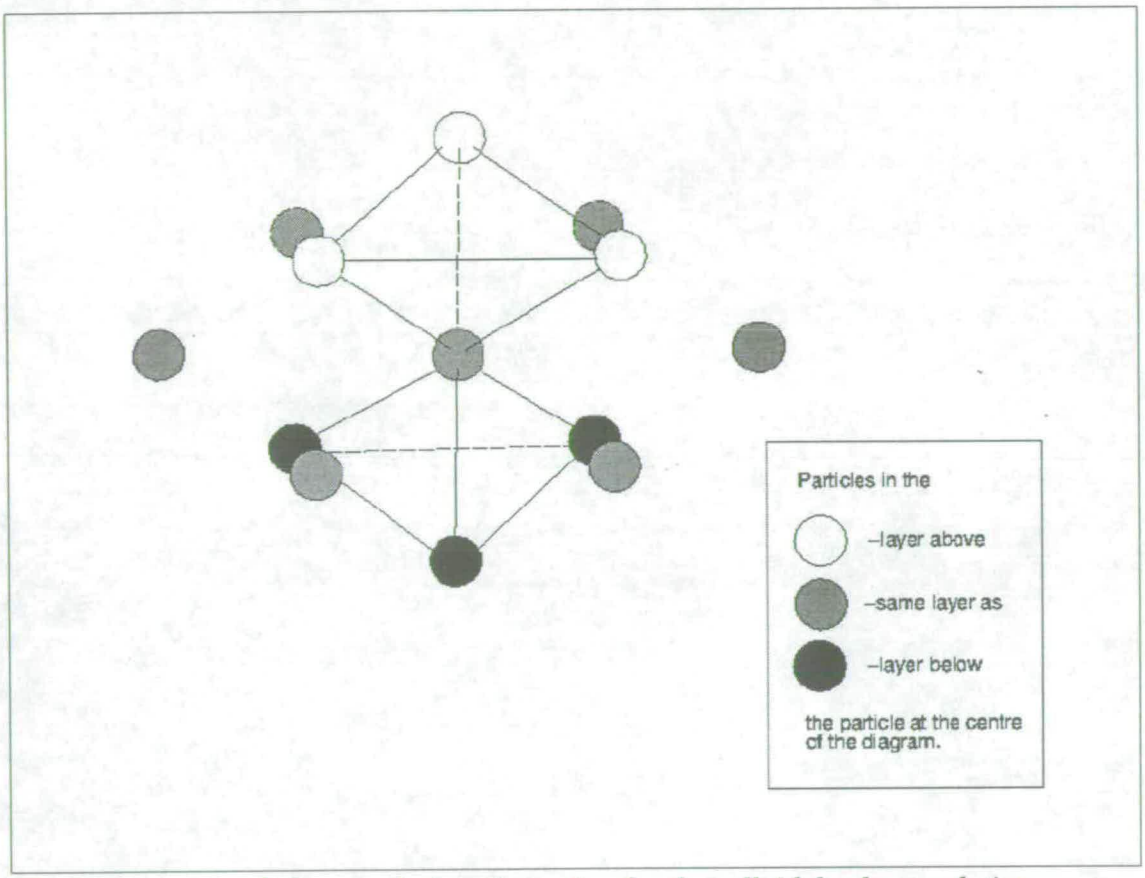

Fig. 2.6: *Hexagonal close-packed configuration for the colloidal cake or solution.*

2.3.3.3. Electrostatic (repulsion) force

a) The electrical double layer and the zeta potential (*Fig 2.7*):

When a charged macromolecule or particle of radius a is in an aqueous solution, charges are likely to appear on its surface: this can be for various reasons, like some local dissociation reactions or some dipoles adsorbing onto the surface. As a result, a tightly bound charged layer is covering the surface. It has the effect of attracting nearby electrolyte ions of the opposite sign. The solution around the particle becomes electrically charged, and a so-called "diffuse layer" is formed. This "double layer" model has been suggested first in 1879 by Helmholtz.

At the plane separating the fixed charged layer and the diffuse charge layer is defined the zeta potential ζ, which is always used to describe the electrical state of the particles in the dispersion. In the Gouy-Chapman model, ions are treated as point charges, whether at the surface or in solution. However, to account for their actual finite size, the depth of the tightly bound-charged layer needs to be known. This limit is known as the Outer Helmholtz Plane (OHP) when taken as between one ion and one hydrated ion diameter from the surface. This position is considered to be coincident with the surface at which zeta potentials are measured.

In the case of sodium, Israelachvili estimated this distance d to be

$$d = 0.55 \text{ nm}.$$

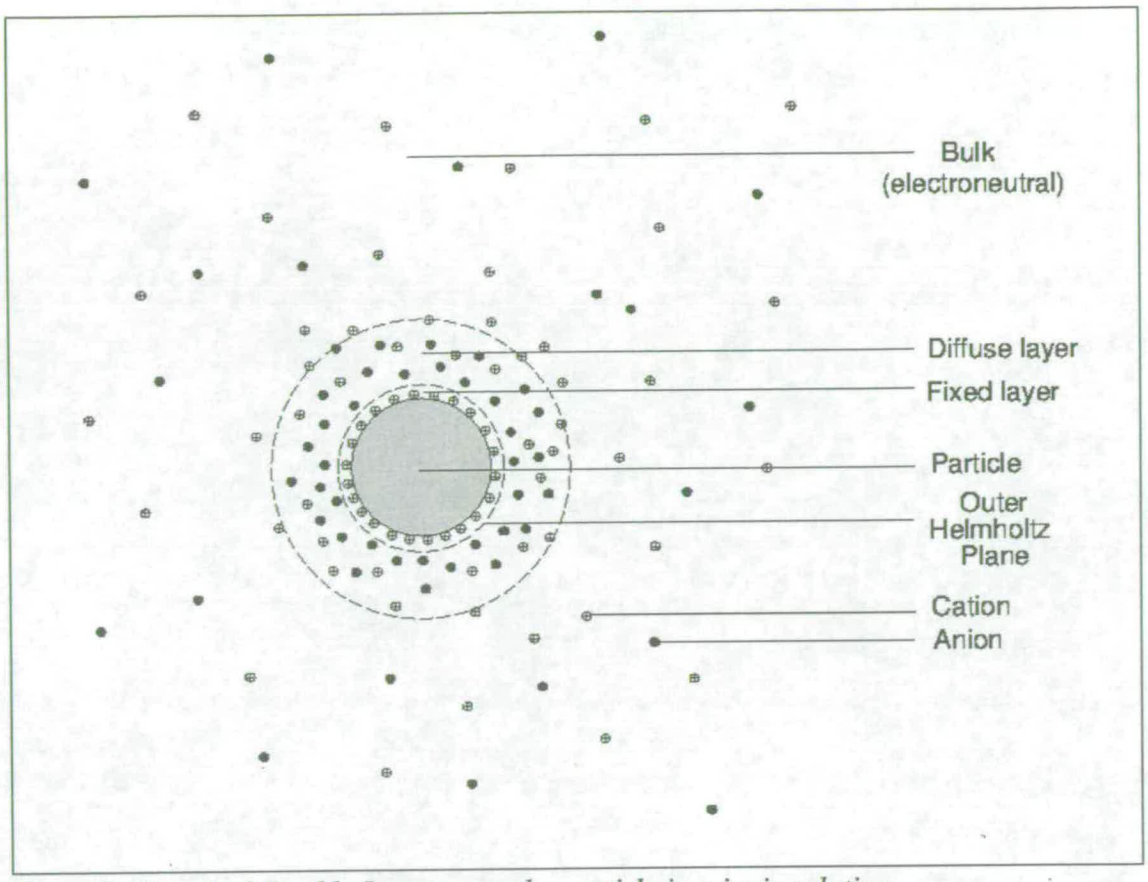

Fig. 2.7: *Electrical Double Layer around a particle in a ionic solution.*

b) The Poisson-Boltzmann Equation (P.B.E.):

If applying Poisson's equation to a Boltzmann distribution of electrolytes around a charged particle in spherical co-ordinates, one obtains the non-linear Poisson-Boltzmann Equation:

$$\frac{d^2\psi}{dr^2} + \frac{2}{r}\frac{d\psi}{dr} = \frac{2n^0 ze}{\varepsilon_0 \varepsilon_r} \sinh\left(\frac{ze\psi}{kT}\right), \qquad \textbf{(2.16)}$$

in which ψ is the electrical potential (V),

r the radius from the particle center (m),

n^0 the bulk ion number concentration (m^{-3}),

z the valence number,

e the elementary charge (1.6×10^{-19} C),

ε_0 the permittivity of vacuum (8.854×10^{-12} $C.V^{-1}.m^{-1}$),

ε_r the relative permittivity of the buffer,

k the Boltzmann constant (1.38×10^{-23} J.K^{-1}),

T the absolute temperature (K).

With the following changes to dimensionless variables,

$$\Psi = \frac{ez\psi}{kT},$$
$$\kappa = \left(\frac{2e^2 z^2 N_A I}{\varepsilon_0 \varepsilon_r kT} \right)^{\frac{1}{2}}, \qquad \textbf{(2.17 - 2.19)}$$
$$R = \kappa r,$$

in which I is the ionic strength I and N_A the Avogadro's number, the P.B.E. is normalised to

$$\frac{d^2\Psi}{dR^2} + \frac{2}{R}\frac{d\Psi}{dR} = \sinh \Psi . \qquad \textbf{(2.20)}$$

c) Boundary conditions:

The P.B.E. must be solved between the distances from the particle center $a+d$ and r_{cell}, as defined in sections 2.3.3.2. and 2.3.3.3 a). In dimensionless terms, these boundaries become

$$\alpha = \kappa(a+d)$$
and **(2.21 and 2.22)**
$$\beta = \kappa r_{cell} .$$

The following boundary conditions then apply:

$$\Psi_{|R=\alpha} = \xi = \frac{ze\zeta}{kT}$$
and **(2.23 and 2.24)**
$$\left.\frac{d\Psi}{dR}\right|_{R=\beta} = 0.$$

The first condition simply expresses the zeta potential at the OHP, whereas the second one is a consequence of Gauss' theorem applied to an electro-neutral cell, or of the symmetry of the system.

d) Solving the Poisson-Boltzmann Equation (P.B.E.):

Using a numerical method to find the potential profile, a first problem is to avoid excessive precision errors due to the fast-growing exponential right hand side: Bowen and Jenner introduced the following change in variable (suggested by Strauss *et al.*, 1987) to overcome this difficulty:

$$\Psi = 4.\operatorname{arctanh}[M(R)]. \qquad \textbf{(2.25)}$$

The P.B.E. can then be rewritten as

$$\frac{d^2M}{dR^2} + \frac{2}{R}\frac{dM}{dR} + \frac{2M}{1-M^2}\left(\frac{dM}{dR}\right)^2 = \frac{M(1+M^2)}{1-M^2}. \qquad \textbf{(2.26)}$$

Bowen and Jenner used the following trial and error method, which we present below as a simplified algorithm:

-1) A starting value for M at β is obtained from the Debye-Hückel approximation for the potential; this simplified equation gives us

$$\Psi(\beta) = \frac{A}{\beta}e^{\beta-\alpha} + \frac{\xi\alpha - A}{\beta}e^{-(\beta-\alpha)} \qquad \textbf{(2.27)}$$

with

$$A = \frac{\xi\alpha\, e^{-2(\beta-\alpha)}}{\frac{\beta-1}{\beta+1} + e^{-2(\beta-\alpha)}}.$$

-2) We are therefore starting knowing a trial value M_β, and the value $M'_\beta = (dM/dR)_\beta = 0$, from the second boundary conditions. The starting position is $R=\beta$.

-3) While $R>\alpha$:

The distance from α to β is subdivised into a number of segments. If the current position is labelled i, then the next position as we move towards α is labelled i-1.

-4) Knowing the step value Δ_i from i to i-1, we write M_{i-1} as a third order Taylor's expansion and the derivative $M'_{i-1} = (dM/dR)_{i-1}$ as a second order Taylor's expansion:

$$M_{i-1} = M_i - M'_i \Delta_i + \frac{M''_i}{2}\Delta_i^2 - \frac{M'''_i}{6}\Delta_i^3;$$

$$M'_{i-1} = M'_i - M''_i \Delta_i + \frac{M'''_i}{2}\Delta_i^2;$$

M_i'' is given by the P.B.E. as a function of M_i' and M_i, which are known;

M_i''' is similarly obtained using the derivative of the P.B.E.

Therefore, M_i' and M_i can be calculated.

-5) Calculation of the fourth derivative of M by taking the second derivative of the P.B.E. allows to estimate the truncation error, and hence to increase or decrease the step Δ_i accordingly: return to -3) if required (with the same i).

-6) The current position i is decreased by one unit, and the new R_i is calculated using the previous value for Δ_i. If R_i is smaller than α, then Δ_i is corrected so that $R_i = \alpha$, and kept constant whatever the truncation error in 5). Return to -3).

-7) When $R = \alpha$ has been reached, the value found for M_α is compared with $M_\xi = \tanh(\xi/4)$.

If $M_\alpha \neq M_\xi$:

-8) Another starting value for M_β has to be interpolated and tried. If $M_\beta{}^k$ refers to the kth attempt for a correct value of M_β, then the following linear interpolation formula is used:

$$M_\beta^{k+1} = \frac{M_\beta^k (M_\alpha^{k-1} - M_\xi) - M_\beta^{k-1}(M_\alpha^k - M_\xi)}{M_\alpha^{k-1} - M_\alpha^k}.$$

When k=0 (i.e. after the first attempt), the two previous profiles used for the interpolation are the Debye-Huckel approximation (see -1)) and the zero-potential profile (M=0 at all positions).

-9) Return to -2).

If $M_\alpha = M_\xi$:

-10) The correct potential profile has been found, and we leave the programme.

e) Calculation of the electrical repulsion force:

We used here the assumption of a close-packed hexagonal geometry. From equating the derivative of the configurational free energy with the sum of the electrical forces exerted onto a particle by its 12 closest neighbour, the following expression for the repulsive force between **two** particles is:

$$f(D) = \frac{4\pi r_{cell}^2}{3} n^0 kT \left(\cosh \frac{ze\psi_{|r=r_{cell}}}{kT} - 1 \right) \qquad \textbf{(2.28)}$$

2.3.3.4. London-Van der Waals (attraction) forces

In a first approximation, these weak attractive forces are inversely proportional to the cube of the distance to a point-charge. The electrical force, on the other hand, is inversely proportional only to the square of the distance. This means that the attractive forces will be dominant at very short distances from the charged surfaces, but will decrease very quickly when the distance increases, leaving the dominant influence to the electrical force.

The exact expression of the London-Van der Waals force is complex, and its derivation requires a knowledge of physics much above the scope of this work. We therefore assumed the following formulae as accurate enough for our purposes.

The starting point is Hamacker's formula for the total attractive interaction energy between two spheres:

$$V_A(D_{ip}) = -\frac{A_H}{6}\left[\frac{2a^2}{D_{ip}^2 + 4aD_{ip}} + \frac{2a^2}{(D_{ip}+2a)^2} + \ln\left(1 - \frac{4a^2}{(D_{ip}+2a)^2}\right)\right], \qquad \textbf{(2.29)}$$

in which A_H is the Hamacker constant, a the particle radius, D_{ip} the inter-particle distance, and V_A the potential energy.

However, this is only a simplified approach, for at least three phenomena contribute to alter the value of A_H with the distance D_{ip}, and the ionic strength I:

-The formula given above does not take into account the presence of several other particles surrounding the pair: these other particles affect the internal repartition of charges within the particles of the pair, hence the London-Van der Waals force too.

-Transmission of electromagnetic waves is not instantaneous, and since the internal changes in molecules occur very rapidly, this affects the intensity of the London-Van der Waals force. This so-called phenomenon of retardation leads to the Hamacker constant decreasing with the interparticle distance D_{ip}.

-The presence of electrolytes in solution "screens" electromagnetic interactions, including the London-Van der Waals force: this introduces in the formula to calculate A_H the Debye parameter κ, which is a function of the ionic strength I (see section 2.3.3.3 b)).

Accounting for these three effects, and adapted from results found for flat plates, the Lifshitz-Hamacker "constant" becomes then:

$$A_H(\kappa, D_{ip}) = A_{\xi 0}(1 + 2\kappa D_{ip})e^{-2\kappa D_{ip}} + A_{\xi \geq 1}F(H), \qquad \textbf{(2.30)}$$

in which

$$A_{\xi 0} = \frac{3}{4} kT \left[\frac{\varepsilon_{r1}(0) - \varepsilon_{r3}(0)}{\varepsilon_{r1}(0) + \varepsilon_{r3}(0)} \right]^2$$

$$A_{\xi \geq 1} = \frac{3\hbar\sqrt{\omega_1 \omega_3}}{64\overline{n}_0^{7/4}} \times \frac{X^2 \overline{n}_0 + 2X\Delta n_0 \sqrt{\overline{n}_0} + \Delta n_0^2 (3 + 2Y)}{[(Y - \sqrt{Y^2 - 1})^{1/2} + (Y + \sqrt{Y^2 - 1})^{1/2}]^3}$$

$$\overline{n}_0 = \frac{n_{0_1} + n_{0_3}}{2}$$

$$\Delta n_0 = n_{0_1}^2 - n_{0_3}^2$$

$$X = \frac{\omega_1}{\omega_3}(n_{0_1} - 1) - \frac{\omega_3}{\omega_1}(n_{0_3} - 1)$$

$$Y = \frac{1}{4\sqrt{\overline{n}_0}} \left[\frac{\omega_1}{\omega_3}(n_{0_1} + 1) + \frac{\omega_3}{\omega_1}(n_{0_3} + 1) \right]$$

$$F(H) = \left[1 + \left(\frac{\pi H}{4\sqrt{2}} \right)^{3/2} \right]^{-2/3}$$

$$H = n_{0_3} \sqrt{(n_{0_1}^2 - n_{0_3}^2)} \frac{D_{ip} \sqrt{\omega_1 \omega_3}}{c}.$$

Subscripts 1 and 3 refer respectively to the protein and to the solvent (pure water). ε_i refers here to the dielectric constant for the compound *i*. The constants n_i and ω_i are respectively the refraction index and the characteristic frequency of electromagnetic radiation for the substance *i*. These data are obtained from examining the refractive index of a protein solution (n_2) over a range of electromagnetic wavelengths.

The resulting attractive force is therefore

$$F_A = -\frac{1}{6}\left\{\left[A_{\xi 0}\,4\kappa^2 D e^{-2\kappa D} + A_{\xi\geq 1}\left(1+\left(\frac{\pi H}{4\sqrt{2}}\right)^{3/2}\right)^{-5/3} \times\left(\frac{\pi}{4\sqrt{2}} n_{0_3}\sqrt{n_{0_1}^2 - n_{0_3}^2}\,\frac{\sqrt{\omega_1\omega_3}}{c}\right)^{3/2}\sqrt{D}\right]\right.$$

$$\times\left[\frac{2a^2}{D^2+4aD} + \frac{2a^2}{(D+2a)^2} + \ln\left(1-\frac{4a^2}{(D+2a)^2}\right)\right]$$

$$+\left[A_{\xi 0}(1+2\kappa D)e^{-2\kappa D} + A_{\xi\geq 1}F(H)\right]$$

$$\left.\times\left[2a^2\left(\frac{2D+4a}{(D^2+4aD)^2} + \frac{2}{(D+2a)^3} - \frac{4}{(D+2a)^3 - 4a^2 D - 8a^3}\right)\right]\right\}$$

(2.31)

2.3.3.5. Non-DLVO forces

In some colloidal systems (e.g. silica), additional short-range repulsive forces F_{hyd} are sometimes present. Not much is known about these forces, usually attributed to hydration of the surfaces, and they were simply ignored in this research work.

2.3.3.6. Entropic pressure

A purely thermodynamical term, it increases when the degree of freedom of the particles decreases, i.e. when they get closer together.

Bowen and Jenner mentioned three formulae for the osmotic pressure, as a function of the particle volume fraction ϕ: one of them applies to disordered phase ($\phi < 0.5$), another one for the ordered phase ($\phi > 0.55$), and the continuous expression derived by Hall, which covers both regions:

$$\Pi_e = \left(\frac{3\phi}{4\pi a^3}\right) kT \frac{(1+\phi+\phi^2-0.67825\phi^3-\phi^4-0.5\phi^5-X\phi^6)}{(1-3\phi+3\phi^2-1.04305\phi^3)} \qquad \textbf{(2.32)}$$

with

$$X = 6.028e^{Y(7.9-3.9Y)}$$

$$Y = \frac{\pi\sqrt{2}}{6} - \phi.$$

2.3.3.7. Disjoining pressure

The effect of the forces listed in the previous sections are taken into account by calculating the total force F_D per unit area perpendicular to the cake (*Fig. 2.8*), exerted onto a cake particle by the cake situated below it. If we insert an hypothetical plane between two contiguous layers of the cake, and estimate an effective area A_e by each particle at this plane, we obtain the disjoining pressure $P_D = F_D / A_e$. In a **hexagonal close-packed array**,

$$A_e = 2\sqrt{3}(a + D_{ip}/2)^2 \qquad \textbf{(2.33)}$$

and

$$P_D = \frac{\sqrt{6}}{A_e}[f(D_{ip}) + F_A(D_{ip}) + F_{hyd}(D_{ip})] + \Pi_e. \qquad \textbf{(2.34)}$$

P_D is in fact equivalent to the osmotic pressure, and was termed Π in our combined modelling (see section 2.4).

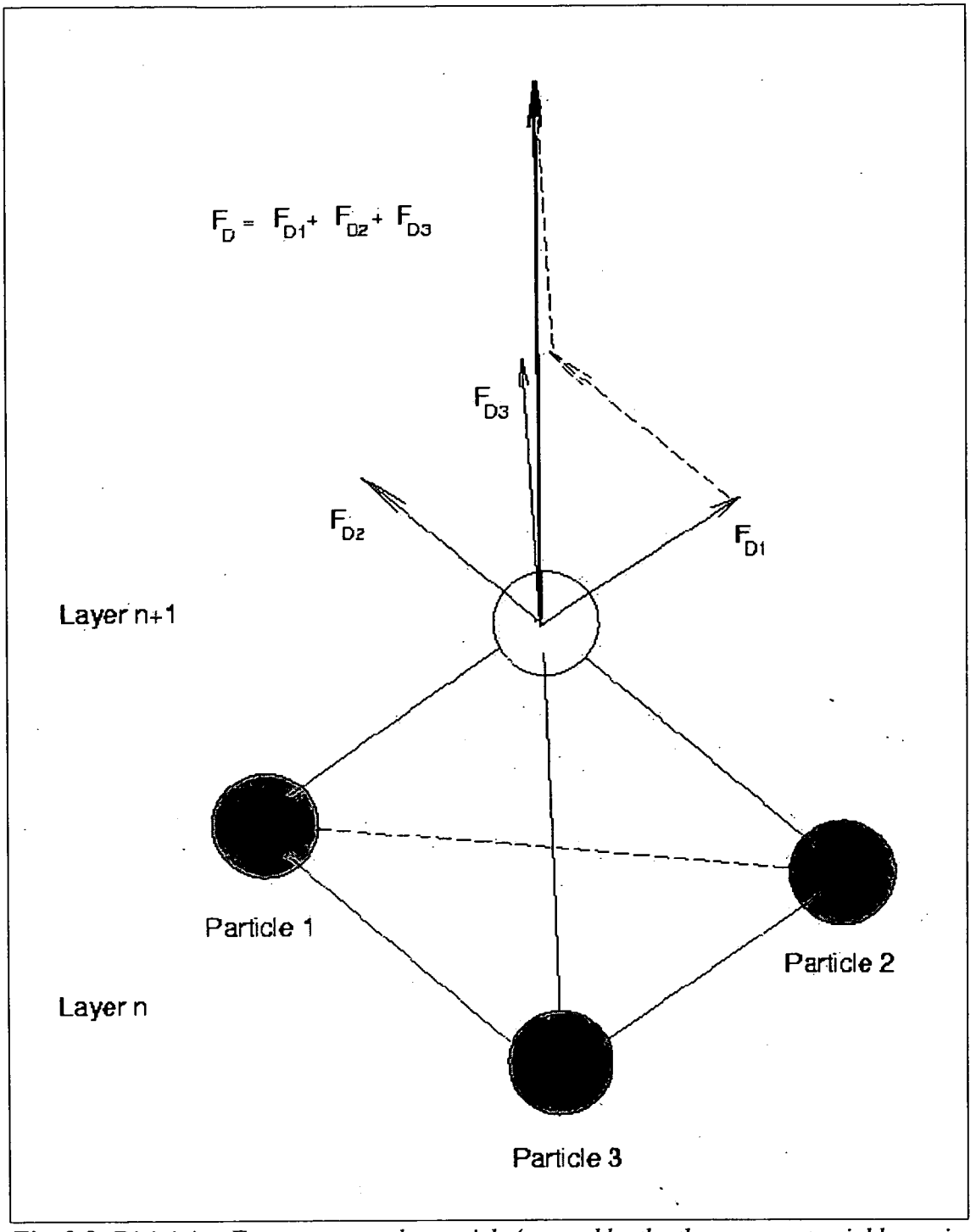

Fig. 2.8: *Disjoining Force onto a cake particle (exerted by the three nearest neighbours in the layer below).*

2.3.4. ELECTROVISCOUS EFFECTS

The flow of an electrolyte against a charged wall, e.g. against capillary walls or particle surfaces in a filter cake, creates a so-called "streaming potential": some ions are held back because of their charge. This causes the flow to be electrically charged: this streaming current causes in return a build-up of charges, and a backward counter-current of ions through the bulk of the liquid. These ions in this conduction current draw a backflow of liquid with them, a phenomenon which is called the "electro-osmotic effect". When a steady state is reached, the apparent viscosity of the fluid through the media is increased, and this phenomenon is referred to as "electroviscous effect".

The following formula was developed by Bowen and Jenner for capillaries:

$$\frac{\mu_a}{\mu} = \left[1 - \frac{8\varepsilon_0 \varepsilon_r \zeta^2}{\mu}(1-G)^2 \times \left(\frac{2\varepsilon_0 \varepsilon_r}{\mu} \int_0^{R_c} R(d\Psi / dR)^2 dR + \frac{ze}{kT} \int_0^{R_c} R(m_+ e^{-\Psi(R)} + m_- e^{\Psi(R)}) dR \right)^{-1} \right]^{-1}$$

(2.35)

with

$$G = \frac{2}{R_c^2 \zeta} \int_0^{R_c} R\Psi(R) dR$$

m_+ and m_- respectively refers to cation and anion electrophoretic mobility ;

R_c refers to the capillary radius;

All other notation is taken from previous sections.

The previous formula can be used for filter cakes made of spherical particles, by replacing R_c with an equivalent hydraulic radius $r_{c,hyd}$ (first introduced by Kozeny):

$$r_{c,hyd} = \frac{\varepsilon}{1-\varepsilon} \frac{a+d}{3} \qquad \textbf{(2.36)}$$

2.3.5. RELATING PRESSURE DROP ACROSS THE CAKE AND DISJOINING PRESSURE

In a plane (or quasi-plane) geometry, for any portion of the cake between the top and any distance y from the membrane surface, the following balance of pressures can be written

$$P_y + P_{D(y)} = P_l \qquad (2.37)$$

in which the layer is subjected not only to the hydraulic pressures P_y and P_l (operating filtration pressure), but as well to the disjoining pressures P_D from the particles below.

2.3.6. FILTRATION LAW FOR A COMPRESSIBLE CAKE

2.3.6.1. Assumptions

In this section, "compressible cake" refers to the particles in suspension as much as to the deposited cake they may form onto the membrane.

a) Geometry:

As already mentioned earlier on, it is assumed that the configuration of the cake is hexagonal close-packed.

b) At any instant t, the permeate flux $z=dV/dt$ is constant throughout the cake:

z is in fact independent of the distance to the cake-membrane interface provided that the amount of liquid gained by compression of the cake is negligible. We reckon this assumption should be checked after running the simulation programme, by using D'Arcy's law with local Happel permeability and pressure gradient (see section 2.3.6.2.).

c) Time stepping procedure:

Bowen and Jenner made this assumption when modelling cake build-up: from top to bottom, the pressure and permeability profiles within the cake do not change with time, apart from the cake thickening and becoming more compact at the bottom. All happens as if with every time-increment *dt*, an extra layer of cake was inserted between the cake and the membrane, lifting up the whole previous cake unchanged (see *Fig. 2.9*).

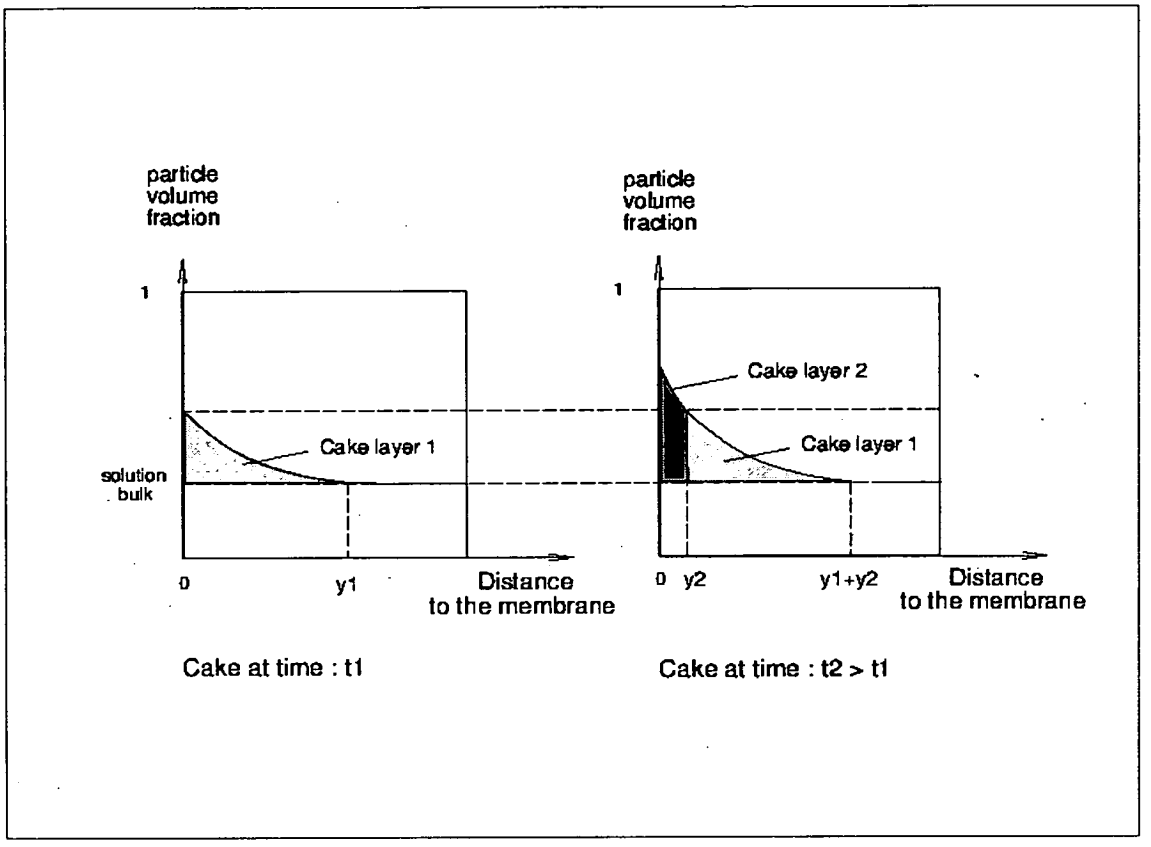

Fig. 2.9: *Time stepping procedure for cake build-up.*

In the derivations for obtaining a filtration equation, this property is used in the following way: Let us consider a quantity $X(y,t)$, which depends only on the pressure and cake voidage. The integration of this quantity over the volume of the cake is equal to the "flux" of X passing through the plane y during the growth of the cake through that plane. With the notations used in *Fig. 2.9*, we get

$$\left(\int_0^{y_2(t)} X(y,t)dy\right)\Bigg|_{t_2} = \int_{t_1}^{t_2}\left(X(y,t)\frac{dy}{dt}\right)\Bigg|_{y_2} dt\,. \qquad \textbf{(2.38)}$$

2.3.6.2. Derivation of the filtration law at the membrane-cake interface

Bowen and Jenner derived a filtration law giving the permeate flux as a function of time in a dead-end filtration with a compressible cake, at constant operating pressure (P_1).

-The starting point is D'Arcy's equation with Happel's expression for the local permeability:

$$\frac{1}{A_m}\frac{dV}{dt} = \frac{K_H}{\mu}\frac{dp_y}{dy} \qquad \textbf{(2.39)}$$

with

$$K_H = \frac{2a^2}{9(1-\varepsilon)} \times \frac{3 - 4.5(1-\varepsilon)^{1/3} + 4.5(1-\varepsilon)^{5/3} - 3(1-\varepsilon)^2}{3 + 2(1-\varepsilon)^{5/3}} \qquad \textbf{(2.40)}$$

in which

-$V(t)$ is the permeate volume collected at the filtration time t,

-A_m is the membrane surface area,

-μ is the solvent viscosity,

-y the distance to the membrane surface,

-$p_y(y, t)$ is the hydrodynamic pressure at y,

-$K_H(y, t)$ is the Happel permeability,

-$\varepsilon(y, t)$ is the cake voidage.

This equation is valid over the entire concentration range ($\varepsilon = 0.26$-1).

-Then, dy is expressed as a function of dV using the relationships for the mass of deposited colloid dm_p:

$$dm_p = c_b\, dV + c_b\,(1-\varepsilon) A_m dy \quad \text{(taking into account the colloid volume)}$$

and

$$dm_p = (1-\varepsilon)\rho_p A_m dy,$$

which gives

$$\frac{1}{A_m}\frac{dV}{dt} = \frac{K_H}{\mu} A_m (1-\varepsilon)(\rho_p / c_b - 1)\frac{dp_y}{dV}, \qquad \textbf{(2.41)}$$

-Then, use is made of equation (2.37) (i.e. P_D=P_1-P_y) and assumption 2.3.6.1. b) (*dV/dt* independent of *y*) to find, after integration throughout the cake (or the permeate volume) the following relationship:

$$V\frac{dV}{dt} = -A_m^2\left(\frac{\rho_p}{c_b} - 1\right) \times \int_{bottom}^{top\ of\ cake} \frac{(1-\varepsilon(P_D))K_H(P_D)}{\mu_a(P_D)} dP_D(y) \qquad \textbf{(2.42)}$$

-Using again Eq. (2.37) for the integral boundaries,

$$V\frac{dV}{dt} = -A_m^2\left(\frac{\rho_p}{c_b} - 1\right) \times \int_{P_1-P_2}^{0} \frac{(1-\varepsilon(P_y))K_H(P_y)}{\mu_a(P_y)} (-dP_y) \qquad \textbf{(2.43)}$$

in which P_1 is the (constant) operating pressure (retentate side), P_2 the (time-dependent) pressure at the membrane-cake interface. This equation may also be written

$$V\frac{dV}{dt} = -A_m^2\left(\frac{\rho_p}{c_b} - 1\right) \times \int_{y_1}^{0} \left\{\frac{(1-\varepsilon(y))K_H(y)}{\mu_a(y)} \cdot \frac{dP_y}{dy}\right\} \cdot (-dy), \qquad \textbf{(2.44)}$$

in which y_1 is the cake thickness.

-using then the time-stepping procedure (equation (2.38)) to change the variable from *dy* to *dt*, we get:

$$V\frac{dV}{dt} = -A_m^2\left(\frac{\rho_p}{c_b} - 1\right) \times \int_0^t \frac{(1-\varepsilon)K_H}{\mu_a}\frac{dP_y}{dt} dt \qquad \textbf{(2.45)}$$

Differentiation with respect to *t* and using the expression for the flux through the clean membrane eventually leads to the following set of equations:

$$\frac{dz}{dt} = -\frac{z^2}{V + A_m R_m \left(\frac{\rho_p}{c_b} - 1\right)(1-\varepsilon)\frac{\mu}{\mu_a} K_H};$$

$$\frac{dV}{dt} = z \quad \text{for all } y; \qquad \textbf{(2.46 - 2.48)}$$

$$P_2(t) = \frac{\mu R_m}{A_m} z + P_3 .$$

in which P_3 is the permeate-side pressure.

2.3.7. AN ALGORITHM FOR MODELLING DEAD-END FILTRATION

-1) Enter physical and system parameters;

Enter duration of the experiment: store in variable *duration*;

-2) Preliminary calculations:

-Find out and store values for the disjoining pressure over the range of cake voidages to be found during a run of the programme (i.e. from bulk concentration or less, to close-packed). This should enable us to find proper initialisation values when calculating actual values for the voidage from estimated disjoining pressures.

-Find out and store values for the corrected viscosity taking into account streaming current effects, over the range of cake voidages. This should enable us to interpolate in a quick and satisfactorily way the corrected viscosity for any voidage, without having to recalculate potential profiles inside the pores (the hydraulic diameter is different from the interparticle distance).

-3) Initialisation:

-t=0;

-Values for the pressures, permeate flux and voidage at t=0;

-Values for the disjoining pressure and the corrected viscosity;

-Value for the time increment *dt*;

-4) While $t < duration$:

-5) $t=t+dt$;

-6) While the permeate flux z has not converged yet, do the following steps:

-7) Calculate the Happel permeability K_H;

-8) Estimate a value for z at $t+dt$ using a Runge-Kutta method;

Return a relative truncature error too;

-9) Check that the truncature error is "not too big", e.g. below 10^{-4};

If it is larger, then:

-start from previous time: $t=t-dt$;

- halve dt;

-initialize voidages, flux and pressures with values at t;

-start again in 5).

Else:

-10) Work out the pressure P_2 at the bottom of the cake, from the relationship

$$z = (P_2 - P_3) / (\mu R_m)$$

in which P_3 is the permeate side pressure, μ the viscosity, and R_m the clean membrane resistance;

-11) Work out the disjoining pressure $P_D = P_1 - P_2$,

where P_1 is the retentate side pressure.

-12) Work out the corresponding cake voidage with a trial and error method; the results of step 2) are used here to get starting trial values;

-13) Work out the corrected viscosity from interpolation on results of step 2);

-14) Check that the truncation error is "not too small", e.g. above 10^{-6};

If it is smaller, then double dt;

-15) Check convergence for z;

-16) Return to -6);

-17) Repeat -4);

-18) Display results: cake voidage and permeate flux versus time.

2.3.8. MODEL VALIDATION

We attempted to reproduce some of the graphs presented by Bowen and Williams (1996) according to Bowen and Jenners' model. *Fig. 4.10 a)* presents the results for a dead-end filtration for various zeta potentials at I = 0.03M, and *Fig. 4.10 b)* for two ionic strengths (0.01M and 0.15M) at a zeta potential of -50 mV.

In *Fig. 4.10 a)*, results were very similar to the original for high values of ζ, but differing by about 40% for low ζ. For a collected volume (V) of 15 L and for ζ= -50mV, the t/V ratio was ca. 1.75 min/L, which was identical to that obtained by Bowen and Williams. However, for the same V and ζ= -2.5mV, t/V was found to be ca. 6.5 min/L instead of the 4.5 min/L found in Bowen and Williams' graph. *Fig. 4.10 b)* shows the influence of ionic strength (I) at ζ= -50mV: For a collected volume of 20 L and I = 0.01M, the t/V ratio of ca. 1.7 min/L was the same as that found on Bowen and Williams' graph. For the same V and I = 0.15M, however, the values for t/V were 30% too high (3.6 min/L was found, instead of the reported 2.7 min/L).

After careful checks on the formula and procedures used in the present work, no explanation could be found for those discrepancies: All that could be said was that the attraction force seemed to be slightly overestimated compared to Bowen and Williams' work, as apparent for low ζ values. However, the results obtained were deemed accurate enough for the purpose of this study.

Those preliminary runs confirmed that reductions in flux are more important when zeta potential decreases, and when ionic strength increases.

Fig. 4.10 a)

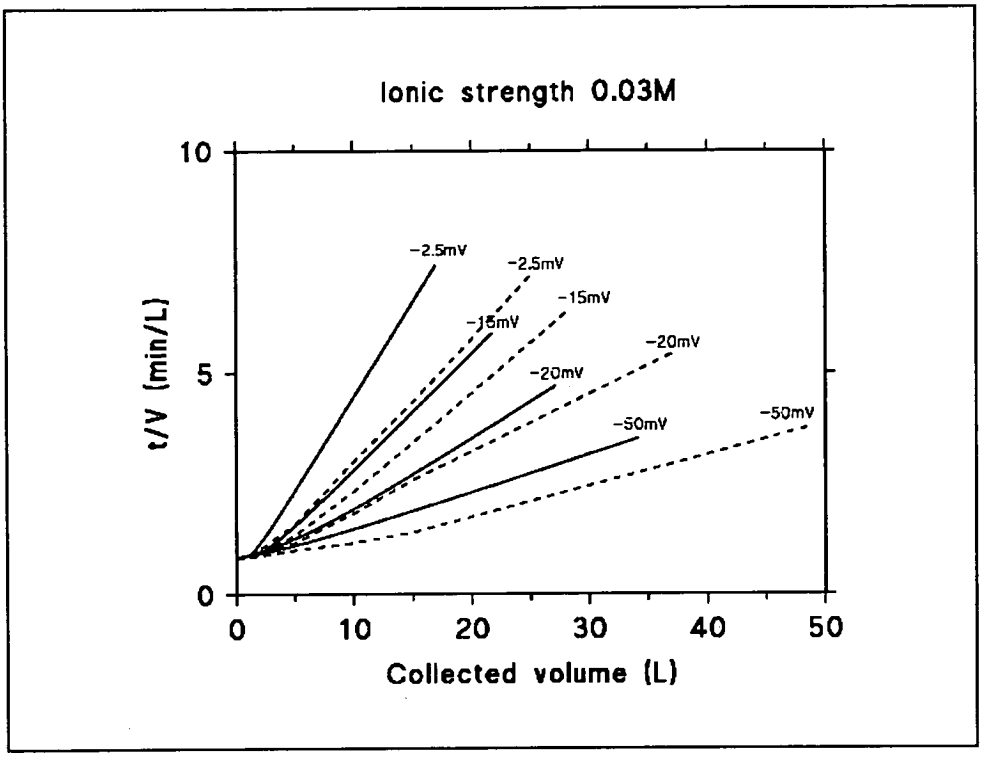

Fig. 4.10 b)

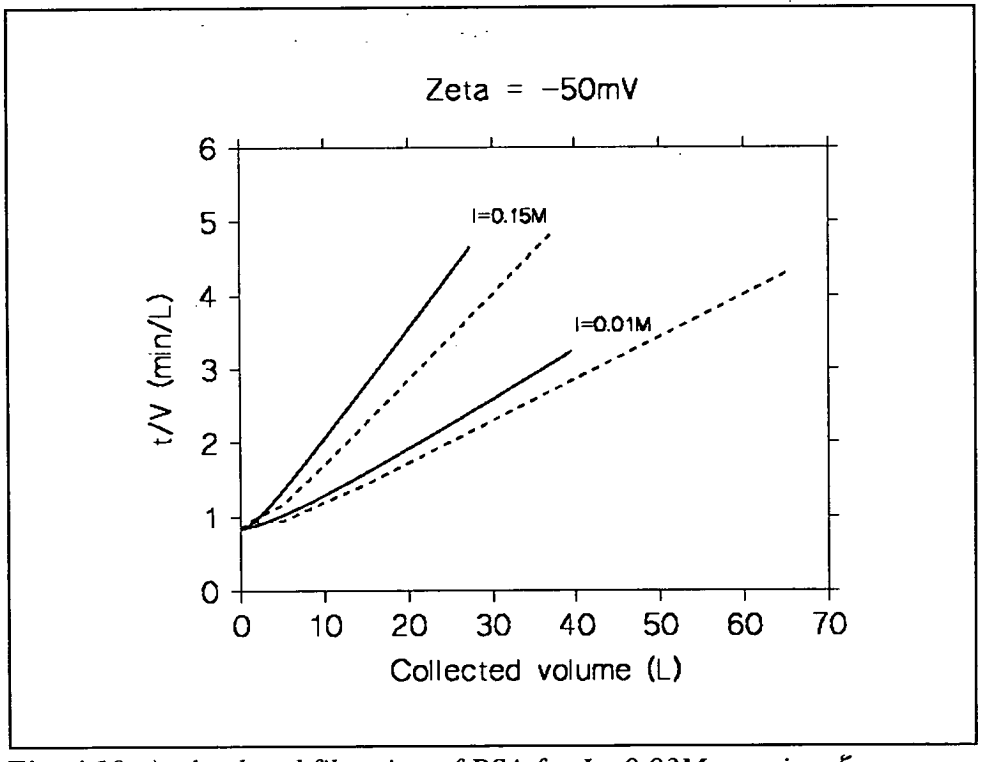

Fig. 4.10 a): *dead-end filtration of BSA for I= 0.03M, varying ζ;*
Fig. 4.10 b): *dead-end filtration of BSA for ζ = -50mV and varying I.*
Conditions for both figures: *TMP = 4 Bars, $R_m = 2 \cdot 10^{13}\ m^{-1}$, $A_m = 1\ m^2$, total rejection.* ***Key:*** ------- *Bowen and Williams's results;* —— *results from this PhD work.*

2.4. MODELLING CROSSFLOW OPERATION WITH CONCENTRATION POLARISATION AND FOULING

2.4.1. AIMS OF THE MODEL

Incorporating the effects from interactions between colloidal particles within the concentration polarisation model should account for pH and ionic strength effects, and predict cake deposition in cross-flow filtration. Cake deposition was defined as a sudden, discontinuous increase in concentration nearby the membrane, from a concentrated solution ($\varepsilon<0.26$) to a close-packed, compact cake ($\varepsilon=0.26$).

2.4.2. ADDITIONAL EQUATIONS AND VARIABLES TO DESCRIBE THE SYSTEM

In Ilias and Govind's model, the velocity field and concentration profiles are related by three equations (continuity, momentum transport, and solute transport). The introduction of surface effects for the charged colloidal particles leads to a fourth variable, which is a non-convective flux J_{nc}, and a fourth equation, which describes the dynamic balance of the particles in solution. The continuity and momentum transport equations remain unchanged, and for them the same assumptions as those drawn out for Ilias and Govind's model prevail. However, the transport equation has to be written with a more complex form for J_{nc}.

The model has to interpret the dynamic balance so that it can predict coagulation of the colloid at the membrane or cake surface.

2.4.3. MASS TRANSPORT EQUATION

The equation written for Ilias and Govin's model has to be written in a more general form: The hypothesis that is not considered valid anymore is the constancy of the diffusion coefficient D for the solute. Here, the diffusion flux, which was meant to cover only Brownian diffusion effects, should be replaced by the non-convective flux J_{nc}, to which Derjaguin-Landau-Verwey-Overbeek (DLVO) forces may contribute much. The equation becomes then

$$U\frac{\partial C}{\partial Z}+V\frac{\partial C}{\partial R}=\frac{1}{R}\frac{\partial}{\partial R}\left(\frac{-J_{nc}}{v_{0,wall}c_0}R\right) \qquad \textbf{(2.49)}$$

2.4.4. DYNAMIC BALANCE

2.4.4.1. Assumptions

Fig. 2.11 describes the forces acting on one particle of solute. These include the double layer forces F_{DL} (electrostatic repulsion plus London-Van der Waals attraction), the Brownian diffusion (or entropic pressure) force F_E, and the drag force F_V. Since the axial non-convective flux is neglected, one need to consider only what happens in the radial direction. Each particle is submitted to a total force $F_{T(bottom)} = (F_{DL}+ F_E)_{(bottom)}$ from the particles below, and a total force $F_{T(top)} = (F_{DL}+ F_E)_{(top)}$ from the particles above it. When repulsion dominates, $F_{T(bottom)}$, which is directed towards the lumen's centreline, is negative, whereas $F_{T(top)}$ is positive.

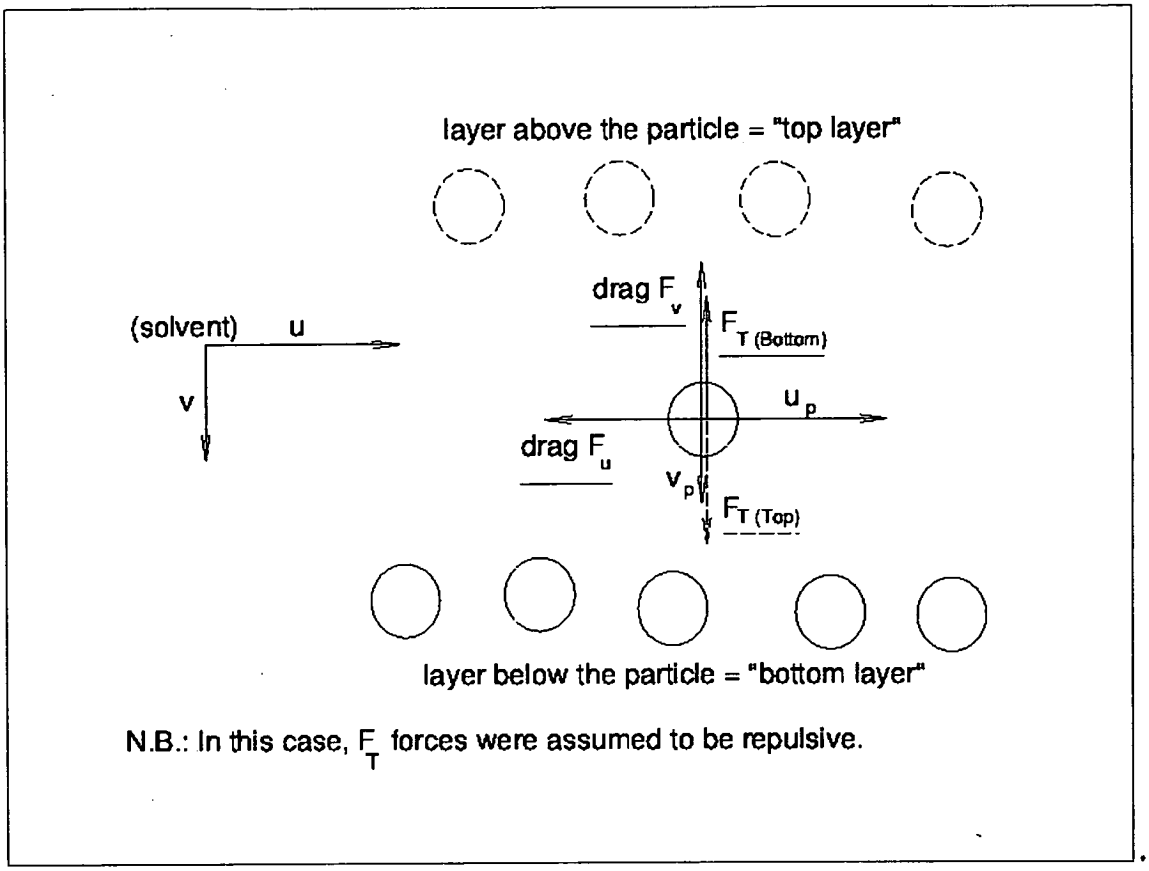

Fig. 2.11: *Dynamic equilibrium for a colloidal particle in cross-flow filtration.*

The following assumptions were made on the interactions between the particles:

-a) the particles, whether in solution or in the compact cake, are assumed to be arranged in a close-packed hexagonal array, and only the effects of those directly adjacent to the one considered are taken into account

-b) the particle is within a monolayer l_j of ordered particles at a distance R from the fibre centreline;

-c) the inter-particle distance D_{ip} is negligible compared to R, allowing approximation to a plane geometry for the interactions between l_j and the adjacent layers l_{j-1} and l_{j+1}.

2.4.4.2. Newton's law of motion

Newton's law applied on one particle of radial velocity v_p and mass m_p gives then:

$$m_p \frac{Dv_p}{Dt} = F_v + F_{T(bottom)} + F_{T(top)}; \qquad \textbf{(2.50)}$$

or, in radial co-ordinates for the local variables, with r = radius and z = downstream axial position:

$$m_p \left\{ \frac{\partial v_p}{\partial t} + u \frac{\partial v_p}{\partial z} + v \frac{\partial v_p}{\partial r} \right\} = F_v + F_{T(bottom)} + F_{T(top)} \qquad \textbf{(2.51)}$$

The following assumptions may also be made:

$$\frac{\partial v_p}{\partial t} = 0 \qquad \text{(steady state from a local standpoint)}$$

$$u_p \approx u$$

$$v_p = \frac{J_{nc}}{c} + v$$

(2.52 - 2.54)

The dynamic balance equation becomes then

$$m_p \left\{ u \frac{\partial}{\partial z}\left(\frac{J_{nc}}{c} + v \right) + v \frac{\partial}{\partial r}\left(\frac{J_{nc}}{c} + v \right) \right\} = F_v + F_{T(bottom)} + F_{T(top)} \qquad \textbf{(2.55)}$$

The different forces can then be calculated.

2.4.4.3. Forces exerted onto a particle from an adjacent layer (below or above):

- $F_{DL} = \sqrt{6}\ .(f(D) + F_{ATT})$, which is the **total surface force**, is calculated according to the method described in section 2.3.3. F_{ATT} is attractive and taken positive always, whereas $f(D)$ is always negative.

F_E is obtained **from the entropic pressure** Π_E (see 2.3.3.6.), multiplied by the suitable equivalent surface area for a half sphere, when considering the influence of the layer below (or above) the particle (Eq. 2.56 below). F_E is repulsive, with a negative sign:

$$F_E = -\pi a^2 \Pi_{E(bottom)}\ ; \qquad \textbf{(2.56)}$$

It is important to note that the sign of $F_{DL}+ F_E$ is independent from the referential (r, z) used in section 2.4.4.2. Instead, $F_{DL}+ F_E$ is defined as a function of the distance to the centre of the particle, and is negative when repulsion prevails, and positive when attraction is stronger.

An expression for $F_{T(bottom)} + F_{T(top)}$ was derived. The starting point is the following approximation on $F_{T(bottom)} + F_{T(top)}$:

$$F_{T(bottom)} + F_{T(top)} \approx -\frac{\partial(F_{DL} + F_E)}{\partial D_{ip}}.2(2a + D_{ip})\ ; \qquad \textbf{(2.57)}$$

The volume fraction φ gives a relationship between the concentration c, and D_{ip}:

$$\varphi = \frac{4\pi a^3 c}{3m_p} = \frac{4\pi\sqrt{2}}{3}\frac{a^3}{(2a + D_{ip})^3}\ ; \qquad \textbf{(2.58)}$$

We get, after simplifications,

$$F_{T(bottom)} + F_{T(top)} \approx 6c\frac{\partial(F_{DL} + F_E)}{\partial c}\ . \qquad \textbf{(2.59)}$$

It is interesting to note that, if $F_{DL} + F_E$ has a minimum at a concentration c^*, then, according to this formula, $F_{T(bottom)} + F_{T(top)}$ will be nil at c^*, and positive beyond c^*. Therefore, if $c > c^*$, it tends to compress the cake, in accordance with colloid theory.

2.4.4.4. Drag force

In the radial direction, the viscous drag force in the solution is given by Happel's version of Stokes law:

$$F_v = 6\pi\mu a f(\gamma)\cdot(v - v_p) \qquad \textbf{(2.60)}$$

with

$$\gamma = \varphi^{1/3}$$

$$f(\gamma) = \frac{3 + 2\gamma^5}{3 - 9/2\gamma + 9/2\gamma^5 - 3\gamma^6}$$

2.4.5. BOUNDARY CONDITIONS

Boundary conditions are essentially the same as those used in Ilias and Govind's model. There are, however, two modifications in the membrane-wall flux condition:

-The condition includes this time the resistance from the deposited material, R_a:

$$V_{wall}(Z) = \frac{(P_{wall} - P_{per}) - (\Pi_{wall} - \Pi_{per})}{R_m + R_a} \quad ; \qquad \textbf{(2.61)}$$

-The osmotic pressure Π_{wall} is the same as the disjoining pressure P_D in (Eq. 2.34):

$$\Pi_{wall} = \frac{\sqrt{6}}{A_e}\left(f(D_{ip}) + F_A(D_{ip})\right) + \Pi_E \; ; \qquad \textbf{(2.62)}$$

with

$$A_e = 2\sqrt{3}(a + D_{ip}/2)^2 .$$

2.4.6. SIMPLIFICATIONS

In order to solve the system of equations, two major simplifications are introduced:

2.4.6.1. Mass transport equation and diffusion coefficient

The non-convective flux is assumed to follow Fick's law:

$$J_{nc} = -D' \frac{\partial C}{\partial R} \qquad \textbf{(2.63)}$$

in which D' depends on the pH and ionic strength of the solution, and on the concentration of the solute. Investigating this dependency, Phillies *et al.* (1976) derived a generalised expression for the Einstein-Stokes law, giving D' as a ratio of the osmotic pressure gradient to the drag force coefficient:

$$D' = \frac{(\partial \Pi / \partial C)_{T,P}}{6\pi\mu a f(\gamma)} \qquad \textbf{(2.64)}$$

However, further research showed that the value found by this team for BSA at infinite dilution and pH=7 were 25% lower than that usually measured (e.g. Shen and Probstein, 1977). In addition, Anderson and Reed (1976) found a subtle but significant mistake in the derivation of this equation: They derived a more exact, but quite complex expression for D'. Given the limited time that was available for this PhD work, Phillies' equation was considered as a good enough approximation, which should provide some reasonably good insights into the impact of a variable diffusion coefficient.

2.4.6.2. Dynamic balance at the membrane wall; assumption of an inert membrane wall

The dynamic balance is considered only at the membrane wall, in the vicinity of which the axial velocity u is negligible (no-slip condition). Also, only those particles that are rejected are of interest for the cake formation, therefore one can assume v_p=0.

For a rejected particle, the simplified dynamic balance at the wall becomes then:

$$0 = F_v + F_{T(bottom)} + F_{T(top)} \qquad \textbf{(2.65)}$$

An assumption has to be made on the interaction of the solute with the clean surface of the membrane. In the absence of theoretical data, we assumed that there was no interaction. When running the model leads to a wall concentration c_g such that adjacent layers of particle would not coagulate, then the particles are considered to be against the membrane wall, at the concentration c_g. If significant differences are observed when comparing the model with the real system, then the experimentally measured adsorbed resistance in static conditions will have to be provided.

2.4.7. METHOD

2.4.7.1. Equations used

-The continuity and the momentum transport equation:

$$\frac{\partial U}{\partial Z} + \frac{1}{R}\frac{\partial}{\partial R}(RV) = 0 \qquad \textbf{(2.66)}$$

$$U\frac{\partial U}{\partial Z} + V\frac{\partial U}{\partial R} = -\frac{1}{2}\frac{dP}{dZ} + \frac{1}{R}\frac{\partial}{\partial R}\left(\frac{1}{\frac{\mu}{\mu_{R,Z}}Re_{0,wall}}R\frac{\partial U}{\partial R}\right) \qquad \textbf{(2.67)}$$

-The mass transport equation:

$$U\frac{\partial C}{\partial Z} + V\frac{\partial C}{\partial R} = \frac{1}{R}\frac{\partial}{\partial R}\left(\frac{1}{\frac{D_0}{D'_{R,Z}}Pe_{0,wall}}R\frac{\partial C}{\partial R}\right) \qquad \textbf{(2.68)}$$

-The dynamic balance at the membrane wall for the retained particles, expressed as

$$v_{dyn} = -\frac{c\frac{\partial(F_{DL} + F_E)}{\partial c}}{\pi\mu a f(\gamma)} \qquad \textbf{(2.69)}$$

Here, $\partial(F_{DL} + F_E)/\partial c$ is a function of c.

When making an assumption on J_{nc}, the number of variables was reduced from four to three. Therefore, the solution found from the first three equations may not satisfy the dynamic balance. Instead, we treat the dynamic balance as a constraint:

If $v_{wall} > v_{dyn}$, then the cake becomes tightly compact. **(2.70)**

2.4.7.2. Discretized equations

Discretization is not necessary for the dynamic balance condition at the membrane wall. The transport equations, however, were affected by the fact that the viscosity and the diffusivity depended on the solute concentration, and solvent properties: $Re_{0,\,wall}$ and $Pe_{0,\,wall}$ had to be replaced by the local, concentration dependent values Re and Pe respectively.

Taylor approximations for the derivatives of Re and Pe with respect to the radial position R had also to be used. Those factors had to be of the second order.

The final results of those calculations are given below.

For the momentum transport equation,

$$A_j U_{i,j-1} + B_j U_{i,j} + D_j U_{i,j+1} = E_j \quad \text{for} \quad 2 \le j \le n-1,$$

with

$$A_j = \frac{-1}{(DR1+DR2).DR2}\left\{DR1\left(V_{i-1,j} + \frac{1}{\mathrm{Re}_{0,\,wall}}.\frac{\partial(\mu/\mu_0)}{\partial R}\right) + \frac{2}{Re} - \frac{DR1}{R_j.Re}\right\};$$

$$B_j = \frac{U_{i-1,j}}{dZ} + \frac{1}{DR1.DR2}\left\{(DR1-DR2)\left(V_{i-1,j} + \frac{1}{\mathrm{Re}_{0,\,wall}}.\frac{\partial(\mu/\mu_0)}{\partial R}\right) + \frac{2}{Re} - \frac{DR1-DR2}{R_j.Re}\right\};$$

$$D_j = \frac{1}{(DR1+DR2).DR1}\left\{DR2\left(V_{i-1,j} + \frac{1}{\mathrm{Re}_{0,\,wall}}.\frac{\partial(\mu/\mu_0)}{\partial R}\right) - \frac{2}{Re} - \frac{DR2}{R_j.Re}\right\};$$

$$E_j = \frac{U_{i-1,j}^2}{dZ} - \frac{1}{2}\frac{dP}{dZ}.$$

(2.71)

The equation giving the radial velocities $V_{i,j}$ is the same as (Eq. 2.9).

The mass transfer equation gives

$$F_j C_{i,j-1} + G_j C_{i,j} + H_j C_{i,j+1} = I_j \quad \text{for} \quad 2 \le j \le n-1,$$

with

$$F_j = \frac{-1}{(DR1 + DR2).DR2}\left\{DR1\left(V_{i-1,j} + \frac{1}{\mathrm{Pe}_{0,\,\mathrm{wall}}}.\frac{\partial(D'/D'_0)}{\partial R}\right) + \frac{2}{Pe} - \frac{DR1}{R_j.Pe}\right\};$$

$$G_j = \frac{U_{i-1,j}}{dZ} + \frac{1}{DR1.DR2}\left\{(DR1 - DR2)\left(V_{i-1,j} + \frac{1}{\mathrm{Pe}_{0,\,\mathrm{wall}}}.\frac{\partial(D'/D'_0)}{\partial R}\right) + \frac{2}{Pe} - \frac{DR1.DR2}{R_j.Pe}\right\};$$

$$H_j = \frac{1}{(DR1 + DR2).DR1}\left\{DR2\left(V_{i-1,j} + \frac{1}{\mathrm{Pe}_{0,\,\mathrm{wall}}}.\frac{\partial(D'/D'_0)}{\partial R}\right) - \frac{2}{Pe} - \frac{DR2}{R_j.Pe}\right\};$$

$$I_j = U_{i-1,j}\frac{C_{i-1,j}}{dZ}.$$

(2.72)

Boundary conditions: Same as (Eqs. 2.12-14), replacing $Pe_{0,\,wall}$ by Pe.

2.4.7.3. Solving the discretized equations

a) Starting point on line *i+1*: Trying a value for c_g to get u and v profiles.

Knowing or assuming, all u, v, c, and D' values at line i, a pressure gradient dP/dZ is first assumed. One also needs a first guess c_g for the wall concentration c_g at line $i+1$, or use of a value c_g from previous iterations at this same line. Eq. (2.61) then gives a starting value for the permeate flux v_{wall}. The coupled equations (2.66) and (2.67) are simultaneously solved by trial and error adjusting dP/dZ, and converged u and v profiles are obtained when $v_{wall} = v_{i+1,n}$.

b) Method for solving the concentration profile and predicting coagulation:

The concentration profile is then found by solving Eq. (2.68), and c_g and $c_{i+1,n}$ compared. New values for c_g are then tried, until $c_g = c_{i+1,n}$. So far, this is the trial and error method presented by Ilias and Govind. However, some modification to this scheme is necessary here. Firstly, according to Eq. (2.6), c cannot take a value higher than that of the maximum osmotic pressure, $c_{\Pi max}$. If $c \geq c_{\Pi max}$, then $D' \leq 0$ (Eq. (2.64)), and coagulation occurs. Coagulation, however, may still occur for values $c < c_{\Pi max}$, since all that is needed for this is convection overcoming diffusion. D' and c profiles being now coupled, Eqs. (2.64) and (2.72) have to be solved simultaneously, and the method for choosing c_g carefully assessed. Appendix I details a procedure that recognises whether divergence of Eq. (2.72) is due to an improper choice of value for c_g, or to coagulation. It is summarised below.

c) Finding the concentration profile for a given diffusivity profile:

An initial $D'_0(R, Z_{i+1})$ profile on line i+1 is first assumed as being equal to that on the previous line, i. A typical curve *(Wall BC)* of v_{wall} against c_g, obtained from the wall flux boundary condition (2.61), is schematically drawn in *Fig. 2.12*.

- *(Wall BC)* has a minimum at a value $c_{\Pi max}$.

- Let c_g^* be the actual solution for the wall concentration, and v_{wall}^* the actual solution for the wall radial velocity.

- Let *(MT)* be the locus of the wall-values $c_{i,n}$, obtained from the mass-transport equation for all the starting values of v_{wall} around v_{wall}^*, for a given D' profile.

- c_g^* is found at the intersection of *(Wall BC)* with *(MT)*.

As can be seen on *Fig. 2.12*, for $c_g^* < c_{\Pi max}$, the solution, if any, can always be found by successive guesses for c_g in the interval between the previous guess and the resulting $c_{i,n}$. However, there has to exist a solution for the coupled transport and diffusivity equations.

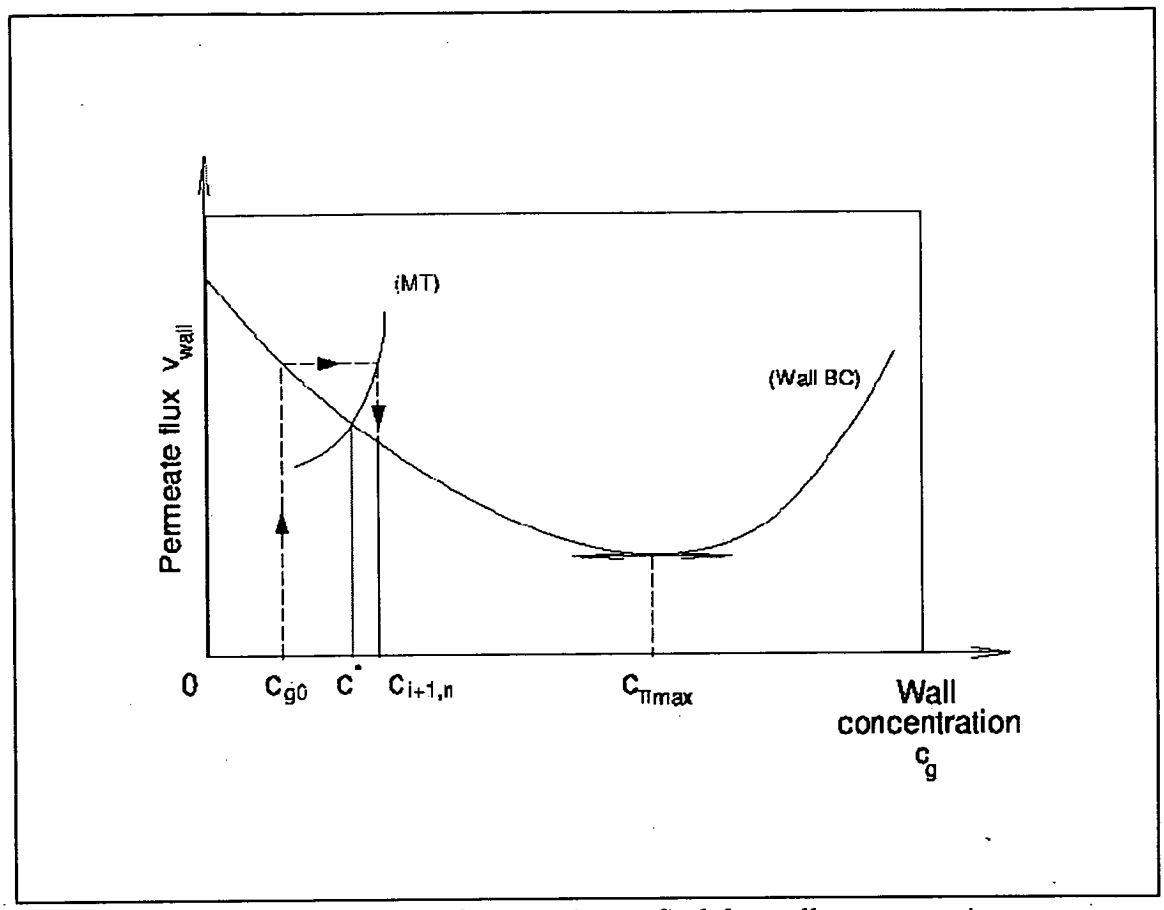

Fig. 2.12: *Solving the mass transfer equation to find the wall concentration.*

d) Solving the coupled transport and diffusivity equations:

In order to calculate all $c(r, z)$ at line $i+1$, one may try successive estimates of values $D'_k(R, Z)$ for the diffusivity profile in the transport equation. The resulting concentration profile $C_{k+1}(R, Z)$ is then used for a better estimate of the diffusivities on the next iteration, and the mass transport equation is solved again. The loop is repeated until a solution at the wall $c_{i+1,n}^*$ is found, or divergence is demonstrated. According to Appendix I, and excluding the simple case where $\zeta=0$ (in which D' had no maximum),

-For $\zeta \neq 0$, D' had a maximum positive value for a concentration $c_{D'max}$.

-For $c_{i+1,n}^* < c_{D'max}$, a solution always existed.

-If $c_{i+1,n}^{*} > c_{D'max}$ was found, and the starting point on section 2.4.7.3 a) was $c_g^0 < c_{D'max}$, then one should try $c_g = c_{D'max}$ and start again from step 2.4.7.3 a).

- If the starting point on section 2.4.7.3 a) was $c_g^0 \geq c_{D'max}$, and convergence does not occur: this value for c_g is too low, a higher value is tried in section 2.7.7.3 a). If no solution at all can be found between $c_{D'max}$ and $c_{\Pi max}$, then this means that diffusion at the wall at the position $i+1$ cannot overcome convection, resulting to the steady-state mass-transfer equation being not valid: coagulation has to occur.

2.4.7.4. Modelling fouling

In this model, fouling is assumed to occur solely as protein coagulation under high enough concentration and permeate flux. When still in solution, the particles against the membrane wall are considered to be at the concentration c_g. If significant differences are observed when comparing the model with the real system, then the experimentally measured adsorbed resistance in static conditions will have to be provided.

a) Conditions for deposition:

The values found for c_g and v_{wall} are now examined. It can be concluded that deposition occurs if either of the following is observed:

- the mass-transfer equation cannot converge due to diffusivity becoming too low to overcome convection (see 2.4.7.3 b)); this is always the case for $c_g > c_{\Pi max}$.
- $v_{wall} > v_{dyn}$ (see section 2.4.4.1.).

The second condition applies in fact only to particles so close to the membrane that their axial velocity is nil: coagulation may still occur elsewhere even if $v_{wall} < v_{dyn}$.

b) Nature of the deposit:

If coagulation occurs first at line i+1, a compact, close-packed monolayer of protein is assumed to deposit there, with a voidage ε=0.26. While the lumen radius r_i is left unchanged, a fouling resistance r_a is added at line i+1. Denoting by τ_{cake} the thickness of the cake, τ_{cake} is increased by $\sqrt{(8/3)}.(a+d)$ for each particle monolayer that deposits. r_a (in m^{-1}) is calculated from τ_{cake} and the Happel permeability K_H at ε=0.26 (Eq. (2.40)):

$$r_a = \frac{\tau_{cake}}{K_H(0.26)} \qquad \textbf{(2.73)}$$

Reinitialising c_g, the resulting new permeate flux v_{wall} is calculated from Eq. (2.61), and new u, v and c profiles recalculated at line i+1 with the new resistance, restarting the whole process again. As many monolayers as required are deposited, until no further coagulation occurs at line i+1. The value obtained for r_a is kept downstream all along the remaining length of the fibre, and increased if further coagulation appears downstream.

2.4.7.5. Algorithm

-1) Enter physical and system parameters (fluid properties, geometry, operating conditions, protein properties, etc...);

-2) Preliminary calculations:

-Find out and store values for the interaction forces, the osmotic pressure and the diffusion coeffient, as well as their derivatives, over the range of cake voidages to be found during a run of the programme (i.e. from bulk concentration or less, to close-packed).

-Find out and store values such as the maximum osmotic pressure, the concentration of maximal diffusivity, etc.

-3) At i=1 (boundary conditions): assume all values for U, V, and C, and cake thicness=0;

-4) i =2;

-5) Assume dP/dZ (Poiseuille equation), and therefore P at i =2;

Assume $C_{2,n}$, and C_g at i=2 different from $C_{2,n}$ (taking an arbitrary large value);

Derive profiles for viscosity and diffusivity.

-6) Work out $V_{2,wall}$ using the membrane flux boundary condition; assume $V_{2,n} \neq V_{2,wall}$;

-7) While i <m+1:

{

-8) While $C_g \neq C_{i,n}$:

{

-9) While $V_{i,n} \neq V_{i,wall}$:

{

-10) Solve momentum transport equations (written for $2 \leq j \leq$ n-1) and find all $U_{i,j}$ at i ;

-11) Solve continuity equation to find all $V_{i,j}$ at i ;

-12) If $V_{i,j} > V_{i,wall}$, increase dP/dZ;

else if $V_{i,j} > V_{i,wall}$, decrease dP/dZ;

-13) Work out P_i ;

-14) Work out $V_{i,wall}$ using the membrane flux boundary condition;

}

-15) With the converged flow field, solve the solute transport equation combined with the diffusivity equation (for $2 \leq j \leq$ n-1) (see section 2.4.7.3 and Appendix I);

-16) Test for finding out if deposition occurs (see section 2.4.7.4):

If "yes", then calculate **new cake thickness** and **go back to -2)** to re-start from scratch on the current line i.

-17) Derive from C profile the profiles for viscosity and diffusivity.

-18) Change the value of C_g to $(C_g + C_{i,n})/2$;

}

-19) i=i+1;

}

-20) Check the overall mass balance.

3.

EXPERIMENTAL MATERIALS AND METHODS

3.1. EXPERIMENTAL WORK

In order to check our model, it was decided to examine the fouling behaviour of some commercially available hollow-fibre devices. Cross-flow filtration of Bovine Serum Albumin (BSA) was studied in three different cartridges that rejected it completely.

3.2. CARTRIDGES

3.2.1. Centrisystem® cartridges

Our first experiments were carried out on Centrisystem® dialysis cartridges, supplied by Cobe ltd.

The first cartridge that was tested was a C-300, with a surface area of 0.8 m^2, and according to a personal communication from Dr. Duncan Pepper (Scottish National Blood Transfusion Service), it has a MWCO between 7 and 15 kD. The fibres are made of Cuprophan®, i.e. regenerated cellulose. The Extra-Capillary Space (ECS) volume was 16 ml.

Two C-400 cartridges were also tested. The difference with the C-300 cartridge was in the fibre-wall thickness, and in the number of fibres. The total surface area provided wa 0.9 m^2. The following table sums-up some of the properties of the cartridge:

Cartridge	Length (mm)	Fibre diameter (μm)	Membrane Thickness (μm)	Surface area (m^2)	Number of fibres
C-300	200	200	8	0.8	6880
C-400	200	200	6.5	0.9	7740

Table 3.1: *Geometric characteristics of the fibres in Centrisystem® cartridges.*

3.2.2. Amicon H1P30-20 cartridges

The other cartridge that was tested was an H1P30-20 supplied by Amicon (a company that has now been taken over by Millipore). It has a MWCO of 30 kDa, and its fibres are made of polysulphone material. The surface area and length available for filtration are 0.06 m^2 and 0.153m respectively, and the diameter of the fibres is 500 μm, resulting in an estimated number of fibres of about 250.

3.3. PREFILTRATION OF BUFFER SOLUTIONS

The aim of prefiltration was to remove any unwanted particulates and debris that were otherwise observed to build-up before the entrance of the fibres. The prefiltration cartridge was a Bioflow 0.1 μm, operated in CF mode with recycle, pulsed by a Watson-Marlow 601S peristaltic pump. Typical inlet relative pressure in operation was 80000-100000 Pa, read with a Bourdon Gauge, while outlet relative pressure was ca. 0 Pa.

Typical flow rates in operation were:

-Outlet: 74 ml/min

-Permeate: 99 ml/min

3.4. EXPERIMENTAL SET-UP

The cartridge was inserted in a circuit designed for CF mode. *Figure 3.1* sums up the features of this circuit. The feed bottle contained 2L of the studied solution, and was kept in a thermostatted bath. No mechanical agitation of the feed solution was provided, in order to minimise aggregation of the BSA protein.

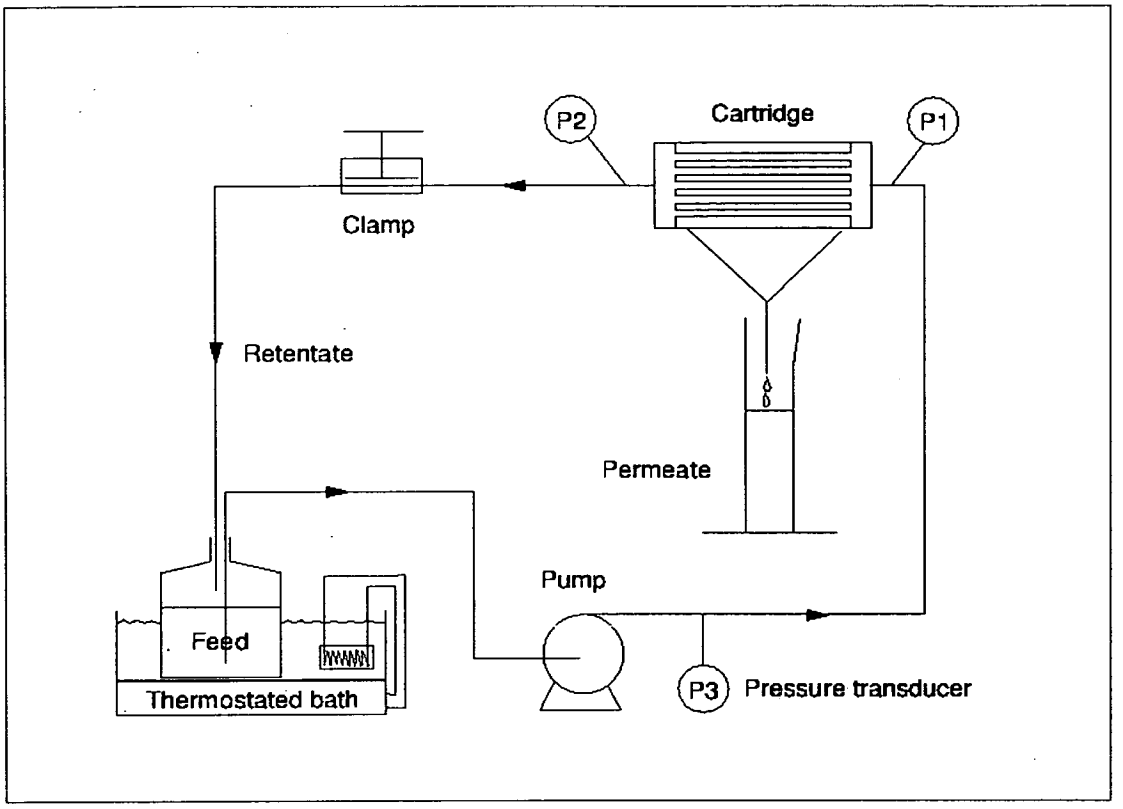

Fig 3.1: *Experimental set-up for Cross-Flow filtration.*

3.4.1. Pump and flow-rates

A Verder, model 2030 Auto gear pump, ensured the circulation of the fluid in the circuit. The head of the pump was a V096.07, with a low shear-to-flow ratio. Its digital display was found not to give the flow rate accurately as a percentage of the maximum capacity of the pump. Therefore, the flow rate of the pump for a range of backpressures and digital displays of the flow rate was measured by reading the outlet volume collected over 1 min. The resulting calibration curves can be found in Appendix II.

3.4.2. Pressure measurement

Clamps on the circuit soft tubes allowed the application of a back pressure, providing a driving force for the filtration.

3.4.2.1. Transducers

Pressures (P_1, P_2, P_3) were measured using pressure transducers supplied by Sensortechnics (Cat. No. PS15GA), interfaced with a computer. The programme was largely derived from one written by J. Burns. Readings were plotted every 5 secs, and stored onto a floppy disk every 60 secs. These were calibrated with a Digital Pressure Indicator (DRUCK) DPI601, supplied by Scotia Instrumental Ltd. Results are reported in Appendix III.

3.4.2.2. Location of the readings

In some preliminary tests, it was found that the pressures measured at the inlet and outlet of the cartridge were affected by the lengths, positions and elements (T-junctions, valves, connectors) of the piping between the pressure gauges and the cartridge ports. Therefore, a special design suggested by K. Wright was chosen for the chambers of the transducers (Figure 3.2): The chamber was a cylinder, with a conical top-part. It had two openings, one near the bottom and the pressure transducer sensitive surface, and the other one at the top. A thin tube was connected to the bottom opening, and introduced inside the cartridge, just before the sealing compound ("potting") and the entrance or exit of the fibres. A large tube was connected to the top opening, and a clamp was fixed on it: This allowed flushing the air from the thin tube and the chamber.

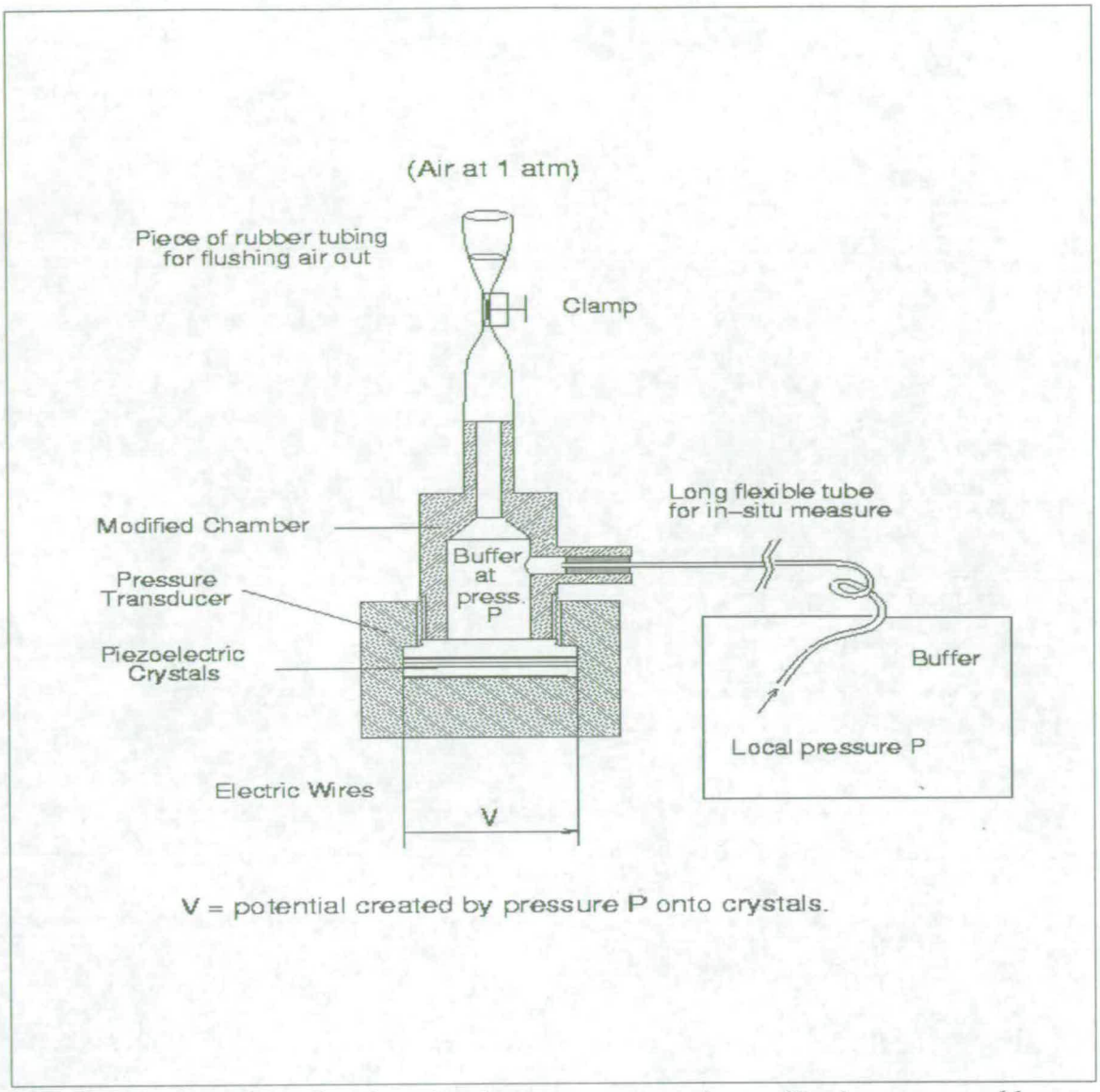

Fig. 3.2: *Design of the chambers for the pressure transducers (Design suggested by Kevin Wright).*

3.4.2.3. Static pressure heights

The axis of the cartridge and the sensitive surface in the pressure transducers were put at the same level. The cartridge was horizontal to avoid taking into account a static height pressure drop along the fibres.

3.5. EXPERIMENTAL PROCEDURE:

3.5.1. Buffer fluxes with clean cartridges

Before all experiments, the flux of Phosphate Buffer Saline (PBS) was measured. This allowed checking that the membrane was clean and without leakage, and obtaining a value for the intrinsic membrane resistance. Flow rates were measured by collecting outlet fluids over a known period of time of at least 5 minutes. The permeate flux, J_v, was obtained by dividing the flow rate by the membrane surface area.

3.5.2. PBS solutions preparation

Phosphate Saline Buffer was chosen as the buffer for protein solutions because it is widely used. The pH was set at 7 in most experiments, but also at 5 and 9, and the ionic strength at either 0.1M, 0.01M or 1M. To obtain a 2L solution of PBS at pH=7 and 0.1M, the following procedure was applied:

-A solution "A" of monobasic sodium phosphate (NaH_2PO_4), at 0.2 M, was prepared by dissolving 48 g of anhydrous salt (SIGMA S0751) in 2L of water.

-A solution "B" of dibasic sodium phosphate (Na_2HPO_4), at 0.2 M, was prepared by dissolving 56.8 g of anhydrous salt (SIGMA S9763) in 2L of water.

-2L of PBS were made up by mixing together 390 ml of solution A, 610 ml of solution B, and 1L of distilled water.

The pH was found to be usually around 6.8-6.85, and was adjusted to 7 adding the required amount of Sodium Hydroxide (NaOH) solution at 1M. When a different pH was required, different proportions of solutions A and B were used. Also, 1M PBS solutions were obtained by adding the required quantity of Sodium Chloride (NaCl). 0.01M solutions were prepared by diluting 10 times 0.1M PBS solutions, and correcting the pH with a 0.01M NaOH solution.

3.5.3. BSA solutions

The BSA was purchased from SIGMA, no. A 7030. This product, with a purity over 98%, is "prepared from pasteurized bovine serum and further processed to be essentially fatty acid free (less than 0.02%)." (from SIGMA catalogue).

2L of PBS were prepared and prefiltered. The BSA was then dissolved into this solution. Because of the influence of temperature, time, aeration and agitation upon the denaturation, aggregation, and subsequent fouling properties of BSA, a strict procedure was followed in the preparation and handling of BSA solutions. Bubbling or foaming in the BSA solution was cautiously avoided throughout to minimize denaturation of the protein:

3.5.3.1. BSA solutions preparation

-Preparation of 1g/L solutions

-Working temperature was 20-23 °C (room temperature).

-Agitation speed was N_s = 80 rpm for 2L, with a magnetic "flea" (length D = 4 cm).

-About 2 g BSA was dissolved by adding the crystals slowly while stirring, avoiding the formation of flocs at the surface.

-The duration of this dissolution and stirring phase was 10 minutes.

3.5.3.2. CF filtration of the BSA

Shortly after the start of the dissolution of the BSA, the solution was cross-flow filtered through the cartridge studied. Special attention was required during the filtration, to make sure no bubbling occurred in the tubing or at the outlet of the

retentate. At the start of the experiment, the tubing was filled with PBS; a 3-way valve was fitted before the cartridge inlet, to expel any bubble.

Again, flow rates were measured by collecting outlet fluids over a known period of time of at least 5 minutes. Rejection ratios were also checked regularly, by measuring the absorbances of the feed solution, the retentate outlet and the permeate (see next section).

3.5.4. Analysis by spectrophotometry

3.5.4.1. Material

BSA concentration, in the retentate and in the permeate, was measured by UV-spectrophotometry at 280 nm, using a JENWAY 6105 VIS/UV spectrophotometer. 2.5 ml UV cuvettes were supplied by Kartell.

3.5.4.2. Procedure

The temperature was checked to be within a range of 20-25 °C. Absorbance at 280 nm was then recorded, and to remain within the range of a linear relationship between the absorbance and the concentration, samples giving absorbance readings over 1.000 were diluted to lower it under this value. Three blanks of distilled water were taken to zero the apparatus, and check the cleanliness of the cuvettes.

3.5.4.3. Calibration

A calibration curve was obtained dissolving known amounts of BSA into a half filled gauged vial, and filling up the vial until the mark of the nominal volume. After thorough mixing of the solution, half of it was collected into another vial and diluted with the same amount of water. This procedure was repeated 5 times, giving solutions of about 2, 1, 0.5, 0.25, 0.125, 0.0625, and 0.03125 g/L. A chart relating absorbance and concentration was then drawn (Appendix IV).

3.5.4.4. Sampling

When no dilution was required (absorbance readings under 1.000), 1 to 2 ml of either permeate or retentate was directly collected respectively either from the feed tank, or from the permeate measuring cylinder.

Where dilution was required (absorbance readings over 1.000), distilled water and sample aliquots of accurately defined volumes were collected into the cuvette using Gibson pipettes. The BSA solution was added to the water with a Gibson pipette, and sucking it up and down in the cuvette 10 times ensured thorough mixing.

3.5.5. Rinsing

In CF mode, after filtration of BSA, CF-filtration of buffer was performed. About 2L of buffer were used, without recycle in the first 2 minutes of the operation. The critical problem here was to preserve any adsorbed or deposited protein while flushing away the concentration polarisation layer. The TMP was decreased to a minimum level, and maintained for 15 minutes to check that steady state was reached. Permeate flow rates were recorded, and then successive higher TMP's were tried.

3.5.6. Cleaning protocols

Protocol 1:

After the membrane was used for cross-flow filtration of BSA stocks, the Extra-Capillary Space (ECS) was drained.

-For the Centrisystem® cartridges, 2 litres of sodium hydroxide at 0.05M were prepared, and used for cross flow filtration, with no back-pressure applied. Recycling at this stage proved to leave significant amounts of protein within the circuit, and it was then always avoided for the first 1L of the solution. The solution was circulated through the circuit for 15 min. The same procedure was repeated with buffer. Restoration of permeate

flux of buffer over the range of TMP's was then checked.

-For the Amicon cartridge, Terg-A-Zyme® at 1% was used, in accordance with the "Cleaning after Operation" chapter of the Operating Instructions supplied by Amicon with the cartridge.

Protocol 2:

For the Centrisystem® cartridges only: whenever the flux was not recovered after applying Protocol 1, the cleaning would then be repeated using protocol 1 again, but with ammonium hypochlorite at 0.01% w/w instead of sodium hydroxide. Protocol 1 would then be repeated again with NaOH for proper conditioning of the membrane.

Protocol 3:

For Amicon cartridges only: backflushing had to be used when protocol 1 sometimes failed to restore the flux. It consists in flushing 0.1M NaOH solution from the ECS into the lumen, which should unclog the membrane pores. The procedure to follow can be found in the chapter on Backflushing, from the "Operating Instructions" supplied with the cartridge.

4.

RESULTS AND DISCUSSION

4.1. CONCENTRATION POLARISATION

4.1.1. SIMULATION ON CENTRISYSTEM CARTRIDGE

A C-programme was written to enable us to reproduce Ilias and Govind's results.

The programme was first tested with Cross-Flow filtration of BSA through C-400 Centrisystem® hemodialysis Hollow-Fibre Cartridges (see 3.2.1).

The geometric characteristics of the C-400 cartridges were:

-Length L = 0.2 m;

-Number of fibres N = 7162;

-Internal diameter of the fibres d_i = 200 µm;

-Total surface area A_m = 0.9 m^2;

-Total rejection of BSA.

The operating conditions were (cf First Year report):

-Inlet Pressure P_1 from 23000 to 60000 Pa;

-Feed Flow rate around 300 ml/min: $4.5 \cdot 10^{-6}$ $m^3/s < \varphi < 5.4 \cdot 10^{-6}$ m^3/s,

where φ is the volume flow rate entering one fibre;

-Concentration of BSA: C_0 = 5 g/L.

The membrane resistance (taking into account the viscosity of the medium at 25 °C) was:

$\mu r_m = 1.05 \cdot 10^{14}$ Pa·s/m;

The medium viscosity was taken as $8.94 \cdot 10^{-4}$ Pa·s, and the diffusivity of BSA was D = $7 \cdot 10^{-7}$ cm^2/s.

For all simulations, the overall mass balances were correct within 0.1%, indicating a correct solution. The following table compares experimental pressure drops and permeate fluxes with those given by the simulation using the same input parameters:

Experiment:				Simulation:	
Parameters		Results			
Inlet pressure (Pa)	Inlet flow rate (m^3/s)	Pressure drop (Pa)	Permeate flux (m/s)	Pressure drop (Pa)	Permeate flux (m/s)
23088	$4.25*10^{-6}$	2619	$1.89*10^{-7}$	2949	$2.03*10^{-7}$
42937	$4.9*10^{-6}$	2963	$3.76*10^{-7}$	3400	$3.90*10^{-7}$
59547	$5.19*10^{-6}$	3234	$5.43*10^{-7}$	3504	$5.48*10^{-7}$

Table 4.1: *Comparison between experiment 4.1.3.3 and simulation 4.1.1 in cross-flow filtration of 5 g/L BSA with C-400 cartridge.*

For the same simulation, figure 4.1 shows the results for the wall concentration profile:

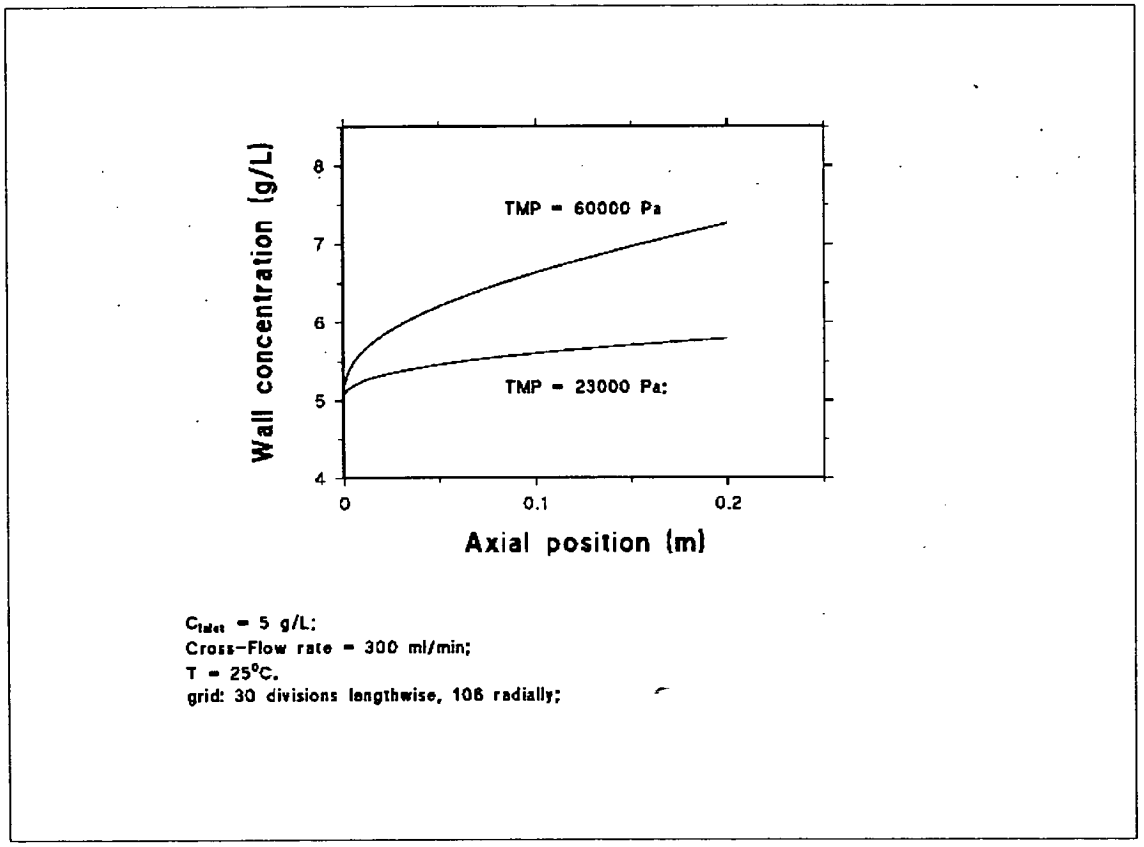

Fig. 4.1: *Wall concentration profile in simulation 4.1.1 for C-400 cartridge in cross-flow filtration of 5 g/L BSA.*

4.1.2. EXPERIMENTS WITH A C-300 CARTRIDGE

4.1.2.1. Buffer Cross-Flow filtration: Influence of TMP and temperature

The buffer used was always PBS at 0.1M and pH=7 (see 3.5.2).

The inlet flow rate was constant, at around 300 ml/min. TMPs were successively taken as 21000, 35000, 46000 and 53000 Pa.

Two temperatures were chosen: 23 °C, and 37 °C. Only the feed temperature was controlled. However, the outlet temperature was checked to be within + or - 1 °C of that set temperature. It was always found at 23 °C when working at that temperature, and at 36-36.5 °C when working at 37 °C.

The temperature was stable within + or - 0.2 °C for the experiments reported here.

4.1.2.2 BSA filtration: 23 °C, 1 g/L

Each experiment comprised the following four phases:

-**Measuring buffer fluxes** in Cross-Flow filtration (section 3.5.1)

-**Filtration of the BSA solution for 2 hours** (see 3.5.3) with an inlet flow rate of 300 ml/min, recording pressures, fluxes (permeate and outlet), and rejection ratios; The studied parameter was the TMP (ca. 21000, 35000, 46000 and 53000 Pa).

-**Rinsing with buffer** (see 3.5.5), repeating the first step.

-**Cleaning** according to Protocol 1 in 3.5.6.

One given TMP for the filtration of BSA (second step) was tried in each experiment:

4.1.2.2.a) TMP=21000 Pa;

4.1.2.2.b) TMP=35000 Pa;

4.1.2.2.c) TMP=46000 Pa;

4.1.2.2.d) TMP=53000 Pa;

4.1.2.2.e) Repeat 4.1.2.2.d);

4.1.2.2.f) Repeat 4.1.2.2.a);

4.1.2.2.g) Repeat 4.1.2.2.b);

4.1.2.2.h) Repeat 4.1.2.2.c);

4.1.3. EXPERIMENTS WITH THE FIRST C-400 CARTRIDGE

4.1.3.1. Buffer Cross-Flow filtration: Influence of TMP and temperature

The buffer, the pressures and the flow-rates were the same as in 4.1.2.1.
Three temperatures were chosen: 23 °C, 25 °C, and 37 °C. Temperature was controlled within + or minus 0.2 °C, except when stated otherwise. The summer having been hot at the time of the experiments, this required constant replacement of the water bath by fresh, cool water.

4.1.3.2. BSA filtration: 23 to 25 °C, 1 g/L

Conditions and parameters were as in 4.1.2.2. However, temperature control often failed due to the hot summer, therefore the temperatures reported here are not 23 °C anymore.

4.1.3.2.a). TMP=21500 Pa; Temperature was 23.8 °C.
4.1.3.2.b). TMP=38000 Pa; Temperature was 24 °C.
4.1.3.2.c). TMP=45000 Pa; Temperature in between 24 and 25 °C.
4.1.3.2.d). TMP=53000 Pa; T= 25 °C.

4.1.3.3. BSA filtration: 25 °C, 5 g/L

Conditions as in 4.1.3.2, except for BSA concentration (5g/L) and temperature (25 °C).

4.1.3.3.a) TMP=22000 Pa;
4.1.3.3.b) TMP=45000 Pa;
4.1.3.3.c) TMP=35500 Pa;
4.1.3.3.d) TMP=55000 Pa.

4.1.4. EXPERIMENTS WITH THE SECOND C-400 CARTRIDGE

Same conditions as in 4.1.1 and 4.1.2 throughout, unless stated otherwise. This was intended to check reproducibility from one cartridge to another. Only buffer filtration at 23 °C was carried out.

4.1.5. EXPERIMENTAL RESULTS WITH CENTRISYSTEM CARTRIDGES

For all BSA filtrations, the rejection ratio was found to be higher than 98%.

Fig. 4.2 and *Table 4.2* report results obtained on buffer filtration with Centrisystem cartridges. *Fig. 4.3* shows the effect of BSA filtration on permeate flux.

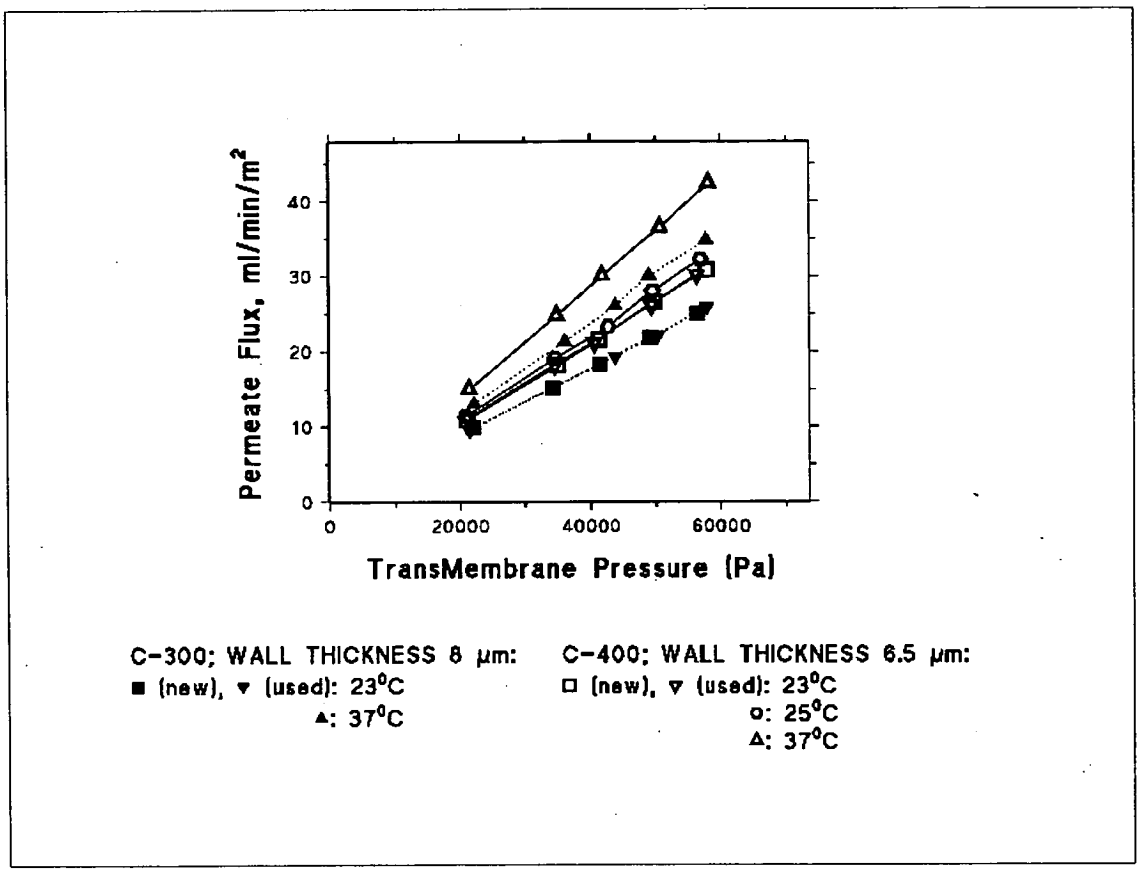

Fig. 4.2: *Buffer filtration with C-300 and first C-400 cartridges, from experiments 4.1.2.1 and 4.1.3.1: influence of TMP and temperature on the permeate flux.*

r_m (m^{-1})	23 °C	24.2 °C	25 °C	37 °C
C-300	$1.46 - 1.53 \cdot 10^{14}$	-	-	$1.46 \cdot 10^{14}$
First C-400	$1.21 - 1.22 \cdot 10^{14}$	$1.18 \cdot 10^{14}$	$1.20 - 1.21 \cdot 10^{14}$	$1.20 \cdot 10^{14}$
Second C-400	$1.04 - 1.06 \cdot 10^{14}$	-	-	-

Table 4.2: *Intrinsic resistances for C-300 and C-400 cartridges with buffer (exp. 4.1.2.1, 4.1.3.1 and 4.1.5), $r_m = TMP / (\mu_0 J_v)$. The slope (TMP / J_v) was obtained from Fig. 4.2. The temperature-dependent viscosity μ_0 was obtained from the International Critical Tables (ed. E.W. Washburn, McGraw-Hill Book Company, Inc., 1926).*

4.1.5.1 Influence of temperature on buffer filtration rates

Experiments with C-300 and C-400 cartridges clearly demonstrated the influence of temperature (T) on buffer filtration rate: *Fig. 4.2* shows that the permeate flux vs. TMP characteristics are linear, and that their slopes increase with T, *i.e.* the cartridges seem more permeable when temperature rises.

This effect is due to the buffer viscosity only: in *Table 4.2*, the intrinsic resistances for all cartridges studied were derived from the slopes of the characteristics in *Fig. 4.2*, and took into account the temperature dependency of the buffer viscosity. The results clearly show that respective intrinsic resistances for C-300 and C-400 did not vary significantly over the range of temperatures considered (23-37 °C).

4.1.5.2. Membrane consistency

Table 4.2 also shows an example of membrane-to-membrane variability: the two C-400 cartridges that were studied displayed significantly different intrinsic resistances at 23°C ($1.05 \cdot 10^{14}$ and $1.21 \cdot 10^{14}$ m^{-1}). In fact, membrane consistency can sometimes be rather difficult to observe. Nilsson and Hallström (1991) observed that with GR61PP membranes, which are retentive to BSA, small sections cut from the same sheet could display buffer permeabilities differing by up to a factor of ten.

4.1.5.3. Comparison with model prediction

The simulation runs reported in *Fig. 4.1* show that, for C-400 cartridges in the conditions described, no significant increase in concentration occurs at the membrane wall. The same result was obtained with C-300 cartridges, or for 1g/L BSA solutions. Experimental results presented in *Fig. 4.3* confirmed that no reduction in flux was observed when filtering BSA solution, suggesting a low concentration polarisation.

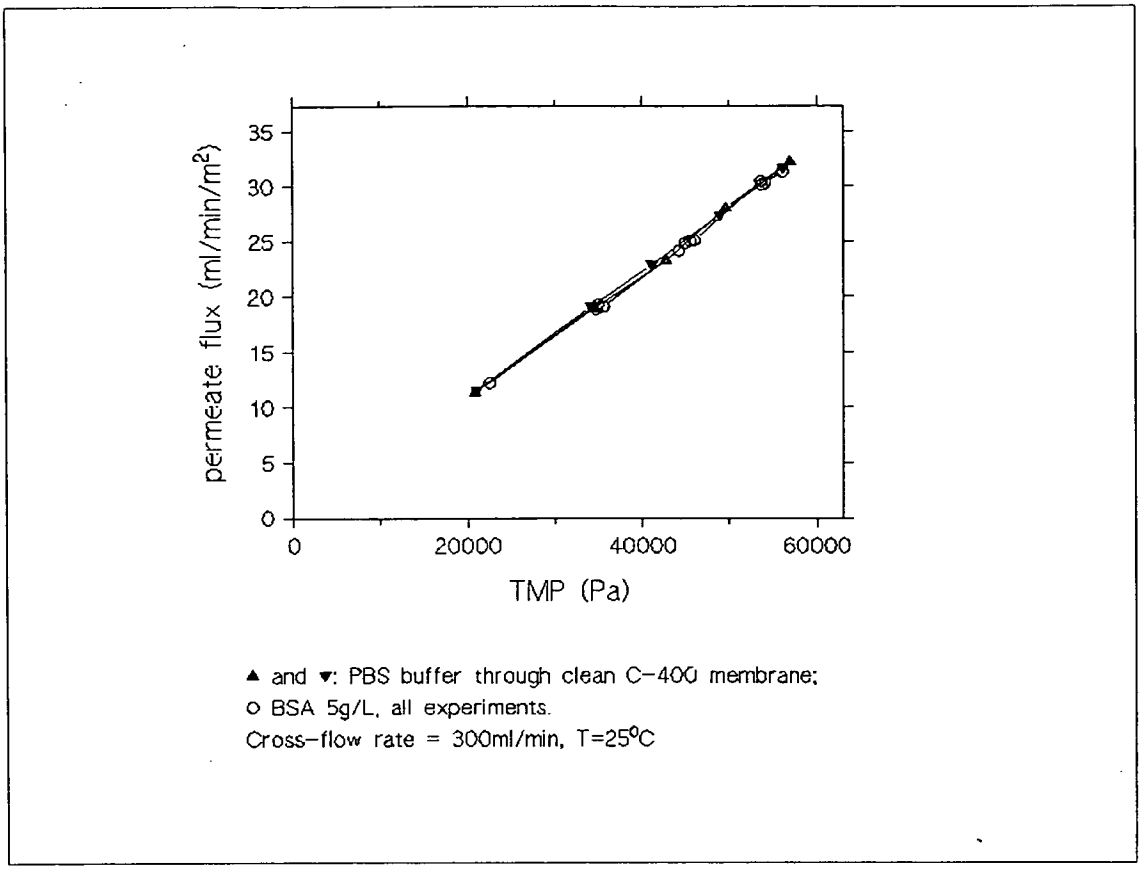

Fig. 4.3: *Permeate fluxes for BSA solutions at 5 g/L with C-400 cartridge (experiments 4.1.3.1-8), compared with buffer fluxes in the same conditions. All other BSA filtration experiments, with C-300 or with 1g/L solutions, yielded similar results, showing no fouling occurred.*

4.1.6. SIMULATION WITH AN AMICON H1P30-20 CARTRIDGE

The programme was then tested with the Ultrafiltration Hollow-Fibre Cartridge H1P30-20, supplied by Amicon (see 3.2.2). Yeh and Cheng (1994) presented in their modelling work their experimental results on the cross-flow filtration of Dextran T-500 with this cartridge: we used their parameters and some of their results in this section.

The geometric characteristics of the Amicon cartridge were:

-Lenght $L = 0.153$ m;

-Number of fibres $N = 250$;

-Internal diameter of the fibres $d_i = 500$ µm;

-Total surface area $A_m = 0.06$ m^2.

-MWCO = 30 kDa, hence total rejection of dextran T-500.

The operating conditions reported in Yeh and Cheng's paper were:

-Inlet Pressure P_1 from 30,000 to 140,000 Pa;

-Feed Flow rates corresponding to a velocity: $u_{0,\,avg} = 0.051$ m/s;

-Concentration in Dextran T-500: 1 g/L $\leq c_0 \leq$ 20 g/L;

In Yeh and Cheng's paper, the membrane resistance at the entrance of the fibres, i.e. in the absence of concentration polarisation, was given as a function of the concentration C_0 and of the cross-flow velocity u_0. If we assume that the contribution from c_0 is due to deposition, then

$$r_m = 2.42 \cdot 10^{12} + 7.49 \cdot 10^{11}\, u_0^{-0.15} \quad (\text{in } m^{-1});$$

The medium viscosity was taken as 0.001 Pa·s.

The diffusivity of Dextran T-500 was given in m^2/s by the following correlation (with c_0 in g/L):

$$D = 10^{-11} \cdot (1.204 + 2.875 \cdot 10^{-1}\, c_0 - 5.042 \cdot 10^{-3}\, c_0^2 + 2.838 \cdot 10^{-5}\, c_0^3).$$

The following correlation gave the osmotic pressure (in Pa) for Dextran T-500 (with c_0 in g/L):

$$\pi_{os} = 37.5\, c_g + 0.725\, c_g^2 + 7.64 \times 10^{-3}\, c_g^3$$

The simulation gave typical wall-concentration profiles along the fibre. We gave an example in the following figure:

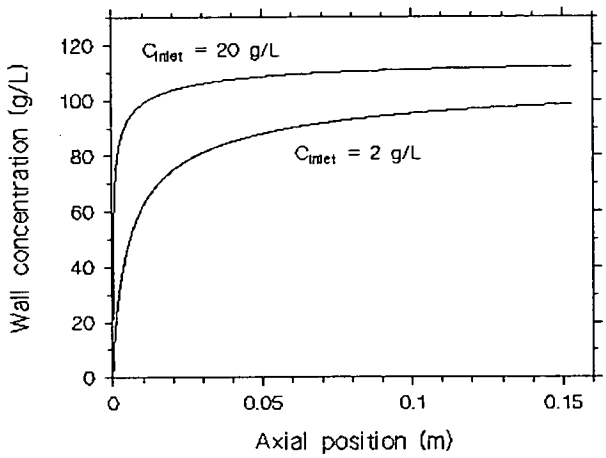

Transmembrane pressure = 30000 Pa;
Crossflow velocity = 0.051 m/s.
Experimental data after Yeh and Cheng.

Fig 4.4: *Example of wall-concentration profile from simulation 4.1.6, showing the development of the concentration polarisation layer during the cross-flow filtration of 2 and 20 g/L Dextran T-500 with Amicon H1P30-20 cartridges.*

The following table reports the final results for permeate flux from simulations 4.1.6:

Pressure (Pa)	Dextran Inlet Concentration (g/L)	Grid Chosen (see section 2.5.4.6)	Overall Mass Balance Factor (see 2.5.4.6)	Average Permeate Flux (m/s)
30000	2	m=1000 n=886	0.999035	$3.93957*10^{-6}$
30000	20	m=300 n=886	1.000000	$1.7651*10^{-6}$
140000	2	m=9000 n=886	0.989885	$6.22234*10^{-6}$
140000	20	m=6000 n=886	0.999934	$2.90144*10^{-6}$

Table 4.3: *Results of simulations 4.1.6, giving permeate flows for the cross-flow filtration of Dextran T-500 with H1P30-20 cartridge (CF velocity = 0.051 m/s).*

These results were combined with the experimental results after Yeh and Cheng (*Table 4.4*) to give estimates of the respective contributions of Concentration Polarisation and of Deposition in the system. The difference between the total resistance, observed by Yeh and Cheng, and the polarisation resistance calculated from our simulations, gives the resistance due to the deposited layer of Dextran. The result can be seen in *Fig. 4.5*.

Pressure (Pa)	Dextran Inlet Concentration (g/L)	Buffer Permeate Flux (clean membrane) (m/s)	Observed Dextran Permeate Flux (m/s)
30000	2	$8.36*10^{-6}$	$2.6*10^{-6}$
30000	20	$8.36*10^{-6}$	$1.1*10^{-6}$
140000	2	$3.59*10^{-5}$	$4.5*10^{-6}$
140000	20	$3.59*10^{-5}$	$1.8*10^{-6}$

Table 4.4: *Some experimental data from Yeh and Cheng on the system used in simulation 4.1.6.*

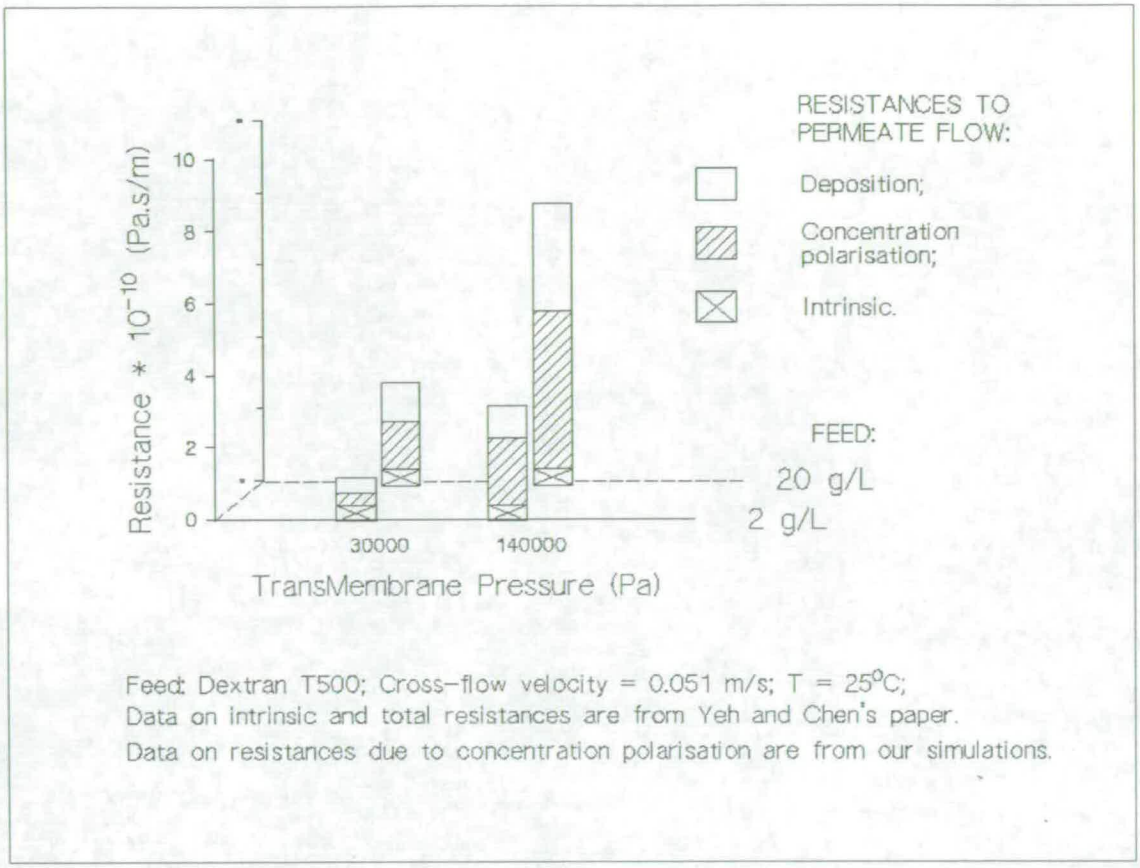

Fig. 4.5: *Respective contributions of concentration polarisation and deposition in fouling, from simulations 4.1.6 and Yeh and Cheng's experimental data (from table 4.3 and 4.4)*

As shown by *Fig. 4.4*, Ilias and Govind's model does predict concentration polarisation occuring for Amicon H1P30-20 cartridges with Dextran T-500 solutions, even under low transmembrane pressure (30000 Pa only). Yeh and Cheng's experimental results show reduction of permeate flux with this system, but do not distinguish between tightly-bound deposition and concentration polarisation. By combining their experimental results with the simulations presented in this work, one may have an idea of the respective contribution of the two factors. *Fig. 4.5* show the results of this approach: It seems that deposition increases when inlet concentration changes from 2 g/L to 20 g/L, even if the pressure is lower. Resistance due to deposition would represent a substantial fraction of the total resistance: between one third (at 140000 Pa) and one half (at 30000 Pa) of the fouling resistance.

4.1.7 CONCLUSIONS

Ilias and Govind's model seem to give good results: The overall mass balance factors are satisfying (see section 4.1.1 and *Table 4.3* in 4.1.5), and the pressure drops and permeate flow rates sensibly match experimental results in the same conditions (see *Table 4.1* and *Fig. 4.5*). Moreover, the model seems able to predict the occurrence or not of significant levels of concentration polarisation and its effect on the permeate flux, as this section has shown.

4.2. CAKE BUILD-UP IN DEAD-END FILTRATION

4.2.1. PROGRAMME

A C-programme was written to reproduce Bowen and Williams' simulation results (1996) on the dead-end ultrafiltration of BSA, according to Bowen and Jenner's model. This allowed checking of the equations for inter-particle forces and disjoining pressure before using these in Cross-Flow situations. It also provided some insights into the way a colloidal cake may build-up.

4.2.2. PARAMETERS TO TEST THE PROGRAMME

The chosen test system was BSA, in a buffer with a viscosity of 10^{-3} Pa·s and a density of 10^3 kg/m^3. The hydrated BSA molecules were taken to have a radius of 2.97 nm and a density of 1268 kg/m^3, and the Helmholtz plane distance was taken as 0.23 nm. Some tests were done as well with aggregated BSA, which was considered to have the same properties as the monomer, except for a larger radius taken arbitrarily at twice the value for the monomer (this could be roughly equivalent to the aggregate of 8 BSA monomers if they were hard spheres). The membrane was chosen to reject BSA completely, and with an intrinsic resistance of $2 \cdot 10^{13}$ m^{-1} and a surface area of 1 m^2.

The standard operating conditions chosen were a feed BSA concentration of 1g/L, a Trans-Membrane Pressure of 4 bars, and a runtime of 2 hours.

Electroviscous effects were not taken into account because they did not seem significant in Bowen and Williams' simulations.

4.2.3. PRELIMINARY TESTS ON THE DISJOINING PRESSURE

To help explain the influence on cake deposition of pH, ionic strength and aggregation, we calculated the disjoining pressure as a function of voidage (in solution or in a cake). The following sets of conditions were chosen:

- **BSA monomers, *I*= 0.01M:** zeta potentials tested were 0, -0.02 and -0.04V.
- **BSA monomers, *I*= 0.1M:** zeta potentials tested were 0, -0.02 and -0.04V.
- **BSA monomers, *I*= 0.5M:** zeta potentials tested were 0, -0.02 and -0.04V.
- **BSA aggregates (radius 5.94 nm), *I*= 0.01M:** zeta potentials tested were 0, -0.02 and -0.04V.

Results were reported in figures 4.6 a) and 4.6 b) below.

Fig. 4.6 a)

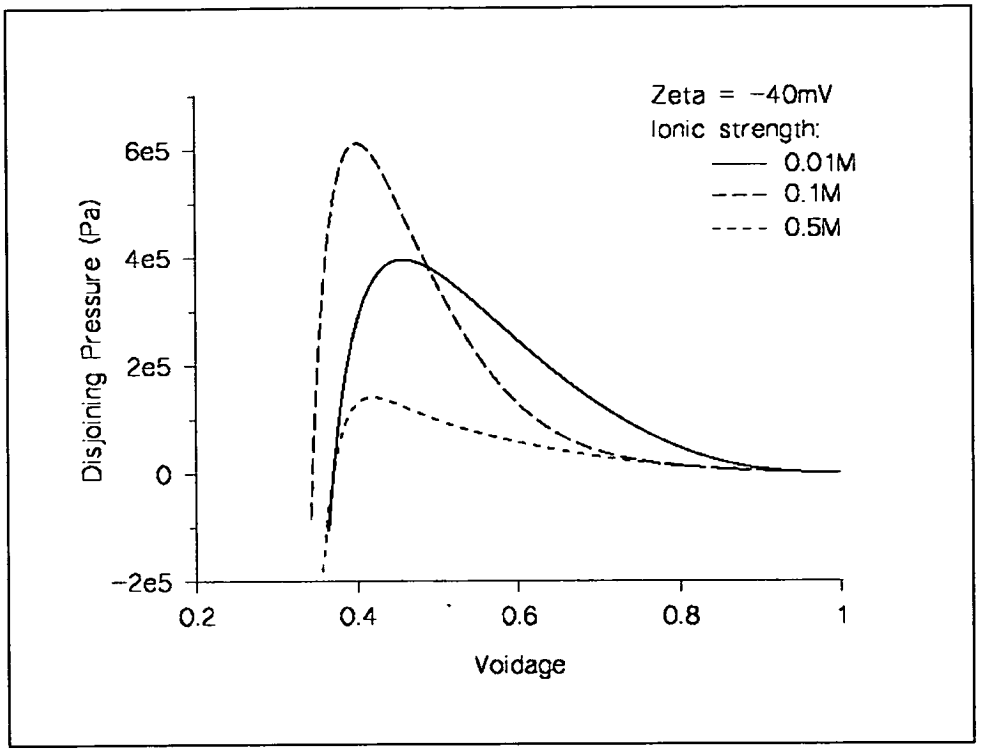

Fig. 4.6 b)

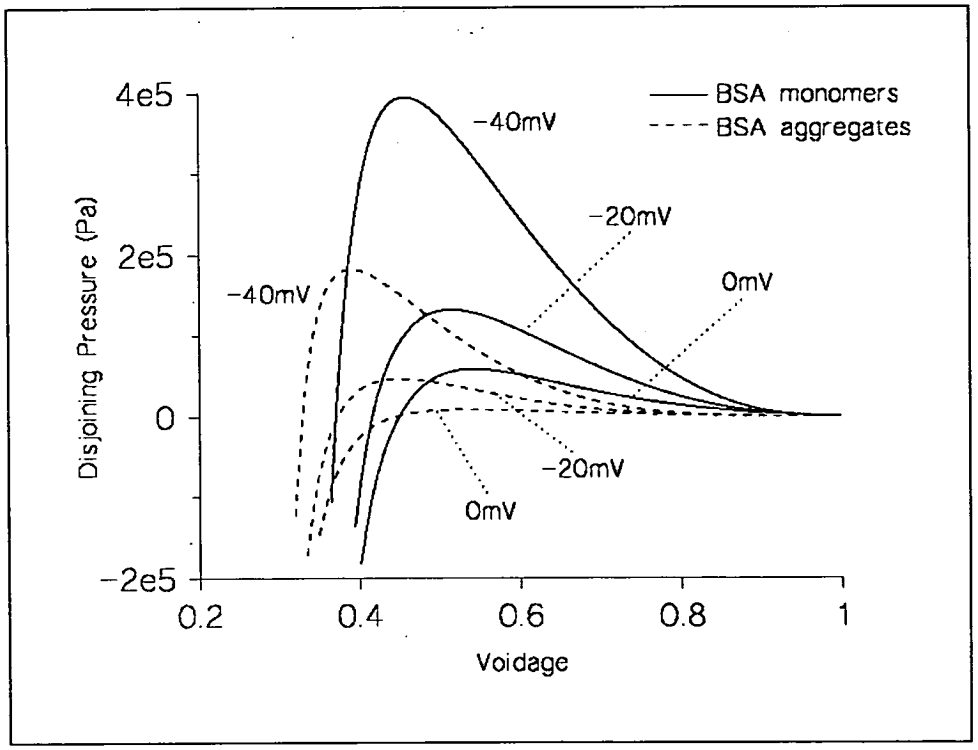

Fig. 4.6 a), b): *Results from simulations 4.2.3 on osmotic pressure profiles for BSA.* ***Fig. 4.6 a)*** *shows the influence of ionic strength for BSA monomers, for ζ= 40 mV.* ***Fig. 4.6 b)*** *shows the influence of aggregation for different zeta potentials (I=10mM).*

4.2.3.1. Influence of ionic strength

Fig. 4.6 a) shows clearly the influence of ionic strength on the value of the maximum disjoining pressure (P_{Dmax}), and the cake voidage for which it occurs. It appears that:

-The value for the maximum P_D first increases with increased ionic strength (from 0.01M to 0.1M in *Fig. 4.6 a)*). At first, this result seems to go against the commonly recognised result that proteins do coagulate more easily in a more saline environment ("salting-out" effect). However, the same trend can be found elsewhere in the Literature on colloids (see Overbeek, 1952). Moreover, disjoining pressures at 0.01M are still higher than at 0.1M over most of the range for voidage values.

-The value for the maximum P_D then decreases sharply with increased ionic strength (from 0.1M to 0.5M).

The initial increase in P_{Dmax} was found to be due to a double effect of the electrolytes in solution when their concentration is increased. Away from a charged colloidal particle, where the short-range attractive forces are quasi-absent, they dampen the long- range repulsive electrical forces. However, closer to the particle, these repulsive forces are less affected than the short-range attractive forces, which are diminished by retardation and screening, and the overall effect is therefore an increased repulsion.

These results are extremely important in interpreting the extent of permanent fouling in dead-end filtration: The maximum disjoining pressure is in fact the critical pressure, above which the solute lattice forms a compact cake of permanent fouling. For concentrations below that corresponding to P_{Dmax}, reversibility is expected, *i.e.* the cake should redissolve into the solution if the pressure is no longer exerted. For concentration above that for P_{Dmax}, the cake will remain coagulated even if the pressure is removed. Therefore, an operating pressure higher than P_{Dmax} eventually leads to permanent fouling.

4.2.3.2 Expected influence of aggregation

In the light of what has been said in section 4.2.3.1, *Fig. 4.6 b)* seems to explain why aggregates can dramatically increase the fouling rate (see section 1.3.4.2 b)). Although aggregates consisting only of about 8 BSA units were considered, the maximum disjoining pressure was found to be much decreased when compared to the monomers - e.g. from 4 bars to less than 2 at ζ = -40 mV, hence coagulation should be easier.

4.2.4 TESTS ON THE FLUXES AND CAKE VOIDAGES

4.2.4.1 Influence of ionic strength on cake voidage

For each of the two following simulations, a given zeta potential was set (-30 mV and -50 mV), and different ionic strengths were tested: 0.01, 0.15, and 0.25M. t/V was then plotted against V, where t is the running time after the start of the filtration and V the total volume of permeate collected. Also plotted for each simulation was the change with time of the cake voidage at the membrane surface (ε), and the disjoining pressure profile for BSA monomers as a function of the cake voidage.

4.2.4.1.a) zeta = -30 mV;

4.2.4.1.b) zeta = -50mV;

Fig. 4.7 a)

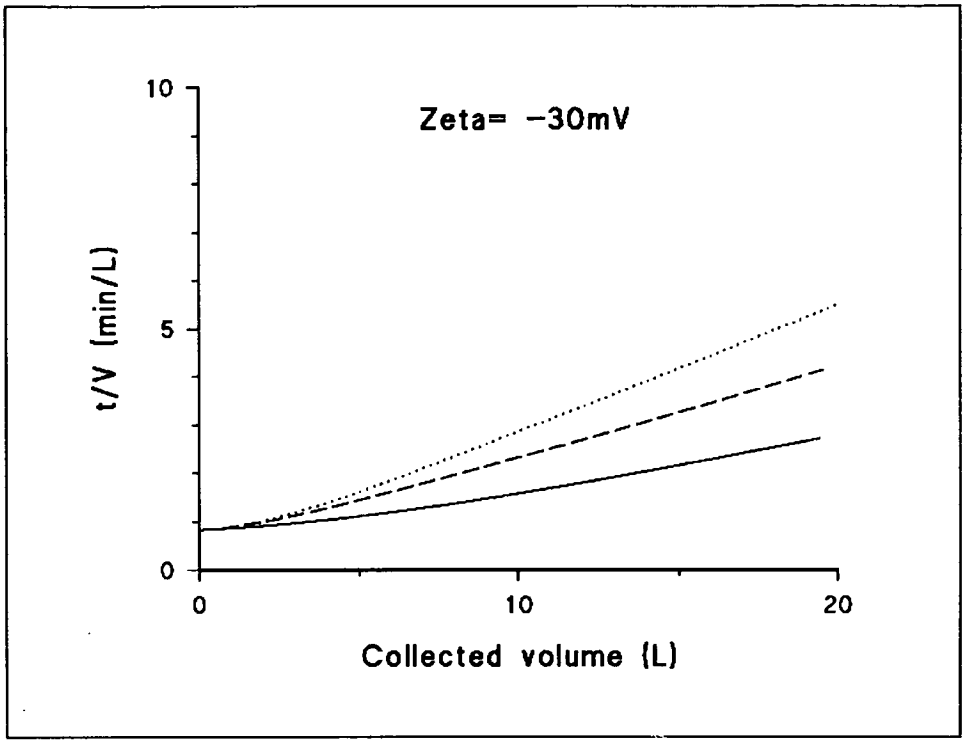

Fig. 4.7 b)

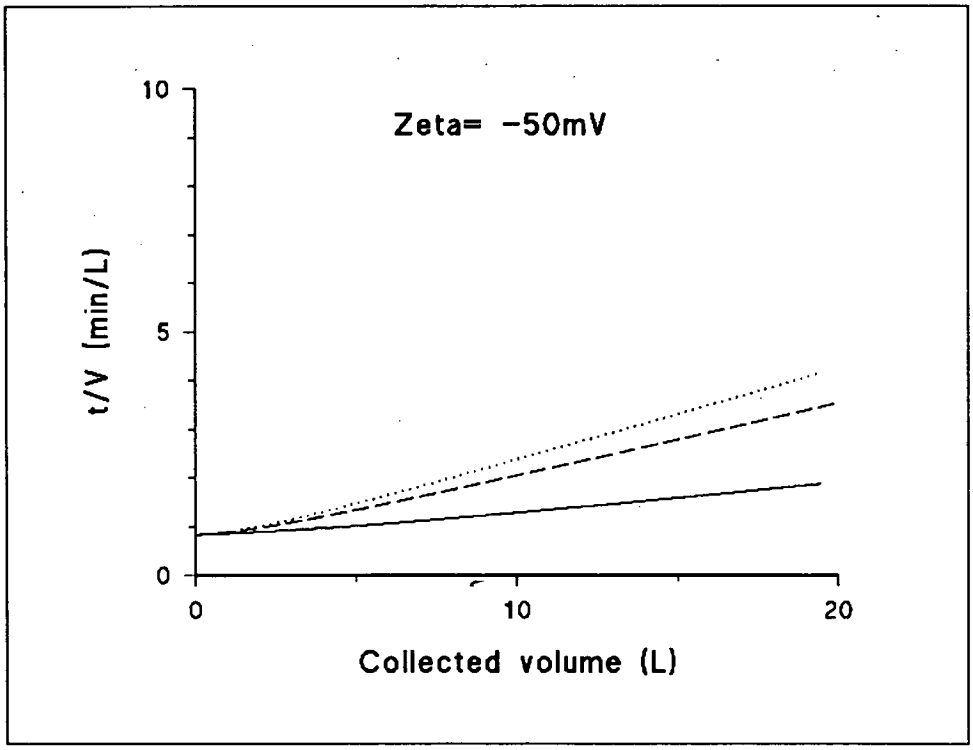

***Fig. 4.7 a) and b)**: filtration time over collected volume V during the dead-end filtration of BSA at ζ = -30 (4.7 a)) and -50mV (4.7 b)).*
***Key:** (Ionic strengths) —— 0.01M; ------- 0.15M; ····· 0.25M;*
***Conditions:** TMP = 4 Bars, $R_m = 2 \cdot 10^{13}\ m^{-1}$, $A_m = 1\ m^2$, total rejection.*

Fig. 4.8 a)

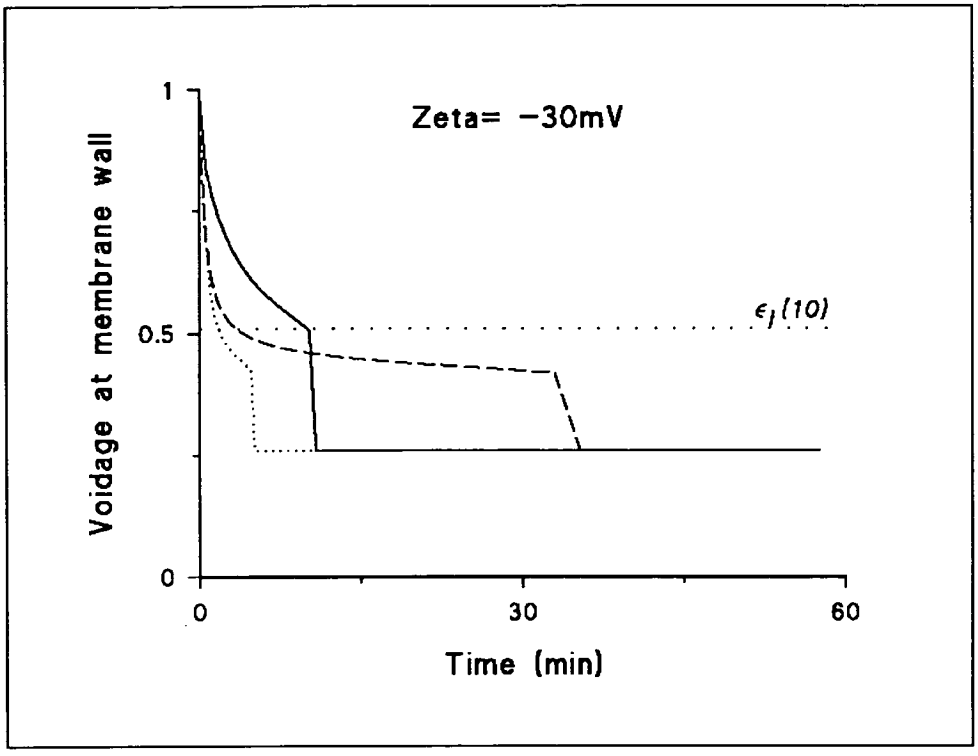

Fig. 4.8 b)

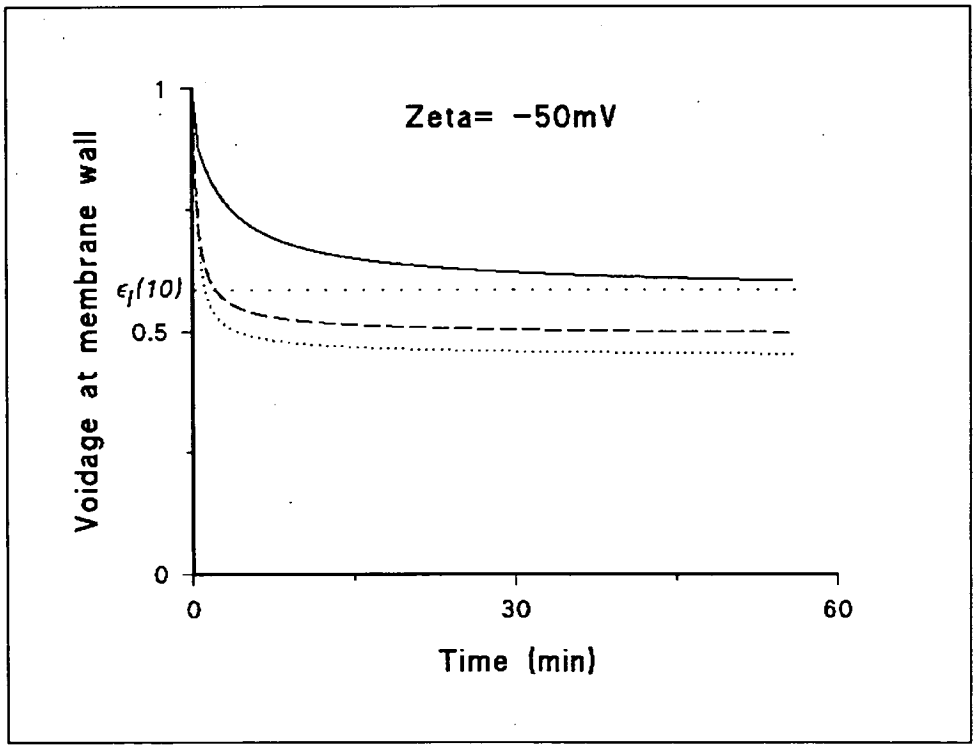

Fig. 4.8 a) and b): *cake voidage at the membrane surface during the dead-end filtration of BSA at ζ = -30 (4.8 a)) and -50mV (4.8 b)).*
Key: *(Ionic strengths) —— 0.01M; ------- 0.15M; ····· 0.25M;*
Conditions: *Same simulations as those presented in Fig. 4.7 a) and b).*

Fig. 4.9 a)

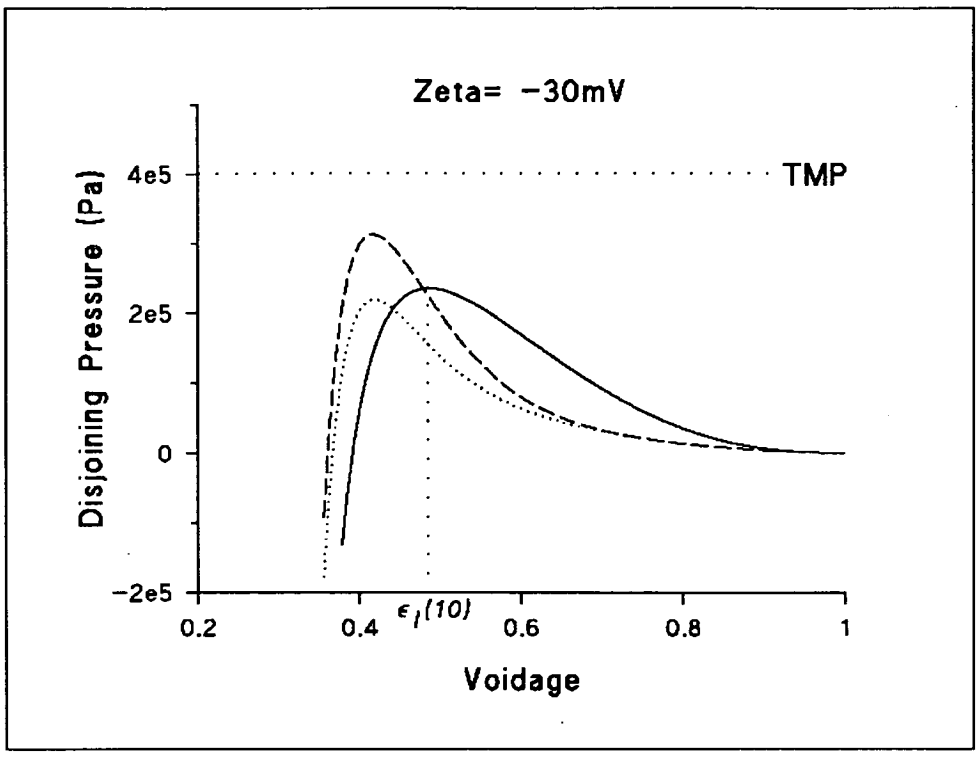

Fig. 4.9 b)

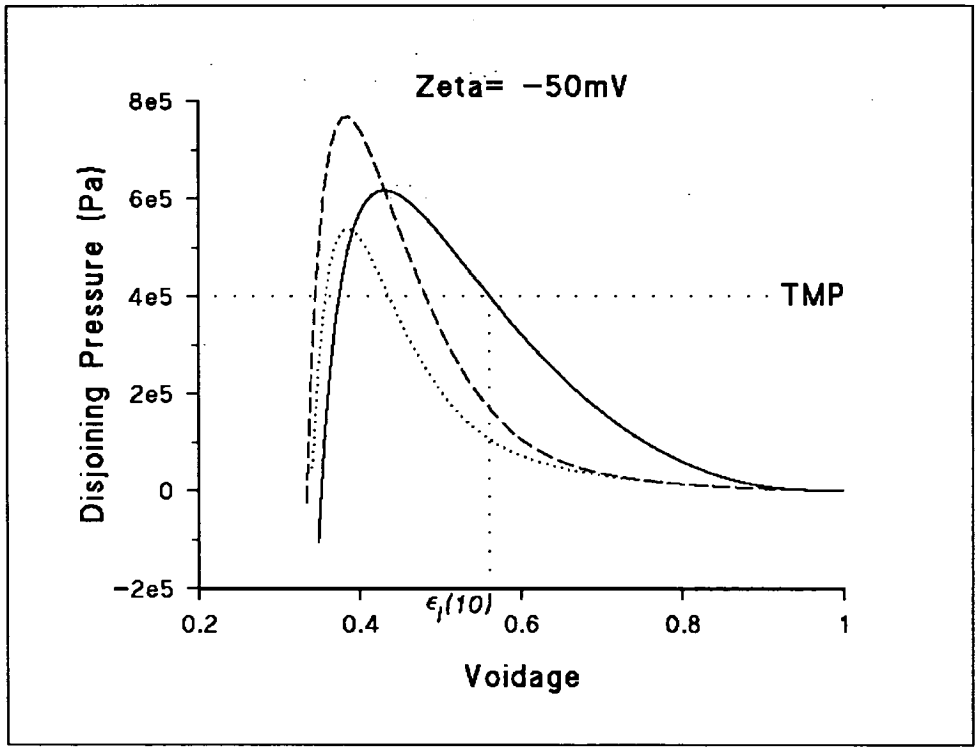

Fig. 4.9 a) and b): *disjoining pressure as a function of cake voidage, at* ζ *= -30 (4.9 a)) and -50mV (4.9 b)).*
Key: *(Ionic strengths) —— 0.01M; ------- 0.15M; ····· 0.25M;*
Conditions: *Same simulations as those presented in Fig. 4.7 a) and b).*

4.2.4.2 Sudden coagulation to a compact cake

In order to be interpreted, *Fig. 4.7* and *4.8* require consideration of Eq. (2.37):

$$P_2 + P_{D,2} = TMP,$$

in which P_2 is the hydraulic pressure at the membrane surface, and $P_{D,2}$ is the disjoining pressure there. *TMP* is constant throughout the filtration. When the filtration starts, $P_2 \approx TMP$ and $P_{D,2}$ is very low. As the filtration proceeds, the solute is getting concentrated at the membrane surface, and $P_{D,2}$ increases while P_2 decreases. Several outcomes are then possible:

-If the maximum disjoining pressure P_{Dmax} for the system is higher than the *TMP*, then an equilibrium will be reached. This is the situation described in *Fig. 4.7 b), 4.8 b) and 4.9 b)*, which all refer to the same BSA solution at $\zeta = -50$ mV: the high zeta potential results in $P_{Dmax} > TMP$ for all three ionic strength (*Fig. 4.9 b)*). For instance, for $I = 0.01$M, $P_{Dmax} = TMP$ for $\varepsilon = 0.55$. This value, noted $\varepsilon_l(10)$, is also the limiting value shown in *Fig. 4.8 b)* for the minimum possible value of the cake voidage during dead-end filtration in those conditions. *Fig 4.8 b)* also shows that ε_l decreases with increasing ionic strength.

-*Fig. 4.8 a)* demonstrates what happens when, on the contrary, $TMP > P_{Dmax}$, at the lower zeta potential of - 30mV. In this case, for all three ionic strengths considered, values for P_{Dmax} are lower than the applied *TMP* (*Fig. 4.9 a)*). In *Fig 4.8 a)*, at some point during the filtration, the cake voidage at the membrane surface suddenly collapses to the tightly-packed configuration ($\varepsilon = 0.26$). The value ε_l reached by ε just before this compaction corresponds to P_{Dmax}. As a function of the ionic strength, the timing of this sudden compaction during the filtration seems to depend on the actual value of P_{Dmax}. At an intermediate ionic strength (0.15 M), compaction occurs after more than 30 min, as opposed to 12 min for low ionic strength (0.01M) and 6 min for high ionic strength (0.25M). This seems to be linked to the particular shapes of the disjoining pressure characteristics, as mentioned in section 4.2.3.1: P_{Dmax} at 0.01M is higher than at 0.15M, and also occurs at a lower voidage - allowing more time to the loose cake to build-up before ε_l is reached.

4.2.5 CONCLUSIONS

It was predicted that a sudden cake compression leading to a tightly bound, irreversible fouling layer, could occur at some stage during the dead-end filtration, provided that the applied transmembrane pressure was greater than the maximum disjoining pressure for the protein in the given conditions of pH and ionic strength. This result was obtained shortly before Harmant and Aimar (1996) published their results on dead-end filtration with full rejection of latex particles in a stirred-cell. Their model considered the balance between drag-forces and surface forces onto a particle, and simulated the cake build-up by incrementing the addition of every single layer of the cake, instead of incrementing the running time of the experiment. They too found that there were critical conditions in which a compact, tightly-bound cake could deposit, and that a critical mass of cake had to build-up before this could occur.

This was confirmed, in the present work on monomeric BSA, by the limiting value of the cake voidage, ε_l, which had to be reached before compaction occurred. As expected, the time taken for this to occur was found to increase with the zeta potential (results not reported here). More surprisingly, this value was also found to present a maximum when the ionic strength of the solution was increased: an intermediate ionic strength seemed to present the longest running time without coagulation. Whenever dead-end filtration with periodic back-flushing is used in an industrial process, this result can be used to maximise running time without creating a tightly bound, hard to remove deposit.

Preliminary simulation results on the disjoining pressure of aggregates also suggested that polymeric BSA was much more easily precipitated into a compact cake due to a lower maximum disjoining pressure.

4.3. COMBINED DEPOSITION AND CONCENTRATION POLARISATION

4.3.1. SIMULATION OF AMICON H1P30-20 CARTRIDGE

4.3.1.1: Programme and parameters:

A C-programme was written according to the equations, principles and algorithm discussed in section 2.4. The same H1P30-20 model of cartridge was used as in section 4.1.6, where its geometric characteristics can be found.
However, this time the solution used for the simulation was one of monomeric BSA at 1g/L at 25 °C. Also, the following assumptions were made:

-pH had an influence (through the zeta potential), and also the ionic strength. Diffusivity and osmotic pressure depended on the local concentration, the pH, and the ionic-strength.

-Viscosity depended on concentration. Kozinski and Lightfoot (1972) found

$$\mu = 10^{-3} / (1.11 - 5.42 \cdot 10^{-3} c + 6.71 \cdot 10^{-6} c^2),$$

with c in g/L and μ in Pa·s. This correlation was obtained from experimental values of up to 450 g/L, at 25 °C.

-Intrinsic membrane resistance and inlet flow-rate were taken from our own experimental data on buffer filtration rates (see *Tables 4.5* and *4.6* in section 4.3.2.1): They depended on the operating *TMP*.

-The losses in permeate flux due to direct interaction between the membrane and the BSA (i.e. due to adsorption) were assumed to be negligible.

-Steady state was assumed.

For each of the following values of the ionic strength: 0.022M, 0.22M and 2.2M, four different values of the zeta potential were tried: 0, -0.01, -0.02 and -0.04V. In each case, the four following values for the *TMP* were used: 7600, 36000, 71000 and 100000 Pa. The choice of 0.022M for the value of the ionic strength stems from the fact that the ionic strength of a 0.01M solution of PBS at pH 7 is 0.022M, and that we used this concentration, and also 0.1M and 1M, in our experiments (see section 4.7).

Numerical results from simulations in this section 4.3 were reported in Appendix V (for permeate fluxes and mass balance factors) and Appendix VI (for resistance and thickness of the deposits along a fibre). As can be seen in Appendix V, all simulations yielded correct mass-balance factors (between 0.990 and 1.000).

4.3.1.2 Typical diffusivity profile

When plotting diffusivity against concentration according to the generalised Stokes-Einstein law, profiles with several local maxima were typically obtained (for $\zeta \neq 0$). The following graph is an example of such profiles:

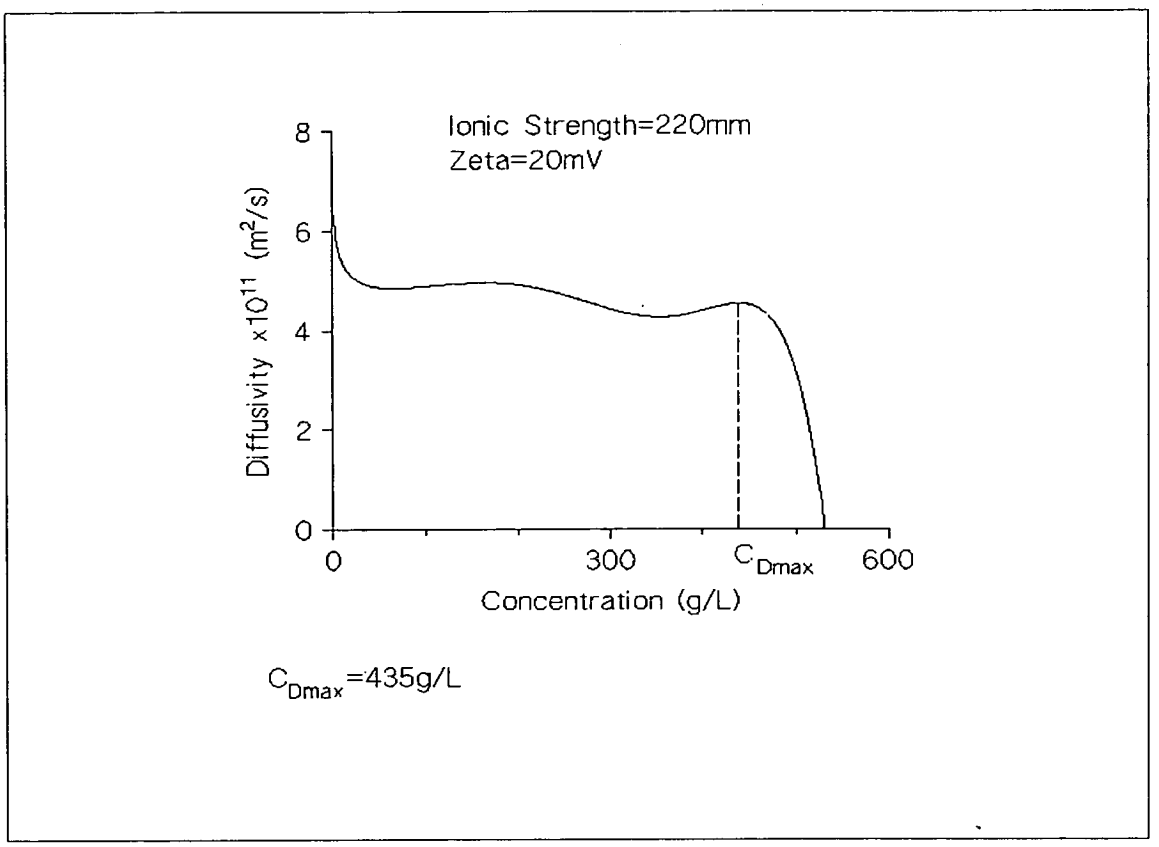

Fig 4.10: Example: *Diffusivity profile of BSA monomers used in simulation 4.3.3.2 at zeta=20mV.*

4.3.1.3: Typical wall concentration and permeate flux profile along a fibre

Fig. 4.11 shows a typical example of wall concentration profile modelled for a cross-flow filtration, in which tightly packed cake deposition was considered. The graph shows coagulation occurring when the wall concentration was about to reach a value corresponding to the highest-concentration local maximum for the diffusivity (c_{Dmax}). In other simulations for different conditions, this value was actually exceeded by a few %. This can be easily understood when considering the rather "flat" shape of the maximum, as seen for instance in *Fig. 4.10*: The situation presented in *Fig. A1.4* in Appendix I, where the solution lies between c_{Dmax} and the concentration for the maximum osmotic pressure $c_{\pi max}$, is likely to occur.

It should be noted that the other coagulation factor mentioned in section 2.4.7.6 did not seem to have a direct influence. The maximum value for the wall velocity v_{dyn} (from the balance of forces onto one particle) was never exceeded by the computed wall-

permeate flux. This is because the balance of forces that was considered applied only to particles at the membrane surface, with no axial velocity (i.e. in Dead-End mode).

Therefore, coagulation occurred due to the build-up of solutes from the transport equation, in the immediate vicinity of the membrane rather than at the membrane wall itself. The concentration at which this happened could not be determined in a simple fashion, but was always equal to or a few per cent higher than c_{Dmax}.

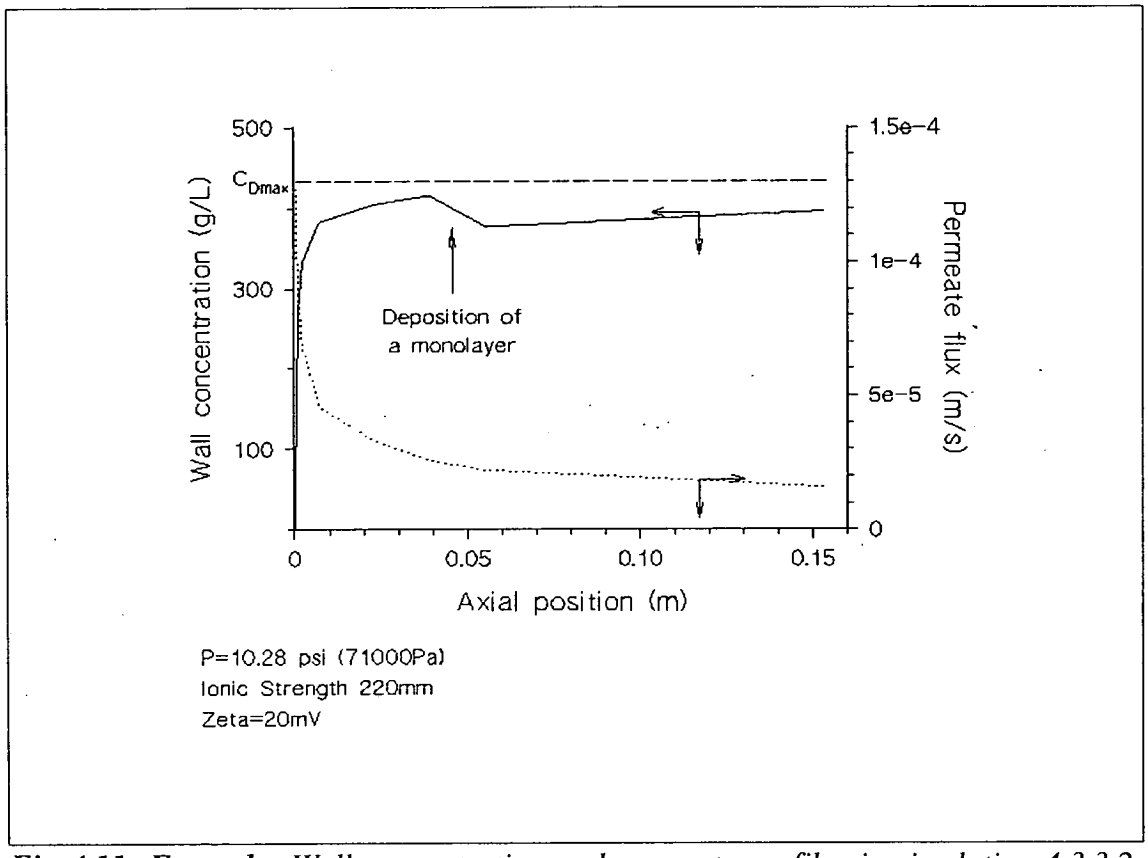

Fig 4.11: Example: *Wall concentration and permeate profiles in simulation 4.3.3.2 at zeta = -20mV. A monolayer of protein was assumed to deposit at this point, and also downstream along the remaining length of the fibre. In other examples, several monolayers could deposit on top of each other.*

4.3.2 EXPERIMENTS WITH H1P30-20 CARTRIGE

The same cartridge was used as in 3.2.2 and 4.1.6, and its geometric characteristics can be found in section 4.1.6. In all experiments, the temperature was set at 25 °C, and for BSA filtration the feed concentration was 1g/L.

4.3.2.1 Buffer cross-flow filtration

PBS buffer concentration was 0.01M, 0.1M or 1M, and the pH was 5, 7 or 9. The average cross-flow rate was defined as the average between the inlet flow-rate and the outlet flow-rate (on the lumen side). We aimed to keep the same average cross-flow rate in the fibre lumen, in spite of running experiments with very different *TMP*'s. Because of heavy losses of permeate with H1P30-20, this was possible only by increasing the inlet flow rate when testing higher *TMP*'s. The following table reports the inlet and average values for the different inlet pressure. It shows that the average cross-flow rate was 345 ml/min ± 33% for all experiments.

Inlet Pressure (Pa)	Permeate flow rate (1) (ml/min)	Outlet flow rate (2) (ml/min)	Inlet flow rate = (1)+(2) (ml/min)	Average flow rate ((2)+(3))/2 (ml/min)
7600	91	280	370	325
36000	260	120	380	280
71000	370	130	500	315
100000	480	220	700	460

***Table 4.5**: Inlet pressures and flow rates with buffer.*

The next table reports the values for the intrinsic membrane resistance r_m as a function of the operating pressure: r_m was found to increase with the TMP - possibly because of electro-osmotic effect of the buffer ions through the membrane pores (see section 2.4.4).

Inlet Pressure (Pa)	Intrinsic Resistance with PBS, r_m (Pa.s / m)
7600	$2.16 \cdot 10^8$
36000	$4.50 \cdot 10^8$
71000	$5.60 \cdot 10^8$
100000	$6.90 \cdot 10^8$

***Table 4.6**: Inlet pressures and intrinsic resistances.*

4.3.2.2 Experiments with BSA 1g/L

Each experiment was run in three phases:

-**Step1:** Buffer filtration at 4 successive TMP's: 7600, 36000, 71000, 100000 Pa (see 3.5.1);

-**Step2:** BSA solution (1g/L) in the same buffer and at a given TMP, **for 2 hours** (see 3.5.3);

-**Step 3:** Rinsing of the membrane with the same buffer, repeating the first step (see 3.5.5).

Permeate flow rates were recorded throughout. Rejection ratio was controlled during BSA filtration (see 3.5.4).

For each experiment, the buffer used in the three phases had the same ionic strength and the same pH.

4.3.2.3. Experiments with BSA 1g/L in PBS buffer at

-0.1M

-pH =7

As described in 4.3.2.2, with the following TMP's:

4.3.2.3 a): TMP=7600 Pa;

4.3.2.3 b): TMP=36000 Pa;

4.3.2.3 c): TMP=71000 Pa;

4.3.2.3 d): TMP=100000 Pa;

4.3.2.4. Experiments with BSA 1g/L in PBS buffer at

-0.01M

-pH =7

As described in 4.3.2.2, with the following TMP's:

4.3.2.4 a): TMP=7600 Pa;

4.3.2.4 b): TMP=36000 Pa;

4.3.2.4 c): TMP=71000 Pa;

4.3.2.4 d): TMP=100000 Pa;

4.3.2.5. Experiments with BSA 1g/L in PBS buffer at

-1M

-pH =7

As described in 4.3.2.2, with the following TMP's:

4.3.2.5 a): TMP=7600 Pa;

4.3.2.5 b): TMP=36000 Pa;

4.3.2.5 c): TMP=71000 Pa;

4.3.2.5 d): TMP=100000 Pa;

4.3.2.6. Experiments with BSA 1g/L in PBS buffer at

-0.1M

-TMP = 71000 Pa

This time, the pH was the studied parameter.

4.3.2.6 a): pH =7 (duplicating 4.3.2.3 c));

4.3.2.6 b): pH =5 (made in duplicate);

4.3.2.6 c): pH =9 (made in duplicate);

4.3.2.7. Experiments on *static adsorption* with BSA 1 g/L

This time, the impact of static adsorption on the permeate flux was studied at the 3 different pH's: No back pressure was imposed onto the cartridge, and we tried to achieve a nil permeate flow rate. At first, we intended to set the inlet flow rate at 345 ml/min, which was the average value in all our dynamic experiments. However, this resulted in a permeate flux due to the pump head pressure and the piping. Therefore, the inlet flow-rate was set at 120 ml/min, which resulted in no significant positive pressure in the fibre lumens, and which also ensured the fibres would not dry up. The three following experiments were carried out:

4.3.2.7 a): PBS buffer at 0.1M, pH =7;
4.3.2.7 b): PBS buffer at 0.1M, pH =5;
4.3.2.7 c): PBS buffer at 0.1M, pH =9;
4.3.2.7 d): PBS buffer at 0.01M, pH =7;
4.3.2.7 e): PBS buffer at 1M, pH =7;

4.3.3 RESULTS ON H1P30-20 CARTRIDGE

4.3.3.1 Steady state, rejection ratio and flux decline in experiments

Fig. 4.12 a) and *b)* show that the cross-flow filtration experiments with BSA was observed to reach quasi steady-state after 2 hours, which is when values for the total resistance to flux and for the permanent fouling resistance (or deposited resistance) were measured.

Fig. 4.13 a) and *b)* show that the rejection ratio for most experiments was greater than 95%, except at the start of experiments with 1M PBS: during the first 30 min of the filtration of BSA 1g/L in 1M PBS, the rejection ratio increased from 72% to 89%. However, the corresponding reduction in flux during that period was only from 92 to 86 $L \cdot hr^{-1} \cdot m^2$, for a steady-state value of 82 $L \cdot hr^{-1} \cdot m^2$. It was therefore decided to neglect the internal fouling that probably did occur during that period.

Fig. 4.12 a)

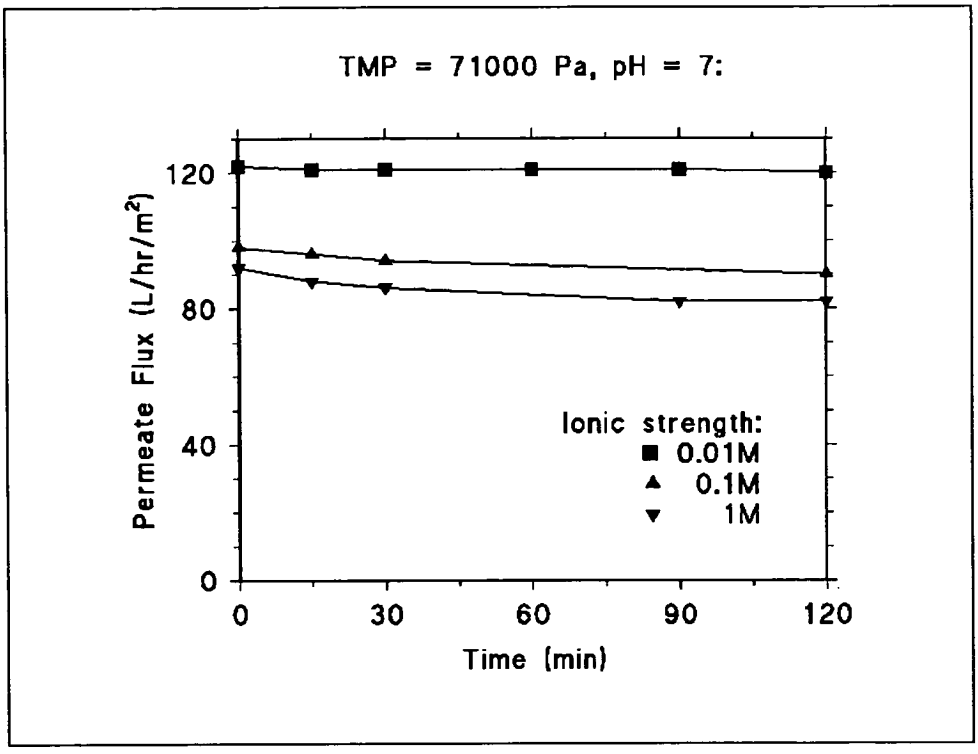

Fig. 4.12 b)

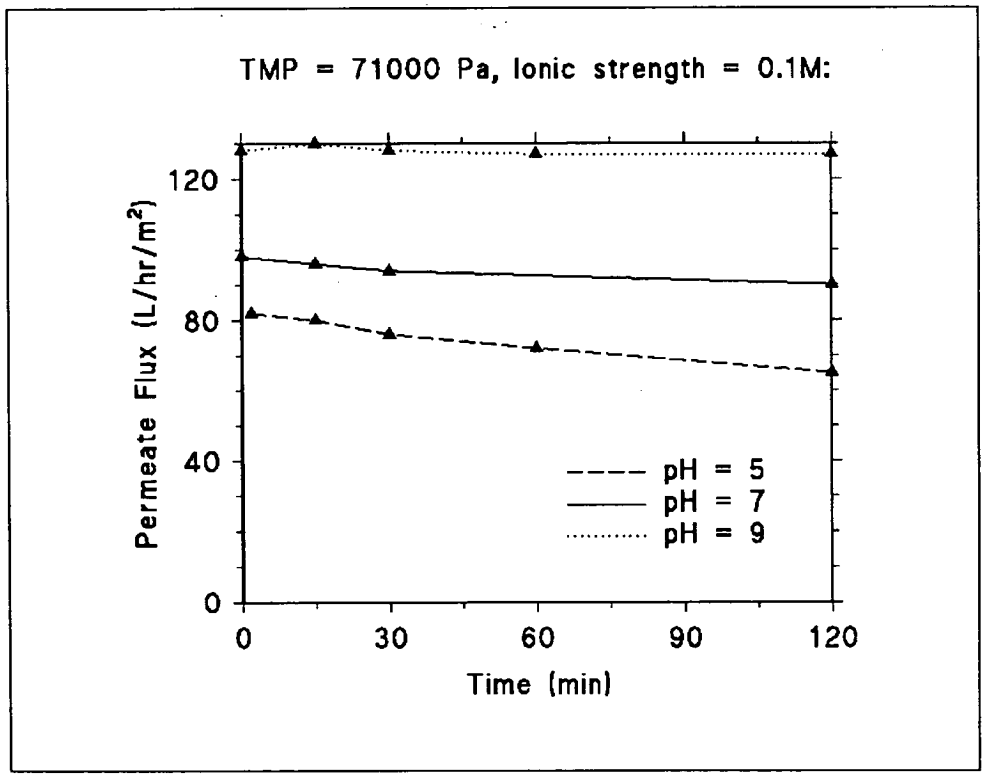

Fig. 4.12: *Permeate flux during the filtration of 1 g/L BSA solutions through H1P30-20 cartridge, at TMP = 71000 Pa and crossflow rate = 345 ml/min.* ***Fig. 4.12 a)*** *shows the effect of ionic strength;* ***Fig. 4.12 b)*** *shows the effect of pH.*

Fig. 4.13 a)

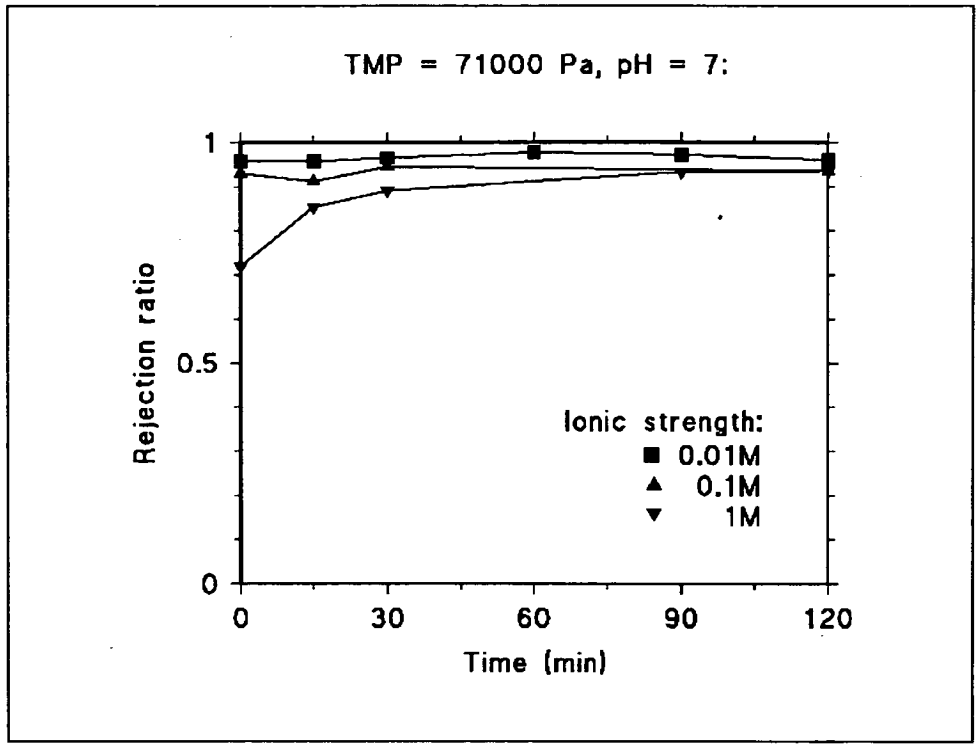

Fig. 4.13 b)

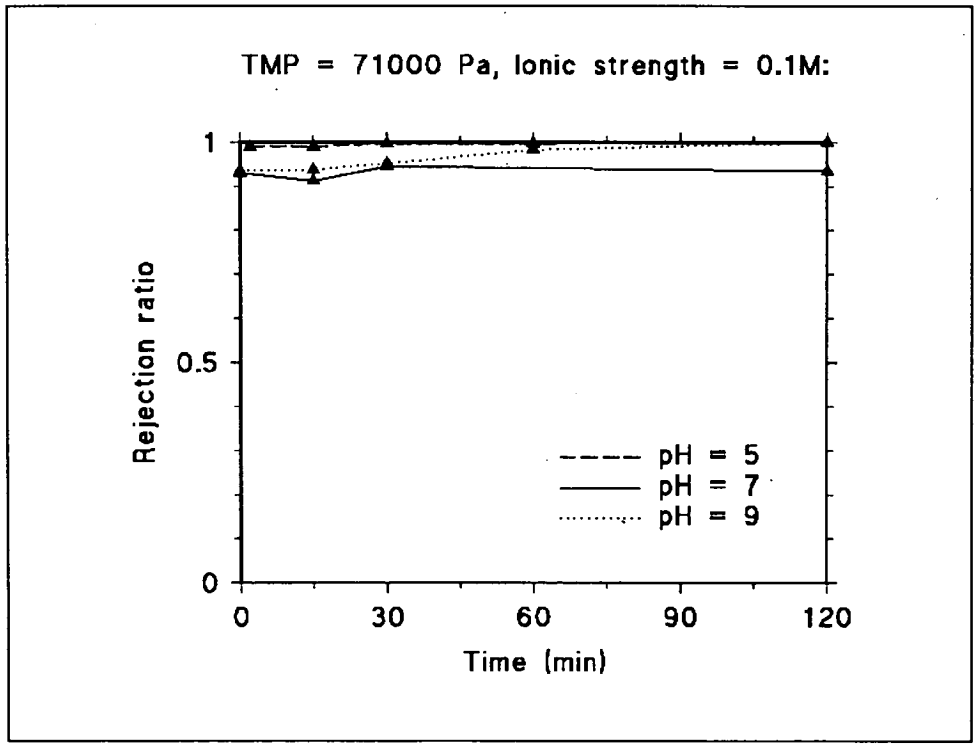

Fig. 4.13: *Rejection ratio during the filtration of 1 g/L BSA solutions through H1P30-20 cartridge, at TMP = 71000 Pa and crossflow rate = 345 ml/min.* ***Fig. 4.13 a)*** *shows the effect of ionic strength;* ***Fig. 4.13 b)*** *shows the effect of pH.*

4.3.3.2 Components of the total resistance to flux during BSA filtration

Numerical results for the experiments are reported in Appendix VII. All resistance values (total, and deposition in static or dynamic conditions) were measured after two hours of BSA filtration, and divided by the intrinsic resistance at the same Transmembrane Pressure (ratio r/r_m , where r_m values are given in *Table 4.6* of section 4.3.2.1).

4.3.3.3 Influence of ionic strength

In the following graphs, the resistances considered are divided by the intrinsic resistance r_m at the same TMP (see *Table 4.6* in section 4.3.2.1).

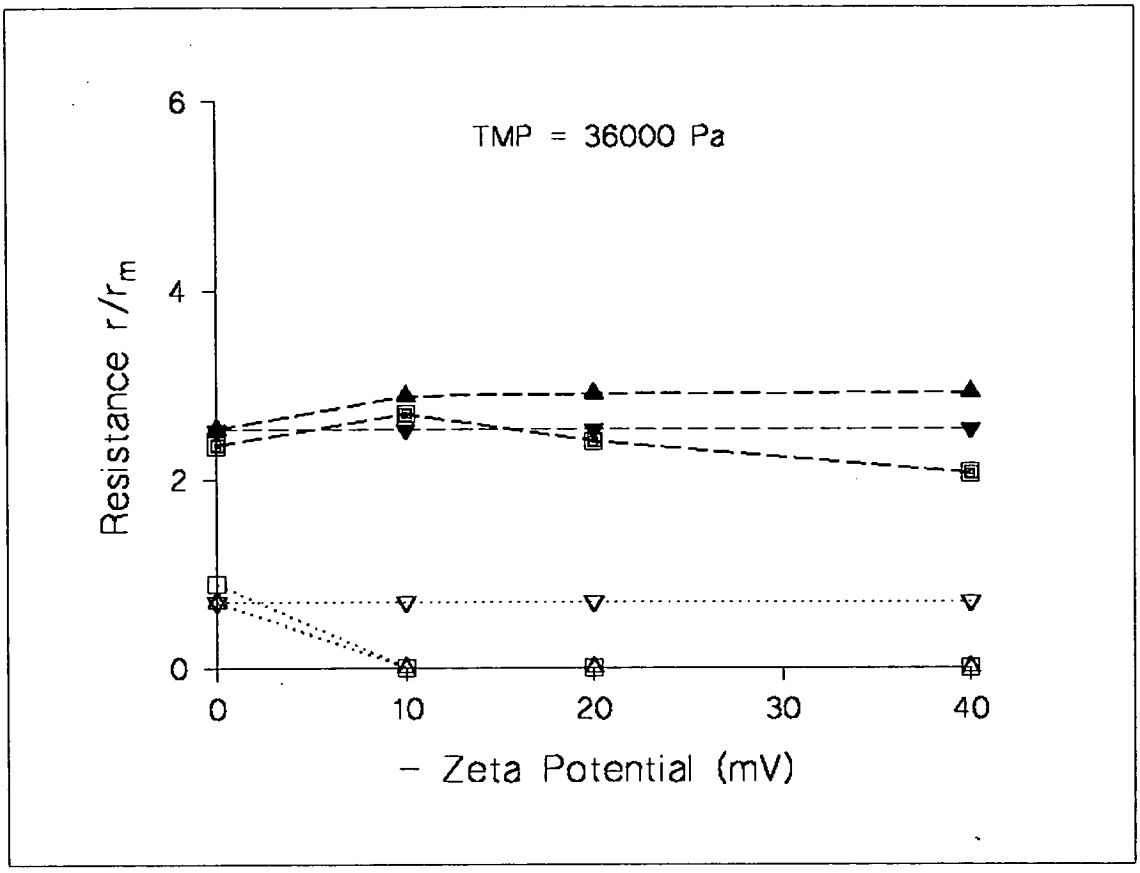

Fig 4.14 a)

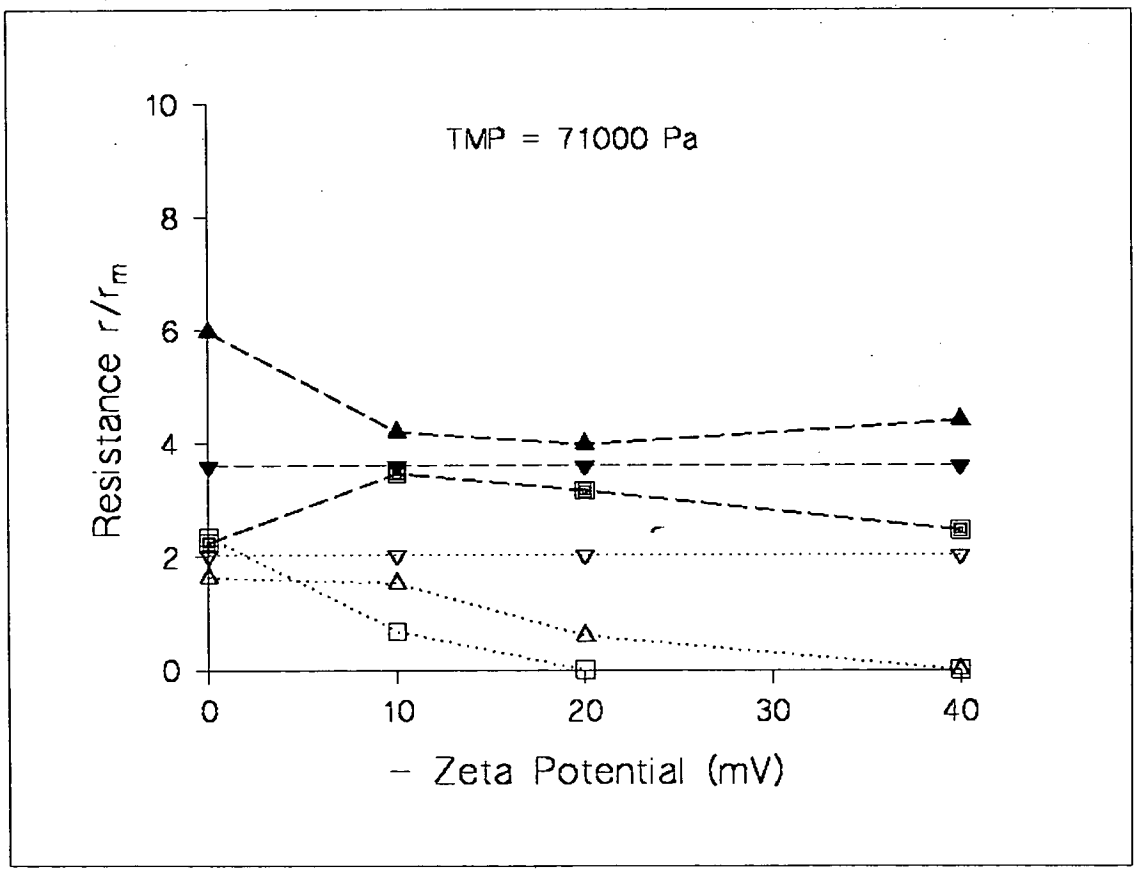

Fig 4.14 b)

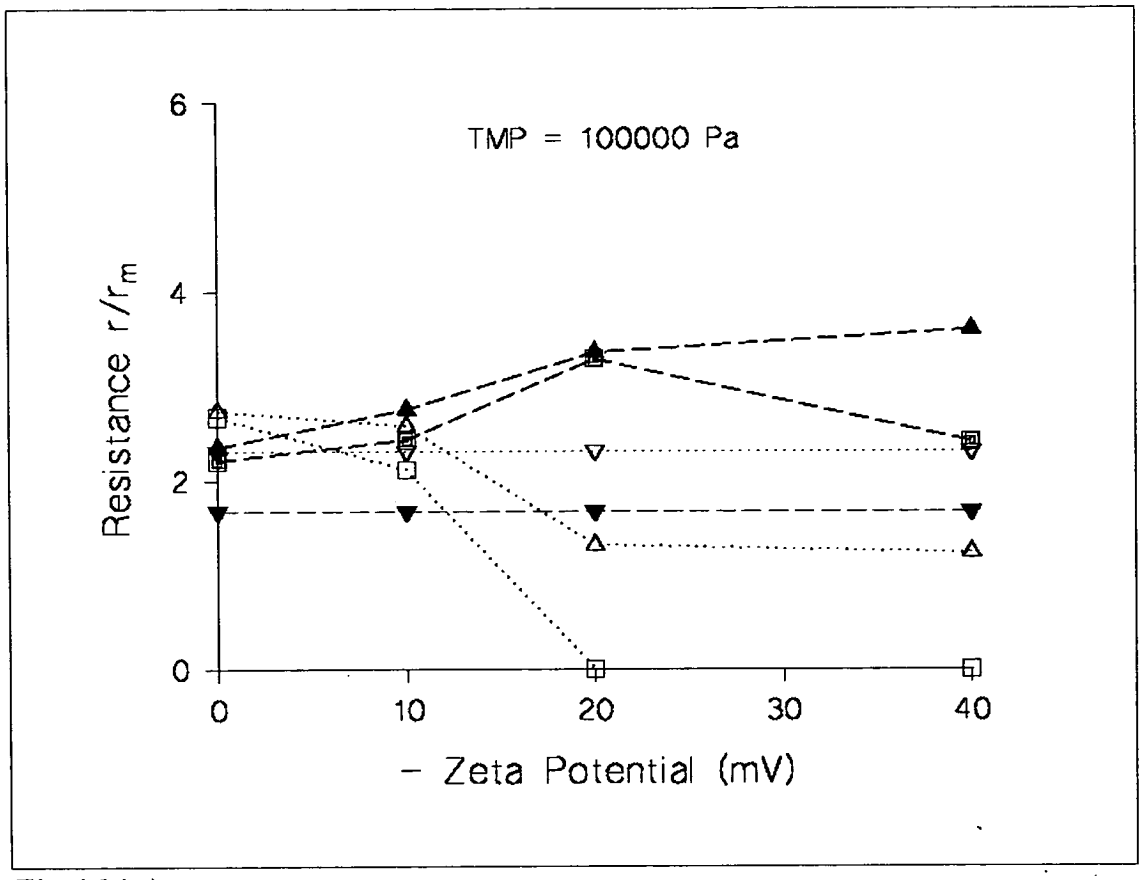

Fig 4.14 c)

Fig 4.14: *Simulations showing the influence of ζ , I, and TMP on the different components of resistance to flux, from simulations 4.3.1.4 (Cross-Flow filtration of BSA 1 g/L with H1P30-20 cartridge, average cross-flow rate = 345 ml/min).*
a): *TMP= 36 kPa;* ***b):*** *71 kPa;* ***c):*** *100 kPa.*
Key for ionic strength: ■ *and* □*: I = 0.022 M;* ▲ *and* Δ*: 0.22 M;* ▼ *and* ∇*: 2.2 M.*
Key for resistances: ····· *Deposition* r_a *(from the cake thickness profile);* ------- *Concentration polarisation* $r_{cp} = r_{total} - r_m - r_a$.

For high zeta potentials (-40 mV ≤ ζ ≤ -20 mV), i.e. away from the protein IEP, simulation showed that deposition increased with ionic strength (*Fig. 4.14 a*) -*c*)). This finding is in accordance with classical results (section 1.3.4.2 d)), and with the experimental results presented here at pH = 7 (away from the IEP for BSA, which is 4.7). All experiments at *I* = 0.02M yielded total and deposition resistances significantly lower than those at *I* = 0.22 and 2.2M, which were similar (*Fig. 4.12 a)* for TMP = 71000 Pa, and *Fig. 4.15* for all pressures). This is due to a screening of the repulsive forces by the electrolyte ions.

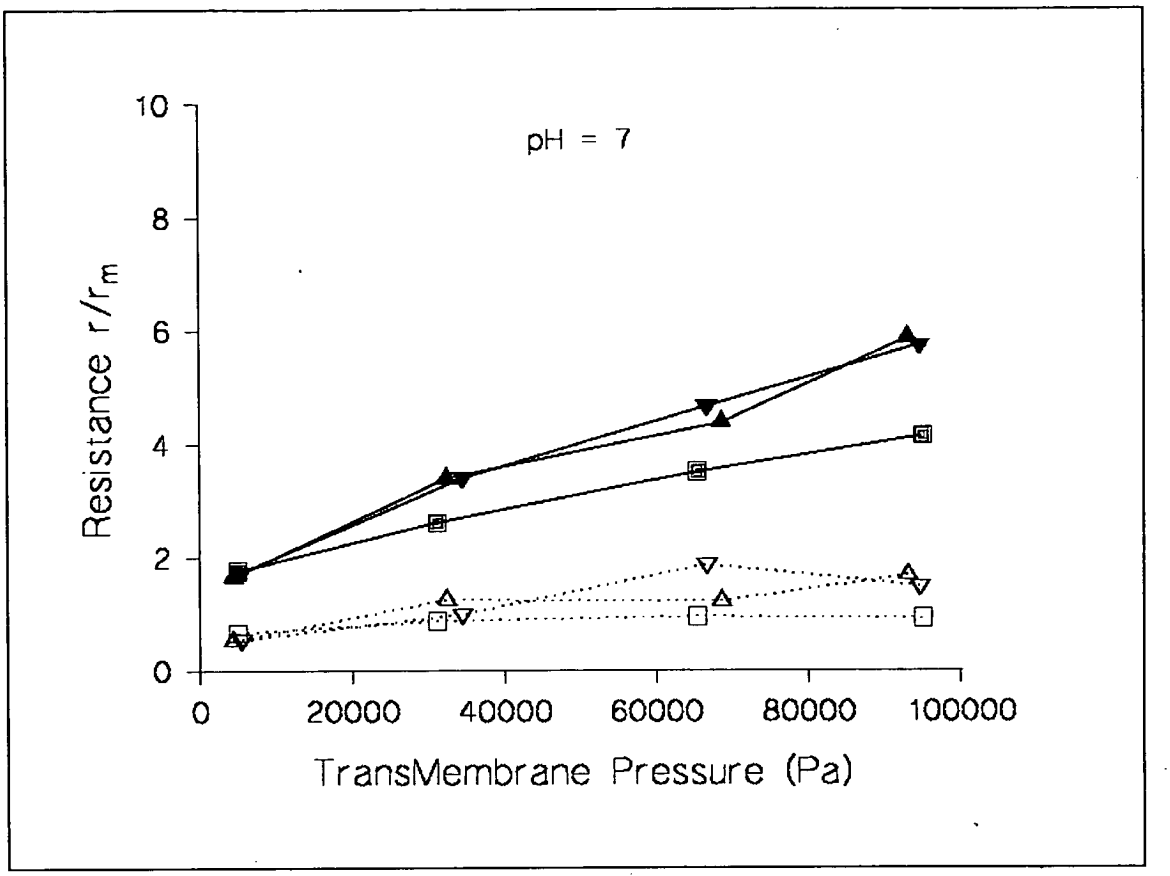

***Fig. 4.15**: Experimental results on the filtration of 1g/L BSA through H1P30-20: influence of I and TMP on the resistance to flux. Conditions: pH=7, cross-flow rate ca. 345 ml/min (Table 4.5) (experiments 4.3.2.3 to 4.3.2.5, i.e. 12 experiments. All resistances were directly measured after 2 hrs of BSA filtration.*
***Key for ionic strength:** ■ and □: I = 0.022 M; ▲ and Δ: 0.22 M; ▼ and ∇: 2.2 M.*
***Resistances:** —— Total resistance r_{total}; ····· Deposition r_a.*

It may be noted that, in *Fig. 4.14 a) - c)*, for ζ = -20 and -40 mV, concentration polarisation decreased when *I* increased from 0.22M to 2.2M. However, this is probably due to a reduction in permeate flux due to heavier deposition.

On the other hand, simulation also showed that, for low zeta potentials (-10 mV ≤ ζ ≤ 0 mV), the amount of deposition was very similar for all ionic strengths. It was, though, lowest at the intermediate ionic strength for *TMP* = 71000 Pa, and the lowest at the highest ionic strength for *TMP* = 100000 Pa (*Fig. 4.14 b)* and *c)*). In *Fig. 4.14 c)*, resistance due to concentration polarisation at the highest ionic strength is also lower than resistances for other ionic strengths. These results are also in accordance with classical experimental results: around the IEP, fouling decreases with *I*. The

interpretation may be, this time, a screening of the attraction forces, which are dominant at low zeta potentials.

However, less deposition may also result in increased concentration polarisation and total resistance: *Fig. 4.14 b)* shows that at $\zeta = 0$, concentration polarisation doubled when I changed from 0.022M to 0.22 M, and this may be due to a decreased deposition allowing a larger and more concentrated polarisation layer.

4.3.3.4 Influence of pH (zeta potential)

As expected (section 1.3.4.2 c)), increasing the zeta potential decreased the amount of deposition, both in simulation (*Fig. 4.14 a) –c)*) and in experiments (*Fig. 4.16*). However, in simulations, a very high ionic strength (2.2M) cancelled-out all effects from ζ, due to the screening of charges. Experiments also showed that concentration polarisation decreased with increased ζ (*Fig. 4.16*, where it represents the gap between deposited and total resistance). However, simulations tended to predict the opposite if deposition decreased with increased ζ: a decrease in deposition allowed higher fluxes, and hence increased concentration polarisation. This can be seen in *Fig. 4.14 a) –c)*, especially for $I = 0.022$M.

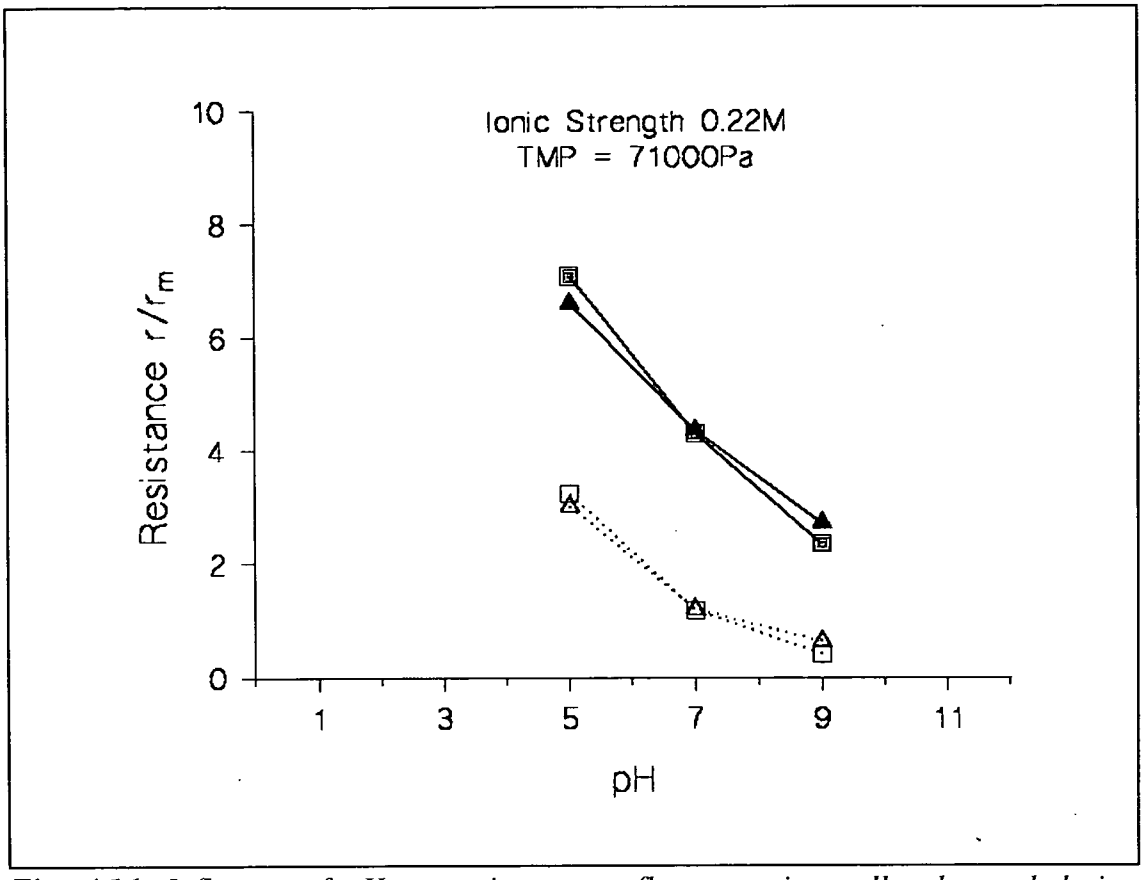

Fig. 4.16**: Influence of pH on resistance to flux, experimentally observed during filtration of 1 g/L BSA through H1P30-20 cartridge (experiments 4.3.2.6, i.e. 6 experiments). All resistances were directly measured after two hours of BSA filtration. (6 experiments). Conditions: I= 0.22M, and average tangential flow-rate=315 ml/min. All resistances were directly measured after 2 hrs of BSA filtration.* ***Key for resistances: *—— Total resistance r_{total}; ····· Deposition r_d.*

4.3.3.5. Critical pressures

The overall range of permeate fluxes predicted by the model seemed in a range in accordance with experimental observations (*Fig. 4.17 and 4.15*). Although the model could overestimate the total resistance to flux by up to 40% (at TMP=71000 Pa), the lack of data relating pH and ζ made comparison difficult.

The model could also be used for predicting critical pressures (see section 1.3.1.3), as shown in *Fig. 4.17*: for ζ = -10 mV, the critical pressure increased when ionic strength was decreased. For I = 0.022 M, deposition was predicted to occur at pressures

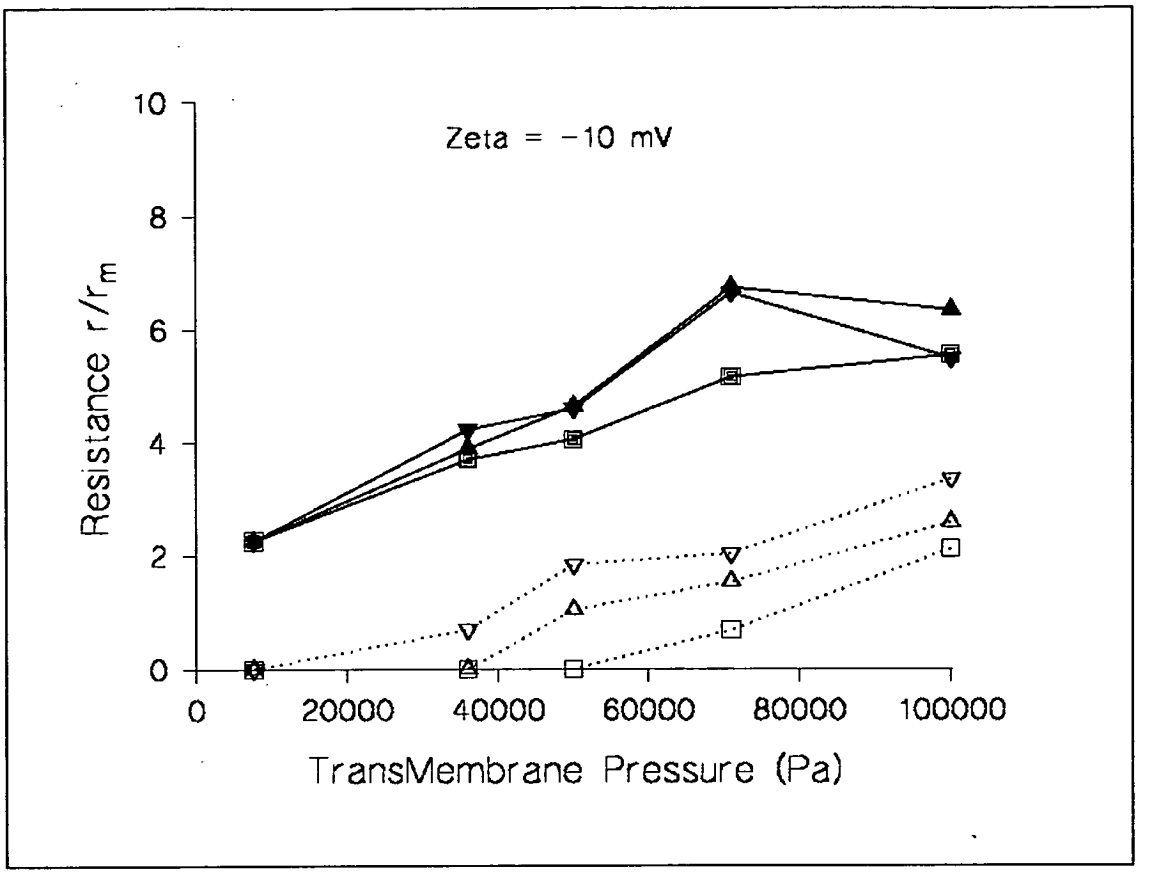

Fig. 4.17: *Total and deposition resistances obtained from simulation runs, for ζ= -10 mV: influence of TMP at various ionic strengths (conditions as in Fig. 4-6).*
Key for ionic strength: ■ *and* □*: I = 0.022 M;* ▲ *and* Δ*: 0.22 M;* ▼ *and* ∇*: 2.2 M.*
Key for resistances: —— *Total resistance* r_{total}*;* ····· *Deposition* r_a *(estimated from thickness profile of the cake along the fibre). (The apparent drop in the ratio* r_{total}/r_m*, from TMP = 71000 Pa to TMP = 100000 Pa at I = 2.2M, seemed to be mostly due to an increase in the intrinsic resistance* r_m *(Table 4.6) combined with a lower flux in the presence of heavier deposition). Intrinsic resistances and cross-flow rates for TMP=50000 Pa were interpolated from Table 4.5 and 4.6.*

between 50000 and 76000 Pa, but this threshold was lowered to between 36000 and 50000 Pa at I = 0.22M, and lower than 36000 Pa at I = 2.2 M.

However, simulation predicted no deposition at the lowest pressure (*TMP* = 7600 Pa) for all zeta potentials and ionic strengths, which was not in accordance with the experimental results reported in *Fig. 4.16*: deposition actually occurred at all *TMP*'s for pH = 7. Even though both simulation and experiments showed deposition increasing with increased *TMP* (*Fig. 4.15* and *4.17*), it was at a slower rate for the experiments,

and only at the higher *TMP*'s (71000 Pa and 100000 Pa) did there seem to be good accordance between experiments and simulation.

-At *TMP* = 71000 Pa, values for the deposited resistance lay between a factor of one and two times r_m, for both the experiments at pH = 7 and all the simulations at -20mV $\leq \zeta \leq$ 0 mV. The total resistances were overestimated by the simulation by up to 40%, with values between 5 and 7 times r_m instead of the values between 3.5 and 5 from the experiments at pH = 7.

-At *TMP* = 100000 Pa, the deposited resistances were overestimated by the simulation, with values between 2 and 3 times r_m instead of the values between 1 and 2 from the experiments at pH = 7. The total resistances were also overestimated, with values between 5 and 7 times r_m instead of the values between 4 and 6 from the experiments at pH = 7.

These problems may point to the absence of a rather major factor in the model: the direct interaction between the membrane and the protein. If direct adsorption accounts for a significant proportion of the fouling resistance, and does develop even for low transmembrane pressures, then, since the model ignores this resistance, it overestimates the permeate flux and hence the concentration polarisation effect associated with it. Thus, it predicts deposited resistances that are too low in the low pressure range, and total fouling resistances that are too high. Moreover, the membrane material, polysulfone, is hydrophobic, and has been reported to strongly modify the shape of BSA molecules adsorbing on it (see section 1.3.4.4). This effect would explain why the observed fluxes were lower than the predicted ones in this work. Another problem may lie in the assumption of a uniform permeate flux through the membrane surface, which certainly does not bear any reality: pores on ultra-filtration membranes are known to be sparsely distributed, resulting in locally high fluxes (*e.g.* Fell *et al.*, 1990).

4.3.3.6 Influence of protein adsorption

Fig. 4.18 and *4.19* compare the fouling resistance of the membrane soaked for 2 hours in 1 g/L BSA solutions in static conditions, with the fouling resistance from cross-flow filtration of 1 g/L BSA after also 2 hours. Clearly, the fouling under static conditions is only a fraction of that obtained under dynamic conditions. However, the static adsorption experiments did not reproduce the high concentrations present at the membrane wall during filtration: static adsorption may still have caused the discrepancies between model and observations reported in the previous section. Therefore, static adsorption experiments should be repeated at high concentrations.

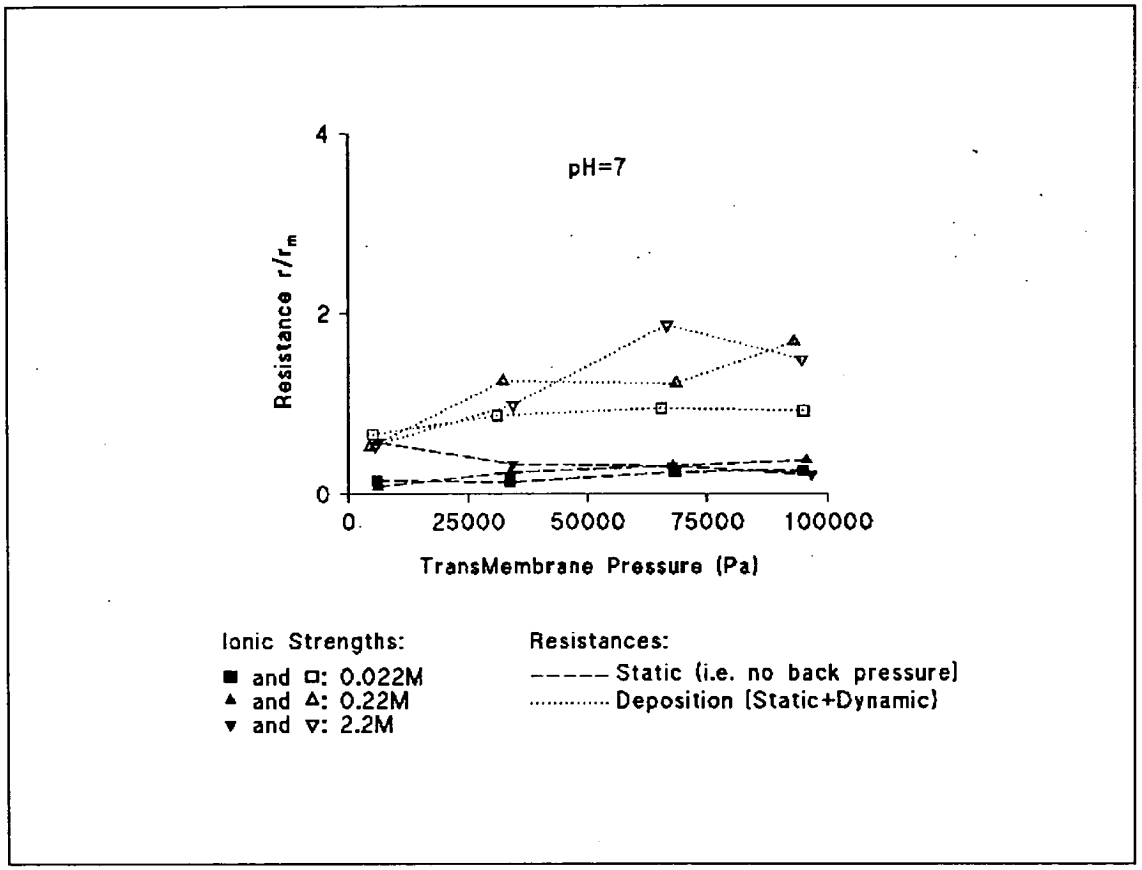

Fig. 4.18: *Influence of ionic strength and TMP on the "static" fouling resistance obtained when passively soaking the membrane in 1 g/L BSA solutions (experiments 4.3.2.7). It is compared with the "static+dynamic" fouling resistance from the cross-flow filtration of 1 g/L BSA through an Amicon H1P30-20 cartridge (experiments 4.3.2.3 -5). Other conditions were: pH=7, and average crossflow-rate around 345 ml/min for the "dynamic" BSA filtration. All resistances were experimentally measured after two hours of BSA filtration.*

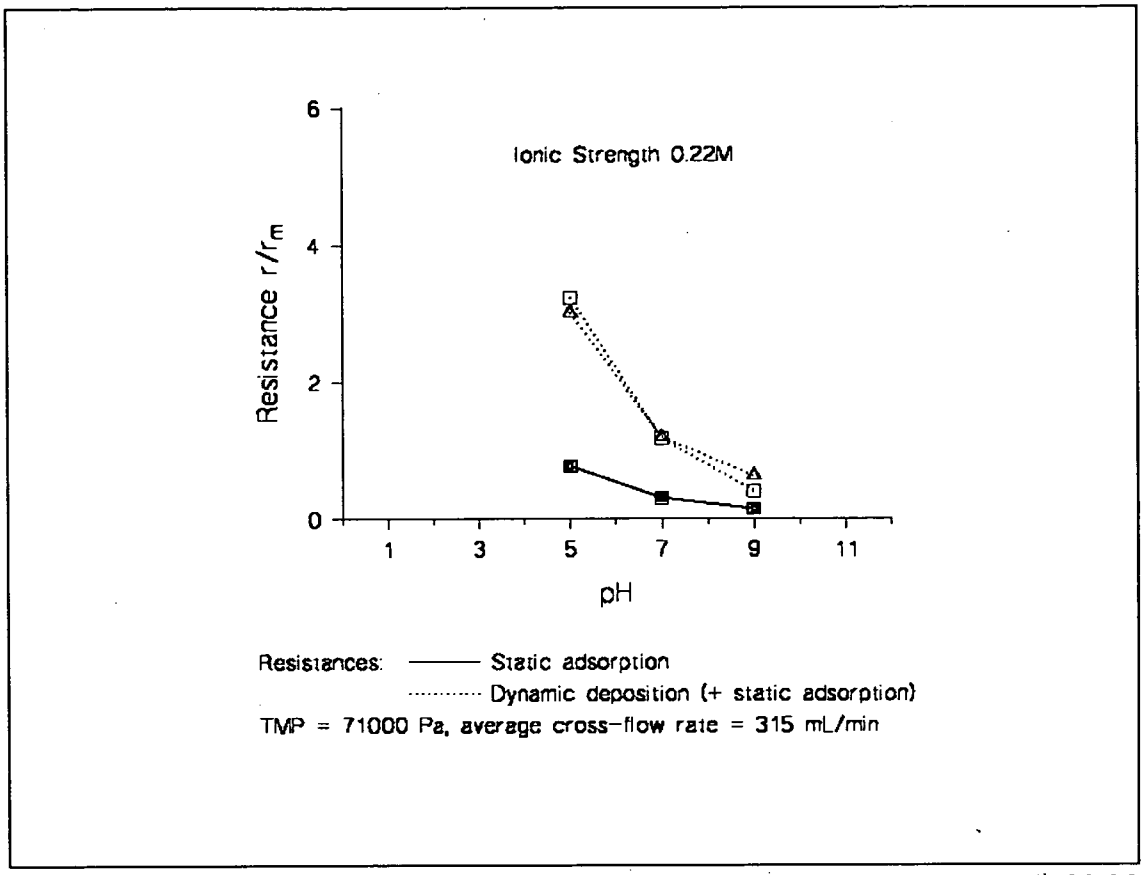

Fig. 4.19: *Influence of pH on the "static" fouling resistance of an Amicon H1P30-20 cartridge passively soaked in 1g/L BSA (experiments 4.3.2.6 a)-c)). It is compared with the "static+dynamic" fouling resistance after the cross-flow filtration of 1 g/L BSA solutions at TMP = 71000 Pa and average crossflow-rate= 315 ml/min (experiments 4.3.2.7 a)-e)). For all experiments, I = 0.22M, and resistances were measured after two hours of BSA filtration.*

4.3.4. CONCLUSIONS

The model yielded interesting results on the influence of zeta potential and ionic strength, which were confirmed by experiments: fouling decreased when ζ increased, and increased with I at high ζ. It was also predicted that fouling could decrease with I at low ζ, a result frequently reported in experimental work. Unfortunately, data relating ζ to pH and I were not available for a more thorough comparison. In spite of this, though, the model provided values for the total resistance and also (at least for the higher pressures) for the fouling resistances, that were in a range in accordance with the experimental results. Discrepancies were found between simulated critical pressures for fouling and observations. Direct adsorption of the protein onto the membrane and the effect of high local pore velocities may both explain these differences.

5.

CONCLUSIONS AND FURTHER WORK

5.1 CONCLUSIONS

A model for practical application, combining concentration polarisation and surface fouling in cross-flow ultrafiltration, was developed. Concentration polarisation was modelled by adapting Ilias and Govind's model to hollow-fibre modules, with variable diffusivity, viscosity and osmotic pressure. Fouling was simulated by a mass-transfer approach considering the conditions for coagulation between charged protein molecules in the concentrated solution near the membrane wall. Bowen and Jenners approach for colloidal interaction was adapted to this purpose, and combined with the concentration polarisation model. Therefore, the combined model was designed to predict filtration characteristics in crossflow mode of hollow-fibre ultrafiltration cartridges that completely reject a solute protein.

Experiments were carried out first to validate the individual parts of the model: Ilias and Govind's approach for modelling concentration polarisation was found to give satisfactory results. It confirmed experimental findings that no permeate flux reduction occurred when cross-flow filtering BSA solutions at 1 and 5 g/L with C-300 and C-400 cartridges. It also gave sensible results for concentration polarisation in the Amicon H1-P30-20 cartridge with Dextran T-500: simulation compared well with experimental results from Yeh and Cheng. Similarly, Bowen and Jenner's model could be used to determine conditions under which BSA would form a tightly-packed, permanent cake in Dead-End filtration: at intermediate zeta potentials (30 mV) and TMP = 4 bars, the loose cake could withstand the applied pressure longest for intermediate ionic strength, before eventually collapsing. Lower or higher ionic strengths would lead to the cake coagulating earlier.

Finally, the model combining concentration polarisation and surface fouling for ultrafiltration hollow-fibre cartridge was experimentally tested using BSA solutions through H1P30-20 Amicon cartridges. It was found to underestimate deposition at low pressures, but nonetheless gave values in a range close to that observed experimentally. It also allowed the estimation of theoretical values for the critical pressure for fouling in cross-flow mode. The lack of data relating pH and zeta potential prevented more

thorough comparison. However, the influence of ionic strength and zeta potential could be confirmed experimentally, with an increase in zeta potential (*i.e.* pH) having the effect of decreasing deposition. The classical result that fouling increases with ionic strength away from the IEP was confirmed by the experiments at pH = 7 and simulation. Simulation also predicted that near the IEP (i.e. at low or nil zeta potential) there was on the contrary an optimal or even maximal ionic strength for which fouling was minimal.

The main needs for improvement of the combined model were found to be in the incorporation of adsorption effects, of changes in the structure of the deposited protein, and of the local wall-permeate velocities nearby the pores: any of these factors may explain the discrepancy observed between experiments and simulations. The consideration of disjoining pressure for aggregates should also help predicting their effect on fouling during filtration. Ultimately, the model could incorporate size distributions for solutes and pores, to account for internal fouling effects.

5.2 FURTHER DEVELOPMENTS

5.2.1 NUMERICAL METHODS, DATA, AND CORRELATIONS USED

The model would benefit from controlling the truncation error on the concentration and velocity profiles as the axial position is incremented along the length of the fibre. This would insure improved mass balance factors for lower computing time. A method has yet to be developed in order to do so, starting with the system of finite difference equations obtained from the Ilias and Govind's approach.

A more accurate correlation than the generalised Stokes-Einstein equation should be used: This would, however, require the use of a rather complex model developed by Anderson and Reed (1976).

Also, data relating zeta potentials, pH and ionic strengths would be required for appropriate comparison between models and experiments.

Finally, some of the assumptions made in Bowen and Jenner's approach may not be true in all situations: Thus, sudden compression of the cake (see section 4.2.4) might compromise the assumption that little permeate is gained by compression of the cake. More significantly, Bowen and Jenners assumed constant zeta potential during filtration, whereas Harmant and Aimar considered constant charge at the colloid surface.

5.2.2 FURTHER WORK ON PROTEIN-MEMBRANE INTERACTION

Adsorption was mentioned in section 4.3.3.6 as a parameter which may deeply influence the outcome of the filtration, and would need consideration if the present model is to be improved. Adorption isotherms of the protein onto the membrane should be determined, with concentrations typical of that created under concentration polarisation conditions (i.e. above 100g/L), in order to make sure all adorption sites are being used. A study on the effect of aggregated species under these conditions could also provide very rewarding results (see section 4.2.3.2). The resulting fouling resistances should then be used within the model that has been presented here.

5.2.3 PORE ENTRANCE VELOCITIES AND SHEAR-STRESS

However, another factor that may contribute to the discrepancies observed between experiments and simulation is the sparsity of pore distribution. Ultrafiltration membranes usually have low pore densities (Fell *et al.*, 1990), and therefore one can expect the normal permeate velocity to be nil over much of the membrane surface, but have a much higher value than the average permeate flow rate at the entrance of the pores. This, in turn, can dramatically affect the rate of coagulation of the protein, or the rate of adsorption of the protein, whether it is through changes in the conformation of the protein, or simply by exceeding the maximum drag force that the surface forces

can withstand. Photographs of the membrane skin using Electronic microscopy should enable estimation of pore diameter and membrane skin thickness, and allow calculation of actual local velocities. A description of the local flow patterns around the pore mouth could be worked-out, using maybe a Computational Fluid Dynamic (CFD) simulation package. This could eventually be combined with a suitable mass-transport equation to allow predicting coagulation of the protein under these local conditions.

5.2.4 A MODEL USING SIZE DISTRIBUTION OF PORES AND SOLUTES

A complete model would eventually be able to deal with systems in which a pore size distribution and a solute size distribution would be present - e.g. microfiltration of an aggregating protein such as BSA. Surface and internal fouling could then be distinguished and predicted, and strategies designed to minimise the latter. Validation of the internal fouling models would simply involve filtration of protein through membrane with a Molecular Weight Cut-Off similar to the molecular weight of the protein.

Literature:

P. Aimar and R. Field (1992), *Limiting flux in membrane separations: A model based on the viscosity dependence of the mass transfer coefficient, in* Chemical Engineering Science, **47**, no. 3, pp. 579-586;

P. Aimar, J.A. Howell, and M. Turner (1989), *Effect of concentration Boundary Layer Development on the Flux Limitation in Ultrafiltration, in* Chem. Eng. Res. Des., **67**, pp. 255-261;

J.L. Anderson and C.C. Reed (1976), *Diffusion of spherical macromolecules at finite concentration, in* Journal of Chemical Physics, **64**, pp. 3240-3250;

B.J. Bellhouse, I.J. Sobey, S. Alani, B.M. DeBlois (1996), *Enhanced Filtration using Flat Membranes and Standing Vortex Waves, in* Bioseparation, **4**, no. 2, pp. 127-138;

W.F. Blatt, A. Dravid, A.S. Michaels, and L. Nelsen (1970), *in* J.E. Flinn (Ed.), *Membrane Science and Technology*, Plenum Press, New York, pp.47-97;

M. Bodzek and K.Konieczny (1993), *Characterisation of Gel Layer formed during Ultrafiltration of Latex Emulsion Waste Waters, in* Desalination, **94**, no. 1, pp. 81-100;

A. Bottino, G. Capanelli, A. Imperato and S. Munari (1984), *Ultrafiltration of Hydrosoluble Polymers: Effect of Operating Conditions on the Performance of the Membrane, in* Journal of Membrane Science, **21**, pp. 247-267;

W.R. Bowen and Q. Gan (1991), *Properties of Microfiltration Membranes. Flux Loss during Constant Pressure Permeation of Bovine Serum Albumin, in* Biotechnology and Bioengineering, **38**, pp. 688-696;

W.R. Bowen and D.T. Hugues (1990), *Properties of Microfiltration Membranes. Part 2. Adsorption of Bovine Serum Albumin at aluminium Oxide Membrane, in* Journal of Membrane Science, **51**, pp. 189-200;

W.R. Bowen and F. Jenner (1995), *Dynamic Ultrafiltration Model for Charged Colloidal Suspensions: A Wigner-Seitz Cell Approach, in* Chemical Engineering Science, **50**, no. 11, pp. 1707-1736;

W.R. Bowen and P.M. Williams (1996), *Dynamic Ultrafiltration Model for Proteins: A Colloidal Interaction Approach, in* Biotechnology and Bioengineering, **50**, pp.125-135;

J.D. Brotherton and P.C. Chau (1995), *Protein-Free Human-Human Hybridoma Cultures in an Intercalated-Spiral Alternate-Dead-Ended Hollow Fiber Bioreactor, in* Biotechnology and Bioengineering, **47**, pp.384-400;

M.J. Campbell, R.P. Walter, R. McLoughlin and C.J. Knowles (1993), *Effect of Temperature on Protein Conformation and Activity during Ultrafiltration, in* Journal of Membrane Science, **78**, pp. 35-43;

M. Cheryan (1986), *UF Handbook*, Technomic Publishing, Lancaster;

W.M. Clark, A. Bansal, M. Sontakke, and Y.H. Ma (1991), *Protein Adsorption and Fouling in Ceramic Ultrafiltration Membranes, in* Journal of Membrane Science, **55**, pp. 21-38;

Z.F. Cui and K. Wright, *Gas-liquid Two-Phase Cross-Flow Ultrafiltration of BSA and Dextran solutions, in* Journal of Membrane Science, **90** (1994), pp. 183-189;

A.G. Fane, C.J.D. Fell, and A. Suki (1983), *Effect of pH and Ionic Environment on the Ultrafiltration of Protein Solutions with Retentive Membranes, in* Journal of Membrane Science, 16, pp. 195-210;

A.G. Fane, C.J.D. Fell, and A.G. Waters (1983), *Ultrafiltration of Protein Solutions through partially Permeable Membranes – The Adsorption and Solution Environment, in* Journal of Membrane Science, **16**, pp. 211-224;

C.J.D. Fell, K.J. Kim, V. Chen, D.E. Wiley, and A.G. Fane (1990), *Factors determining Flux and Rejection of Ultrafiltration Membranes, in* Chem. Eng. Process., **27**, pp. 165-173;

P.R. Foster (1995), *Fractionation, Blood Plasma Fractionation, in* Kirk-Othmer Encyclopedia of Chemical Technology 4th ed., **11**, pp. 990-1021;

P. Gatenholm, A.G. Fane and C.J.D. Fell (1988), *Influence of the Membrane Structure on the Composition of the Deposit Layer during Processing of Microbial Suspensions, in* Desalination, **70**, pp. 363-378;

G. Grund, C.W.Robinson and B. Glick (1992), *Protein Type Effects on Steady-State Crossflow Membrane Ultrafiltration Fluxes and Protein Transmission, in* Journal of Membrane Science, **70**, pp.177-192;

J.H. Hanemaaijer (1985), *Microfiltration in Whey Processing, in* Desalination, **53**, pp. 143-155;

J.H. Hanemaaijer, T. Robbertsen, Th. van den Boomgaard and J.W. Gunnick (1989), *Fouling of Ultrafiltraiton Membranes: The Role of Protein Adsorption and Salt Precipitation, in* Journal of Membrane Science, **40**, pp. 199-217;

J.H. Hanemaaijer, T. Robbertsen, Th. van den Boomgaard, C. Olieman, P. Both and D.G. Smith (1998), *Characterization of Cleaned and Fouled Ultrafiltration Membranes, in* Desalination, **68**, pp. 93-108;

P. Harmant and P. Aimar (1996), *Coagulation of Colloids Retained by Porous Wall, in* AIChE Journal, **42**, pp.3523-3532;

S. Ilias and R. Govind (1993), *A Study on Concentration Polarization in Ultrafiltration, in* Separation Science and Technology, **28(1-3)**, pp. 361-381;

G. Jonsson (1984), *Boundary Layer Phenomena during Ultrafiltration of Dextran and Whey Protein Solutions, in* Desalination, **51**, pp. 61-77;

S.T. Kelly, W.S. Opong and A.L. Zydney (1993), *The influence of Protein Aggregates on the Fouling of Microfiltration Membranes during Stirred-Cell Filtration, in* Journal of Membrane Science, **80**, pp. 175-187;

K.J. Kim, V. Chen, and A.G. Fane (1993), *Some factors determining Protein Aggregation during Ultrafiltration, in* Biotechnology and Bioengineering, **42**, pp.260-265;

K.J. Kim, V. Chen and A.G. Fane (1994), *Characterization of Cleaned and Fouled Membranes using Metal Colloids, in* Journal of Membrane Science, **88**, no. 1, pp. 93-101;

K.J. Kim, A.G. Fane, C.J.D. Fell and D.C. Joy (1992), *Fouling Mechanisms of Membranes during Protein Ultrafiltration, in* Journal of Membrane Science, **68**, pp. 79-91;

Kirk-Othmer Encyclopedia of Chemical Technology, 4th ed., ed. J.I. Kroschwitz and M. Howe-Grant, **16**, pp. 135-193 (1995);

M.K. Ko, J.J. Pellegrino, R. Nassimbene and P. Marko (1993), *Characterization of the Adsorption-Fouling Layer using globular proteins on Ultrafiltration Membranes, in* Journal of Membrane Science, **76**, no. 2-3, pp.101-120;

A.A. Kosinski and E.N. Lightfoot (1972), *Protein Ultrafiltration: A General Example of Boundary Layer Filtration, in* AIChE Journal, **18** no. 5, pp.1030-1040;

M.S. Le, L.B. Spark and P.S. Ward (1984), *Separation of Aryl-Acylamidase by Crossflow Microfiltration and the Significance of Enzyme/Cell Interaction, in* Journal of Membrane Science, **21**, pp. 219-232;

A.D. Marshall, P.A. Munro and G. Trägårdh (1993), *The Effect of Protein Fouling in Microfiltration and Ultrafiltration on Permeate Flux, Protein Retention and Selectivity: A Literature Review, in* Desalination, **91**, pp. 65-108;

E. Mathiasson (1983), *The Role of Macromolecular Adsorption in Fouling of Ultrafiltration Membranes, in* Journal of Membrane Science, **16**, pp. 23-36;

M. Meireles, P. Aimar, V. Sanchez (1991), *Albumin Denaturation During Ultrafiltration: Effects of Operating Conditions and Consequences on Membrane Fouling, in* Biotechnology and Bioengineering, **38** no. 5, pp. 528-534;

S. Mercille, M. Johnson, R. Lemieux, and B. Massie (1994), *Filtration-Based Perfusion of Hybridoma Cultures in Protein-Free Medium: Reduction of Membrane Fouling by Medium Supplementation with DNAase I, in* Biotechnology and Bioengineering, **43**, pp. 833-846;

S. Munari, A. Bottino, G. Capanelli and P. Moretti (1987), *in* Proceedings of the 1987 International Congress on Membranes and Membrane Processes (ICOM 87), Tokyo, pp.299-300;

J. Murkes and C.G. Carlsson (1988), *Crossflow Filtration*, ed. John Wiley & Sons;

R.M. McDonough, H. Bauser, N. Stroh and H. Chmiel (1990), *Concentration Polarisation and Adsorption Effects in Crossflow Ultrafiltration of Proteins, in* Desalination, **79**, pp. 217-231;

S.-I. Nakao, T. Nomura, and S. Kimura (1979), *Characteristics of Macromolecular Gel Layer Formed on Ultrafiltration Tubular Membranes, in* AIChE Journal, **25**, pp. 615-622;

S.-I. Nakao, H. Osada, H. Kurata, T. Tsuru and S. Kimura (1988), *Separation of Proteins by Charged Ultrafiltration Membranes, in* Desalination, **70**, 191-205;

J. Nilsson and B. Hallström (1991), *Deviations in the Fouling Resistance of UF Membranes due to Clean Membrane Permeability Variations, in* Journal of Membrane Science, **67**, pp. 177-189;

M. Nyström (1989), *Fouling of Unmodified and Modified Polysulfone Ultrafiltration Membranes by ovalbumin, in* Journal of Membrane Science, **44**, 183-196;

J.Th.G. Overbeek (1952), in *Colloid Science*, edited by **H.R. Kruyt**, vol. 1: *Irreversible systems*, Elsevier Publishing Company (p. 272);

N. Papamichael and M.-R. Kula (1987), *Hydrodynamic Study of the Retention of Polyethylene Glycols by Cellulose Acetate Membranes in the Presence and Absence of Proteins, in* Journal of Membrane Science, **30**, 259-272;

G.D.J. Phillies, G.B. Benedek and N.A. Maser (1976), *Diffusion in Protein Solutions at High Concentrations: a Study by Quasi-Elastic Light Scattering Spectroscopy, in* Journal of Chemical Physics, **65**, pp. 1883-1892;

M.C. Porter (1988), *in* P. Schweitzer (Ed.), *Handbook of Separation Techniques for Chemical Engineers*, 2nd Edn., McGraw-Hill Book Company, New York, pp. 2.3-2.103;

M. Pritchard (1990), *The Influence of Rheology upon Mass Transfer in Cross-flow Membrane Filtration*, PhD thesis, University of Bath, (UK);

H. Reihanian, C.R. Robertson and A.S. Michaels (1983), *Mechanisms of Polarization and Fouling of Ultrafiltration Membranes by Proteins, in* Journal of Membrane Science, **16**, 237-258;

E. Renner and M.H. Abd El-Salam (1991), *Application of the UF in the Dairy Industry*, Elsevier Applied Science, London;

J.M. Sheldon, L.M. Reed, and C.R. Hawes (1991), *Fine Structure of Ultrafiltration membranes, II. Protein Fouled Membranes, in* Journal of Membrane Science, **62**, pp. 87-102;

J.J.F. Shen and R.F. Probstein (1977), *On the Prediction of Limiting Flux in Laminar Ultrafiltration of Macromolecular Solutions, in* Ind. Eng. Chem, Fundam., **16**, no. 4, pp. 459-465;

C.M. Tam and A.Y. Tremblay (1991), *Membrane Pore Characterization – Comparison between single and Multicomponent Solute Probe Technique, in* Journal of Membrane Science, **57**, pp. 271-287;

E.M. Tracey and R.H. Davis (1994), *Protein Fouling of Track-Etched Polycarbonate Microfiltration Membranes, in* Journal of Colloid and Interface Science, **167**, pp. 104-116;

H.M. Yeh and T.W. Cheng (1994), *Concentration Polarization Model for Hollow-Fiber Membrane Ultrafiltration, in* Separation Science and Technology, **29**, no. 4, pp. 497-512;

Yoshihito Osada and Tsutomu Nakagawa (editors) (1991), *Membrane Science and Technology*, pp. 293-298, published by Marcel Dekker Inc.;

APPENDICES

APPENDIX I:
MASS TRANSPORT AND DIFFUSIVITY EQUATIONS

A1.1: Problem

As stated in sections 2.4.7.3-2.4.7.5, we started with an initial value c_g for the wall concentration at line $i+1$, and all values of the concentration and velocities profile are known on the previous line i (see section 2.2.2.6 for grid notations). From c_g, the wall velocity v_{wall} is obtained from equation (2.61), and this starting value is used to work out U and V velocity profiles with the momentum transport and continuity equations. With those values, we have to solve the mass transport equation and the diffusivity equation simultaneously, i.e. the following system:

$$\begin{cases} U\dfrac{\partial C}{\partial Z}+V\dfrac{\partial C}{\partial R}=\dfrac{1}{R}\dfrac{\partial}{\partial R}\left(\dfrac{1}{\dfrac{D_0}{D'_{R,Z}}Pe_{0,wall}}R\dfrac{\partial C}{\partial R}\right) & (2.68) \\ D'_{R,Z}=\dfrac{(\partial\Pi/\partial C)_{T,P}}{6\pi\mu af(\gamma)} & (2.64) \end{cases}$$

In this appendix, we do not consider the case in which the zeta potential ζ is nil, because convergence always occur for $D'>0$. Also, values for $D'\leq 0$ (i.e. $c \geq c_{\Pi max}$) are ignored, because they mean a transient state of compaction of the cake (and the boundary condition (Eq. 2.7) would not be valid).

A1.2: Characteristic plots

A1.2.1. Diffusivity:

D' is calculated using equations (2.62) and (2.64). When the zeta potential ζ is significantly different from zero, repulsion forces result in at least one local maximum for the plot *(D'=f(C))*, which represents the diffusivity D' as a function of the wall concentration. In particular, the highest-concentration local maximum is crucial in determining whether the system has a solution at all, or if coagulation occurs. The co-ordinates for this maximum are noted $c_{D'max}$ and D'_{max} (see *fig. A1.1* below).

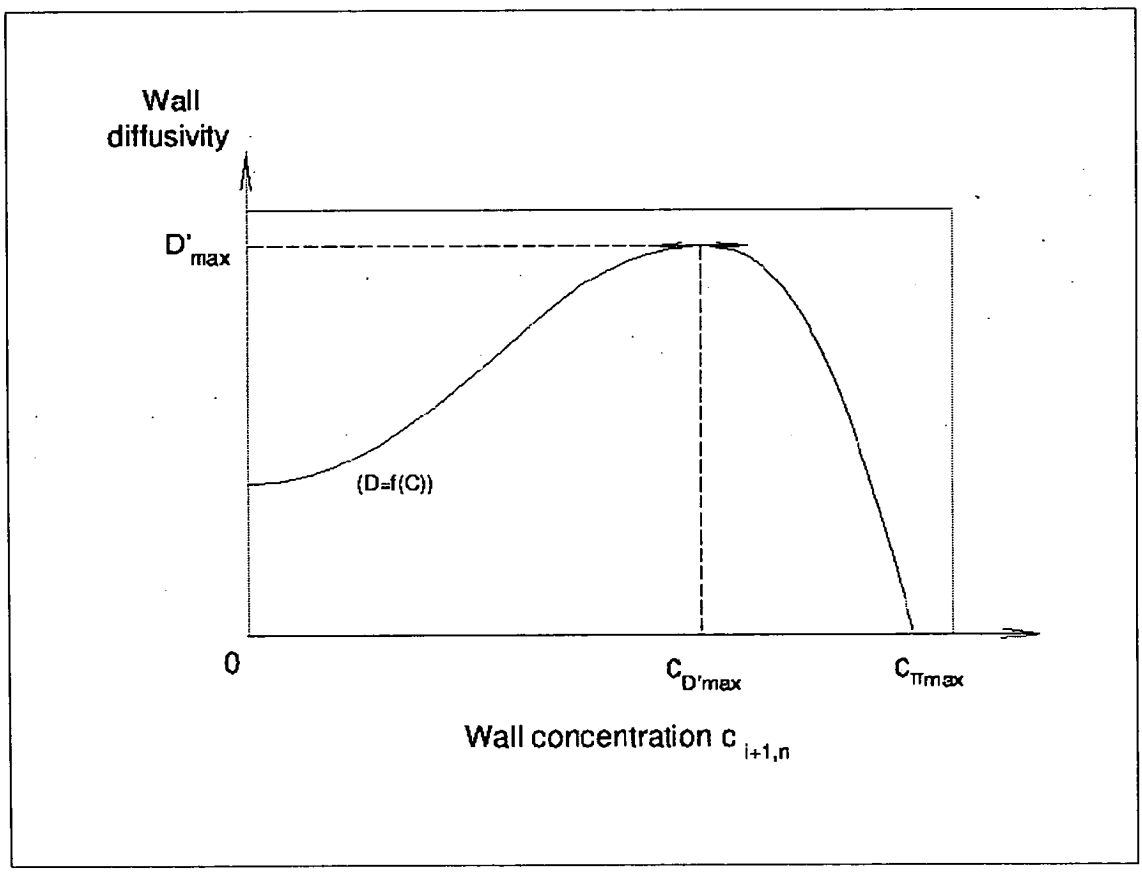

Fig. A1.1: *Diffusivity as a function of concentration, for $\zeta \neq 0$.*

A1.2.2. Mass transport:

Figure *A1.2* shows a typical plot (MT1) for the wall concentration $c_{i+1,n}$, obtained from the mass transport equation as a function of the diffusivity profile. For simplification, D' profiles are represented solely by their values at the membrane (or compact cake) surface, D'_{wall}. For a given v_{wall}, with $D'>0$ (see previous section), $c_{i+1,n}$ decreases when D'_{wall} increases. Also, if v_{wall} is taken bigger (i.e. c_g is taken lower), then this leads to increased concentration polarisation and the plot on *Fig. A1.2* is shifted to the right.

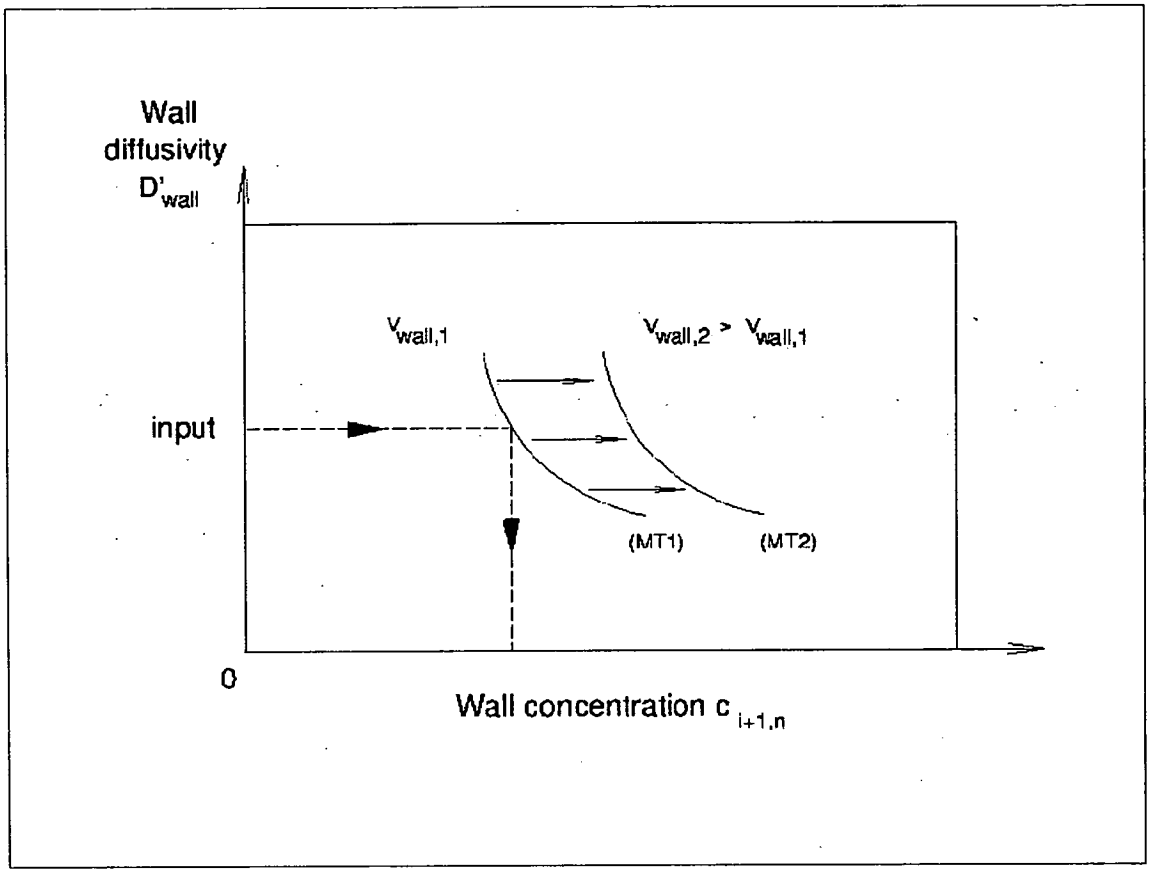

Fig. A1.2: *Mass transport equation giving wall concentrations depending on diffusivities, for two different initial values of permeate flux* v_{wall1} *and* v_{wall2}.

A1.3: Solving the system

Solving the system in section A1.1 is equivalent to finding the intercepts of the plots ($D'=f(C)$) and (MT) we have just defined. We adopted the following method:

-**Step 1:** Starting with an initial value for c_g ($c_g = c_g^0$) we follow the different steps given in A1.1 to establish U and V velocity profiles.

-**Step 2:** We solve the mass-transport equation. We use for D'(R, Z) values those from the previous line, i.e. $D'_{i+1,j}$ at a given radial position j is taken as $D'_{i,j}$. We note $c^0_{i+1,n}$ the resulting value for the wall concentration.

-**Step 3:** Do we have $c_0 \leq c^0_{i+1,n} \leq c_{D'max}$? (c_0 is the bulk inlet concentration)

-If **YES:** We go to step 4. If **NO:** We go to step 5.

-**Step 4:** $c_0 \leq c^0_{i+1,n} \leq c_{D'max}$. A solution $c^*_{i+1,n}$ to the system in A1.1 does exist below $c_{D'max}$ (see *Fig. A1.3*), and is eventually found by successive guesses.

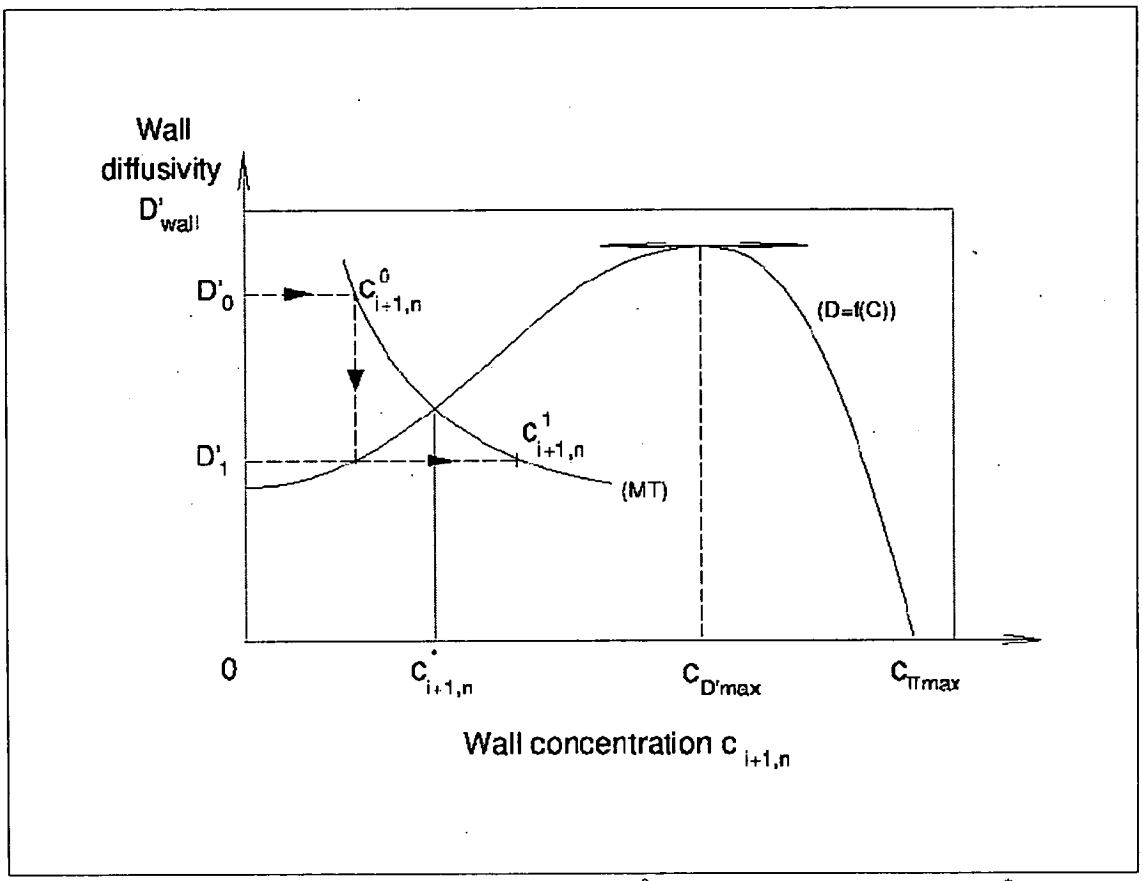

Fig. A1.3: *Solution of the system in A1.1 for* $c_0 \leq c^0_{i+1,n} \leq c_{D'max}$ *(solution noted* $c^*_{i+1,n}$*).*

-**Step 5:** If $c^0_{i+1,n} \leq c_0$ or $c_{D'max} \leq c^0_{i+1,n}$, then there is divergence. In this case, we set $c_g^0 = c_{D'max}$, and go back to step 1, but using there values for the D' profile corresponding to D'_{max} at the wall. From there, we obtain a value $c^1_{i+1,n}$ for the wall concentration. There are then three possibilities:

-case 1: $c_0 \leq c^{1}_{i+1,n} \leq c_{D'max}$. We can go to step 4, the problem is solved.

-case 2: In this case, illustrated in *fig. A1.4*, there actually is a solution such that $c_{D'max} < c^{*}_{i+1,n} < c_{\Pi max}$. From taking D' values corresponding to D'_{wall} given by $c^{1}_{i+1,n}$, then solving the mass-transport equation again and again with successive values of D' profiles, convergence to the solution $c^{*}_{i+1,n}$ is eventually found. Continuity was assumed for the (MT) plot and its intercept with ($D'=f(C)$): beyond $c_{D'max}$, the solution – if any - is still the first of the two intercepts that may occur, *i.e.* the one with the lower value for $c_{i+1,n}$.

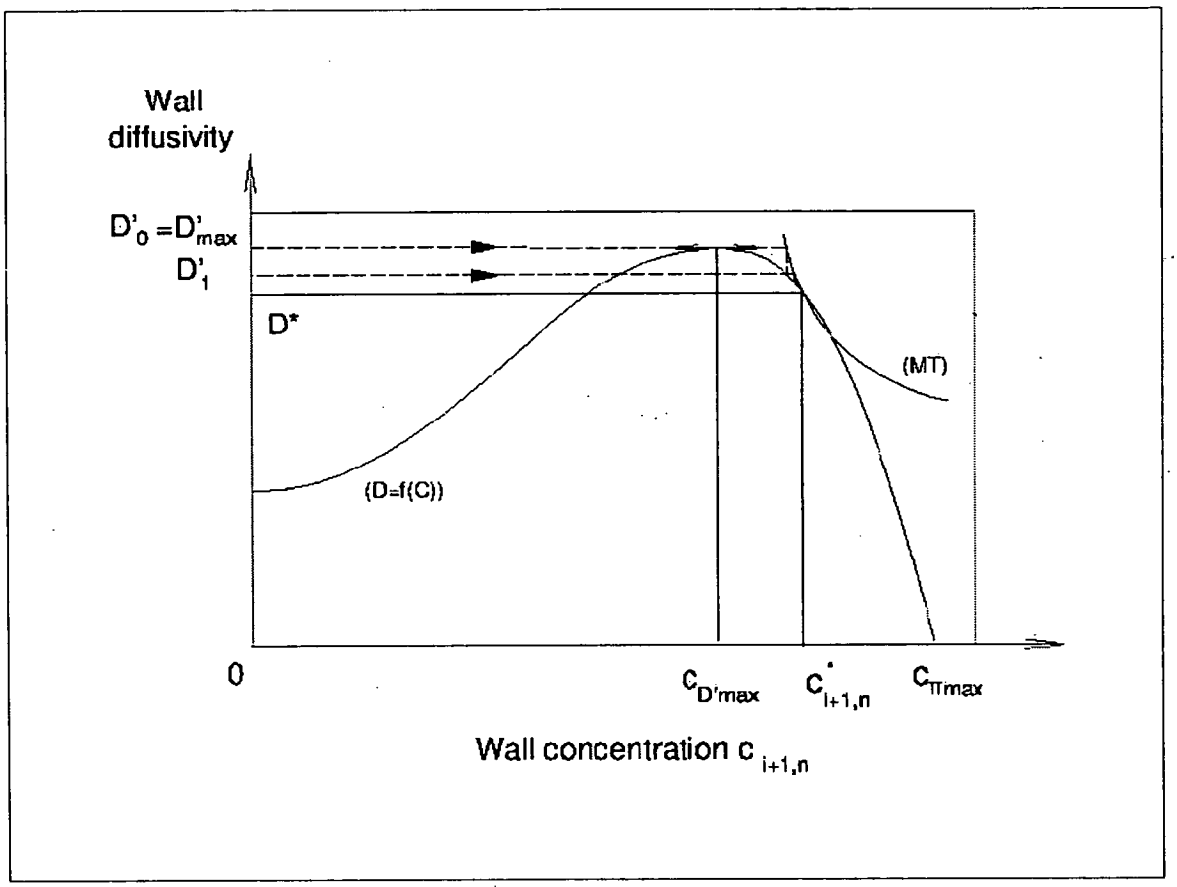

Fig. A1.4: *Solution such that* $c_{D'max} < c^{*}_{i+1,n} < c_{\Pi max}$.

-case 3: Just as in case2, but this time no convergence is observed, and eventually we get $c^{k}_{i+1,n} \leq c_0$ or $c_{D'max} \leq c^{k}_{i+1,n}$ at the k^{th} attempt. This case is illustrated in *fig A1.5*. What happens here is that c_g^{0} was taken too low in step 1 (see section A1.2.2), and a new value c_g^{1} such as $c_g^{0} < c_g^{1} < c_{\Pi max}$ has to be tried in step 1 now. If after several such

attempts, we get c_g^k converging to $c_{\Pi max}$ and still no solution, then there is deposition of an extra layer of compact cake onto the membrane.

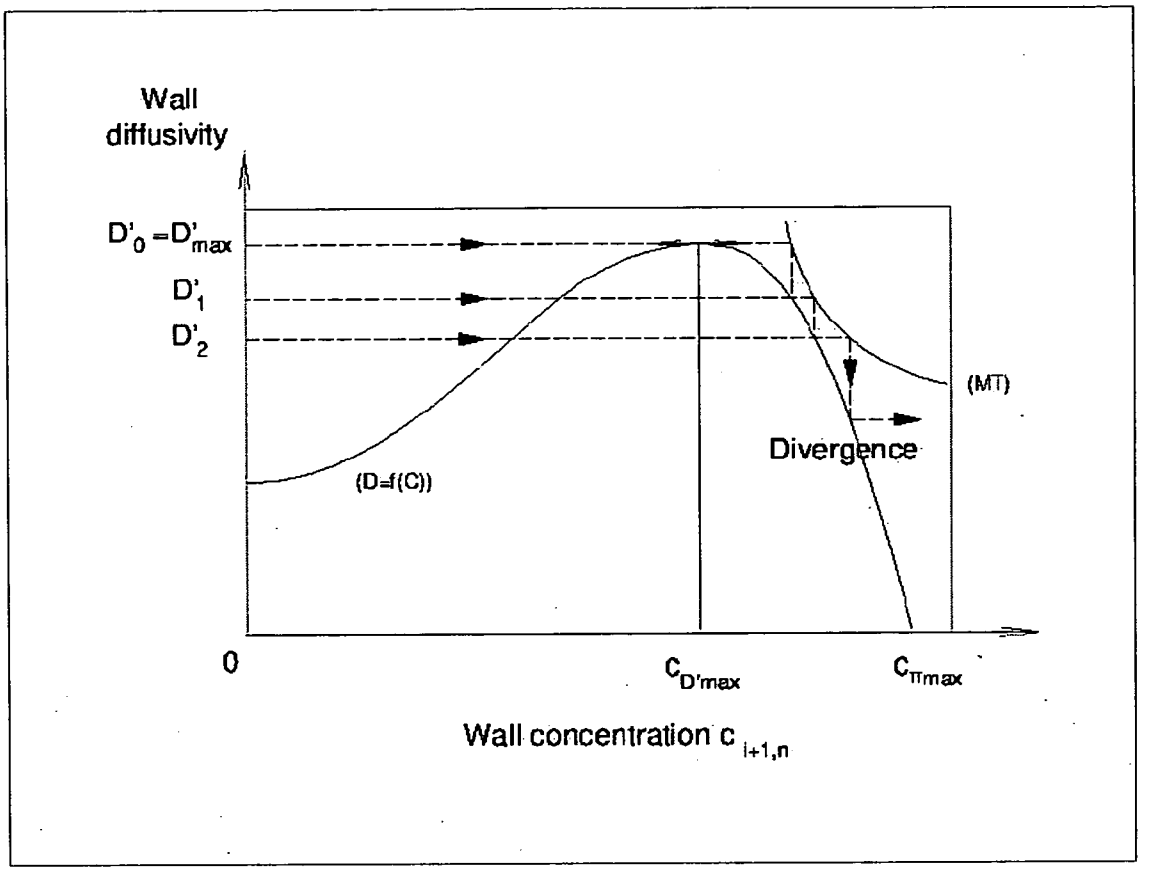

Fig. A1.5: No solution to the system.

APPENDIX II:
GEAR PUMP CALIBRATION

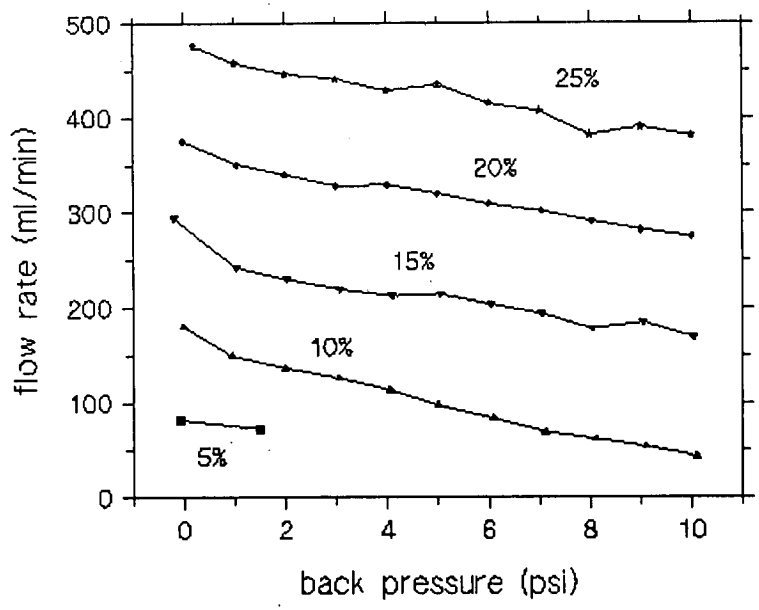

APPENDIX III:

PRESSURE TRANSDUCERS CALIBRATION

At room temperature (22 °C), a linear relationship was found between the output voltage from the transducer, and the actual pressure:

$$P = a.V + b$$

For the transducers P_1 and P_2, two lengths of thin tubes were tried (25 and 50 cm), and as expected, no difference was found for these two lengths.

The following table sums-up the values for a and b found for the three transducers:

P. Transducer:	A	b	r
P_1	1.487	+0.065	0.99999
P_2	1.372	-0.2622	0.99999
P_3	1.502	+0.1339	0.99998

APPENDIX IV:

ABSORBANCE OF BSA AT 280 NM (21-22^{0}C)

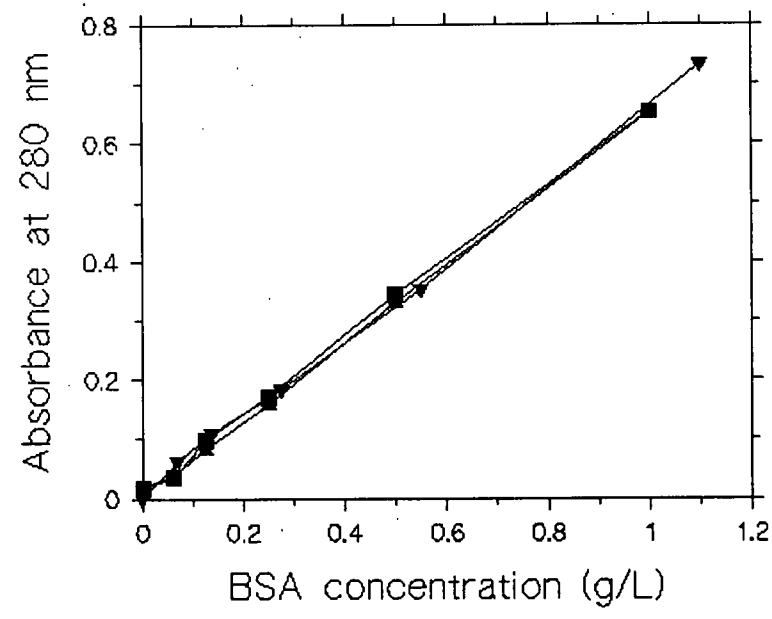

APPENDIX V:

PERMEATE FLUXES AND MASS BALANCE FACTORS FROM MODELLING OF COMBINED CONCENTRATION POLARISATION AND CAKE BUILD-UP

IONIC STRENGTH 0.02M

P 7600

zeta 0
permeate flux1.56456e-05
global mass balance factor 1.0028
solute mass balance factor 1.0018

zeta 10
permeate flux1.5661e-05
global mass balance factor 1.0028
solute mass balance factor 1.0017

zeta 20
permeate flux1.56927e-05
global mass balance factor 1.00284
solute mass balance factor 1.00182

zeta 40
permeate flux1.57766e-05
global mass balance factor 1.003
solute mass balance factor 1.00215

P 36000

zeta 0
permeate flux1.88657e-05
global mass balance factor 1.00592
solute mass balance factor 1.00814
z (m) thickn. (*1e9m)
0.0256441 0
0.0413144 5.22558

zeta 10
permeate flux2.1652e-05
global mass balance factor 1.00865
solute mass balance factor 1.0170

zeta 20
permeate flux2.35067e-05
global mass balance factor 1.01007
solute mass balance factor 1.02122

zeta 40
permeate flux2.61536e-05
global mass balance factor 1.01036
solute mass balance factor 1.02237

P 50000

zeta 10
permeate flux2.02451e-05
global mass balance factor 1.00274
solute mass balance factor 0.98928
z (m) thickn. (*1e9m)
0.007753 0
0.008979 5.22558

P 71000

zeta 0
permeate flux2.26225e-05
global mass balance factor 1.00274
solute mass balance factor 0.98928
z (m) thickn. (*1e9m)
0.0013811 0
0.00162595 5.22558
0.0219637 5.22558
0.0376341 10.4512
0.066465 10.4512
0.0703826 15.6767

zeta 10
permeate flux2.46054e-05
global mass balance factor 1.00692
solute mass balance factor 1.01057
z (m) thickn. (*1e9m)
0.0311111 0
0.0467815 5.22558

zeta 20
permeate flux3.04039e-05
global mass balance factor 1.00958
solute mass balance factor 1.02976
0

zeta 40
permeate flux3.65116e-05
global mass balance factor 1.01092
solute mass balance factor 1.03195

P 100000

zeta 0
permeate flux2.46654e-05
global mass balance factor 1.00185
solute mass balance factor 0.975672
z (m) thickn. (*1e9m)
0.000837556 0
0.000875845 5.22558
0.014315 5.22558
0.0241168 10.4512
0.0318128 10.4512
0.033038 15.6767
0.0918871 15.6767
0.101689 26.1279
0.136034 26.1279
0.145835 31.3535

zeta 10
permeate flux2.61534e-05
global mass balance factor 1.00349
solute mass balance factor 1.01018
z (m) thickn. (*1e9m)
0.00083277 0
0.000985923 5.22558
0.016799 5.22558
0.0216999 10.4512
0.0510287 10.4512
0.0608305 15.6767

zeta 20
permeate flux3.38245e-05
global mass balance factor 1.01069
solute mass balance factor 1.044

zeta 40
permeate flux4.24543e-05
global mass balance factor 1.00866
solute mass balance factor 1.03632

****
****

IONIC STRENGTH 0.22M

P 7600

zeta 0
permeate flux1.56455e-05
global mass balance factor 1.0028
solute mass balance factor 1.0018
0

zeta 10
permeate flux1.56455e-05
global mass balance factor 1.0028
solute mass balance factor 1.0018

zeta 20
permeate flux1.56455e-05
global mass balance factor 1.0028
solute mass balance factor 1.0018

zeta 40
permeate flux1.56455e-05
global mass balance factor 1.0028
solute mass balance factor 1.0018

P 36000

zeta 0
permeate flux1.89588e-05
global mass balance factor 1.00624
solute mass balance factor 1.0074
z (m) thickn. (*1e9m)
0.0413144 0
0.0569848 5.22558

zeta 10
permeate flux2.06198e-05
global mass balance factor 1.00795
solute mass balance factor 1.01126

zeta 20
permeate flux2.05368e-05
global mass balance factor 1.00793
solute mass balance factor 1.01443

zeta 40
permeate flux2.04662e-05
global mass balance factor 1.00847
solute mass balance factor 1.01805

P 50000

zeta 10
permeate flux2.18372e-05
global mass balance factor 1.00204
solute mass balance factor 0.99511
z (m) thickn. (*1e9m)
0.00576239 0
0.00698761 5.22558

P 71000

zeta 0
permeate flux1.47346e-05
global mass balance factor 1.00442
solute mass balance factor 0.986266
z (m) thickn. (*1e9m)
0.00102341 0
0.00166304 5.22558
0.0353077 5.22558
0.115262 10.4512

0.143917 10.4512
0.153 15.6767

zeta 10
permeate flux1.88379e-05
global mass balance factor 1.00866
solute mass balance factor 0.986614
z (m) thickn. (*1e9m)
0.00102341 0
0.00166304 5.22558
0.0832801 5.22558
0.103269 10.4512
0.108897 10.4512
0.153 15.6767

zeta 20
permeate flux2.26763e-05
global mass balance factor 1.01392
solute mass balance factor 1.02833
z (m) thickn. (*1e9m)
0.0390815 0
0.0550723 5.22558

zeta 40

permeate flux2.34e-05

P 100000

zeta 0
permeate flux2.38408e-05
global mass balance factor 1.00104
solute mass balance factor 0.980843
z (m) thickn. (*1e9m)
0.000976351 0
0.00101464 5.22558
0.0108164 5.22558
0.0157173 10.4512
0.0274336 10.4512
0.0286588 15.6767
0.0801948 15.6767
0.0997984 20.9023
0.109677 20.9023
0.114578 26.1279

zeta 10
permeate flux2.28896e-05
global mass balance factor 1.00189
solute mass balance factor 0.983129
z (m) thickn. (*1e9m)
0.00111712 0
0.00117834 5.22558
0.0191594 5.22558
0.0269946 10.4512
0.0390993 10.4512
0.039589 15.6767
0.0725059 15.6767
0.0881762 20.9023
0.0934099 20.9023
0.10908 26.1279

zeta 20
permeate flux2.55804e-05
global mass balance factor 1.00384
solute mass balance factor 0.994887
z (m) thickn. (*1e9m)
0.00252501 0
0.0035044 5.22558

zeta 40
permeate flux2.48915e-05
global mass balance factor 1.00261
solute mass balance factor 1.01422
z (m) thickn. (*1e9m)
0.00641329 0
0.00763851 5.22558

****
*

IONIC STRENGTH 2.2M

P 7600

zeta 0
permeate flux1.56455e-05
global mass balance factor 1.0028
solute mass balance factor 1.0018

P 36000

zeta 0
permeate flux1.89555e-05
global mass balance factor 1.00623
solute mass balance factor 1.00744
z (m) thickn. (*1e9m)
0.0413144 0
0.0569848 5.22558

P 50000

zeta 0
permeate flux2.20451e-05
global mass balance factor 1.00214
solute mass balance factor 0.988732
z(m) thickn. (*1e9m)
0.00775338 0
0.0089786 5.22558

P 71000

zeta 0
permeate flux1.91011e-05
global mass balance factor 1.00526
solute mass balance factor 0.993168
z(m) thickn. (*1e9m)

0.00102341 0
0.00166304 5.22558
0.0273123 5.22558
0.0672893 10.4512
0.0959448 10.4512
0.108737 15.6767

P 100000

zeta 0
permeate flux2.90938e-05
global mass balance factor 1.00079
solute mass balance factor 0.91521

zeta 40
permeate flux2.64399e-05
global mass balance factor 1.00361
solute mass balance factor 0.99877
z(m) thickn. (*1e9m)
0.000306613 0
0.000900676 5.22558
0.0061131 5.22558
0.0288025 15.6767
0.0729548 26.1279
0.153 31.3535

APPENDIX VI:

Fouling resistances due to deposition and due to concentration polarisation, calculated from Appendix V:

Total area:	0.06	m2						NOTATION:						
Length:	0.153	m		Deposited resistance				P	Pressure (Pa)					
Monolayer	5.23E-09	m		Ra with 1 monolayer:		6.3342E+11	m-1	Rtotal	Total Fouled Membrane Resistance (m-1)					
K(Happel)	8.25E-21	m2						Rm	Intrinsic Resistance (m-1)					
μ=	1.00E-03	Po	(Viscosity)					Ra	Deposited Resistance (m-1)					
									Ra is calculated from the cake thickness profile.					
								Rc	Concentration polarisation Resistance (m-1)					
									Rc = Rtotal - Ra - Rm					
								J	Permeate Flux (m/s)					
								X	Axial position along the fibre (m)					
								Ai	Membrane Surface Area From X=0 to X (m2)					
								A	Total Membrane Surface Area for a fibre (m2)					
Ionic Strength		**0.022M**												
				Ra/Rm								Rc/Rm		
	P	Rm*mu	zeta 0mV	10mV	20mv	40mV		P	Rm*mu	zeta 0mV	10mV	20mv	40mV	
	7600	2.16E+08	0	0	0	0		7600	2.16E+08	1.24888692	1.246676	1.242137	1.230072076	
	36000	4.50E+08	0.883537	0	0	0		36000	4.5E+08	2.35696277	2.694809	2.403285	2.058852319	
	50000	4.94E+08		0				50000	4.94E+08		3.048761			
	71000	5.60E+08	2.35833	0.682011	0	0		71000	5.6E+08	2.24607739	3.470749	3.170048	2.472477631	
	100000	6.9E+08	2.667359	2.115276	0	0		100000	6.9E+08	2.20838346	2.426165	3.284691	2.41373044	
											Rtotal/Rm			
								P	Rm*mu	zeta 0mV	10mV	20mv	40mV	
								7600	2.16E+08	2.25E+00	2.25E+00	2.24E+00	2.23E+00	
								36000	4.50E+08	4.24E+00	3.69E+00	3.40E+00	3.06E+00	
								50000	4.94E+08		4.05E+00			
								71000	5.60E+08	5.60E+00	5.15E+00	4.17E+00	3.47E+00	
								100000	6.9E+08	5.87574239	5.541442	4.284691	3.41373044	
	zeta=0mV							**zeta=0mV**						
	P (Pa)	Rm*mu	X (m)	# of layers	Ai/A	J(buffer)		P (Pa)	Rm*mu	X (m)	# of layers	Ai/A	J(buffer)	
	36000	4.50E+08	0.025644	0	0.167608	1.34E-05		100000	6.90E+08	0.00083756	0	0.005474	7.93366E-07	
			0.041314	1	0.10242	4.81E-06				0.00087585	1	0.00025	2.48587E-08	
			0.153	1	0.729971	2.43E-05				0.014315	1	0.087838	6.63717E-06	
					Total J	4.25E-05				0.0241168	2	0.064064	3.90604E-06	
					Ra * mu	3.98E+08				0.0318128	2	0.050301	2.5705E-06	
					Ra/Rm	0.883537189				0.033038	3	0.008008	3.52218E-07	
										0.0918871	3	0.384635	1.48493E-05	
	zeta=0mV									0.101689	5	0.064065	1.98732E-06	
	P (Pa)	Rm*mu	X (m)	# of layers	Ai/A	J(buffer)				0.136034	5	0.224477	5.81984E-06	
	71000	5.60E+08	0.001381	0	0.009027	1.14447E-05				0.145835	6	0.064059	1.53478E-06	
			0.001626	1	0.0016	1.29602E-07				0.153	6	0.04683	1.04E-06	
			0.021964	1	0.132926	7.90818E-06						Total J	3.95182E-05	
			0.037634	2	0.102421	4.8154E-06						Ra * mu	1.8405E+09	
			0.066465	2	0.188437	7.3236E-06						Ra/Rm	2.667358925	
			0.070383	3	0.025605	8.48113E-07								
			0.153	3	0.539983	1.55832E-05								
					Total J	3.77526E-05		**zeta=10mV**						
					Ra * mu	1.32E+09		P (Pa)	Rm*mu	X (m)	# of layers	Ai/A	J(buffer)	
					Ra/Rm	2.358330358		100000	6.90E+08	0.00083277	0	0.005443	7.88832E-07	
										0.00098592	1	0.001001	9.94328E-08	
	zeta=10mV									0.016799	1	0.103353	7.80957E-06	
	P (Pa)	Rm*mu	X (m)	# of layers	Ai/A	J(buffer)				0.0216999	2	0.032032	1.95302E-06	
	71000	5.60E+08	0.031111	0	0.203341	2.57807E-05				0.0510287	2	0.191692	9.79597E-06	
			0.046782	1	0.102421	8.29452E-06				0.0608305	3	0.064064	2.8178E-06	
			0.153	1	0.694239	4.13023E-05				0.153	3	0.602415	2.32569E-05	
					Total J	7.53775E-05						Total J	4.65216E-05	
					Ra * mu	3.82E+08						Ra * mu	1.4595E+09	
					Ra/Rm	0.682011092						Ra/Rm	2.115276133	

APPENDIX VI:

Fouling resistances due to deposition and due to concentration polarisation, calculated from Appendix V:

Ionic Strength	0.22M					
				Ra/Rm		
P	Rm*mu	zeta 0mV	10mV	20mv	40mV	
7600	2.16E+08	0	0	0	0	
36000	4.50E+08	0.692632	0	0	0	
50000	4.94E+08		1.038374			
71000	5.60E+08	1.636767	1.533554	0.606346	0	
100000	6.9E+08	2.7315	2.57759	1.315065	1.236632475	

				Rc/Rm		
P	Rm*mu	zeta 0mV	10mV	20mv	40mV	
7600	2.16E+08	1.25E+00	1.25E+00	1.25E+00	1.25E+00	
36000	4.50E+08	2.53E+00	2.88E+00	2.90E+00	2.91E+00	
50000	4.94E+08		2.60E+00			
71000	5.60E+08	5.97E+00	4.20E+00	3.98E+00	4.40E+00	
100000	6.9E+08	2.34747156	2.753998	3.350504	3.585738062	

				Rtotal/Rm		
P	Rm*mu	zeta 0mV	10mV	20mv	40mV	
7600	2.16E+08	2.25E+00	2.25E+00	2.25E+00	2.25E+00	
36000	4.50E+08	4.22E+00	3.88E+00	3.90E+00	3.91E+00	
50000	4.94E+08		4.63E+00			
71000	5.6E+08	8.60462546	6.730353	5.591111	5.395136778	
100000	6.9E+08	6.07897119	6.331589	5.66557	5.822370537	

zeta=0mV

P (Pa)	Rm*mu	X (m)	# of layers	Ai/A	J(buffer)
36000	4.5E+08	0.041314	0	0.270029	2.16023E-05
		0.056985	1	0.102421	4.80906E-06
		0.153	1	0.62755	2.08523E-05
				Total J	4.73E-05
				Ra * mu	311684300
				Ra/Rm	0.692631778

zeta=0mV

P (Pa)	Rm*mu	X (m)	# of layers	Ai/A	J(buffer)
71000	5.6E+08	0.001023	0	0.006689	8.48064E-07
		0.001663	1	0.004181	3.38563E-07
		0.035308	1	0.2199	1.30825E-05
		0.115262	2	0.522577	2.45694E-05
		0.143917	2	0.187288	7.28E-06
		0.153	3	0.059366	1.96636E-06
				Total J	4.81E-05
				Ra * mu	916589524.6
				Ra/Rm	1.636767008

zeta=10mV

P (Pa)	Rm*mu	X (m)	# of layers	Ai/A	J(buffer)
50000	5.94E+08	0.001023	0	0.006689	8.48064E-07
		0.001663	1	0.004181	3.38563E-07
		0.08328	1	0.533445	3.17362E-05
		0.103269	2	0.130646	6.14245E-06
		0.108897	2	0.036784	1.42962E-06
		0.153	3	0.288255	9.55E-06
				Total J	5.00426E-05
				Ra * mu	4.05E+08
				Ra/Rm	0.682067319

zeta=10mV

P (Pa)	Rm*mu	X (m)	# of layers	Ai/A	J(buffer)
71000	5.6E+08	0.005762	0	0.037663	4.77509E-06
		0.006988	1	0.008008	6.49E-07
		0.153	1	0.954329	5.67758E-05
				Total J	6.21994E-05
				Ra * mu	581489546.4
				Ra/Rm	1.03837419

zeta=20mV

P (Pa)	Rm*mu	X (m)	# of layers	Ai/A	J(buffer)
71000	5.6E+08	0.039082	0	0.255435	3.23855E-05
		0.055072	1	0.104515	8.46411E-06
		0.153	1	0.64005	3.80784E-05
				Total J	7.8928E-05
				Ra * mu	339553791.6
				Ra/Rm	0.606346057

zeta=40mV

P (Pa)	Rm*mu	X (m)	# of layers	Ai/A	J(buffer)
100000	6.9E+08	0.006413	0	0.041917	6.07492E-06
		0.007639	1	0.008008	7.9546E-07
		0.153	2	0.950075	5.79268E-05
				Total J	6.47972E-05
				Ra * mu	853276407.8
				Ra/Rm	1.236632475

zeta=0mV

P (Pa)	Rm*mu	X (m)	# of layers	Ai/A	J(buffer)
100000	6.9E+08	0.00097635	0	0.006381	9.24838E-07
		0.00101464	1	0.00025	2.48587E-08
		0.0108164	1	0.064064	4.84078E-06
		0.0157173	2	0.032032	1.95302E-06
		0.0274336	2	0.076577	3.91331E-06
		0.0286588	3	0.008008	3.52218E-07
		0.0801948	3	0.336837	1.3004E-05
		0.0997984	4	0.128128	4.40762E-06
		0.109677	4	0.064566	2.00287E-06
		0.114578	5	0.032033	9.04779E-07
		0.153	5	0.251124	6.5107E-06
				Total J	3.8839E-05
				Ra * mu	1884734740
				Ra/Rm	2.731499624

zeta=10mV

P (Pa)	Rm*mu	X (m)	# of layers	Ai/A	J(buffer)
100000	6.9E+08	0.00111712	0	0.007301	1.05818E-06
		0.00117834	1	0.0004	3.97464E-08
		0.0191594	1	0.117523	8.88027E-06
		0.0269946	2	0.05121	3.12E-06
		0.0390993	2	0.079116	4.04303E-06
		0.039589	3	0.003201	1.4078E-07
		0.0725059	3	0.215143	8.30585E-06
		0.0881762	4	0.10242	3.52327E-06
		0.0934099	4	0.034207	1.06112E-06
		0.10908	5	0.102419	2.89287E-06
		0.153	5	0.287059	7.44235E-06
				Total J	4.05098E-05
				Ra * mu	1778537432
				Ra/Rm	2.58E+00

zeta=20mV

P (Pa)	Rm*mu	X (m)	# of layers	Ai/A	J(buffer)
100000	6.9E+08	0.00252501	0	0.016503	2.39179E-06
		0.0035044	1	0.006401	6.35858E-07
		0.153	2	0.977095	5.95743E-05
				Total J	6.26019E-05
				Ra * mu	907394964.4
				Ra/Rm	1.315065166

APPENDIX VI:

Fouling resistances due to deposition and due to concentration polarisation, calculated from Appendix V:

Ionic Strength	2.2M					
				Ra/Rm		
P	Rm*mu	zeta 0mV	10mV	20mv	40mV	
7600	2.16E+08	0	0	0	0	
36000	4.50E+08	0.692632	0.692632	0.692632	0.692631778	
50000	4.94E+08		1.834489			
71000	5.60E+08	2.030102	2.030102	2.030102	2.030102264	
100000	6.9E+08	3.346383	3.346383	3.346383	3.34638279	
		(zeta has no influence)				

P	Rm*mu	zeta 0mV	Rc/Rm 10mV	20mv	40mV	
7600	2.16E+08	1.24890129	1.248901	1.248901	1.248901293	
36000	4.50E+08	2.52777918	2.527779	2.527779	2.527779185	
50000	4.94E+08		1.756762			
71000	5.60E+08	3.72375946	3.723759	3.723759	3.723759459	
100000	6.9E+08	1.13501223	1.135012	1.135012	1.135012232	
		(zeta has no influence)				

P	Rm*mu	zeta 0mV	Rtotal/Rm 10mV	20mv	40mV	
7600	2.16E+08	2.24890129	2.248901	2.248901	2.248901293	
36000	4.50E+08	4.22041096	4.220411	4.220411	4.220410963	
50000	4.94E+08		4.59125			
71000	5.60E+08	6.63761324	6.637613	6.637613	6.637613241	
100000	6.9E+08	5.48139502	5.481395	5.481395	5.481395022	

zeta has no influence:

P (Pa)	Rm*mu	X (m)	# of layers	Ai/A	J(buffer)
36000	4.50E+08	0.041314	0	0.270029	2.16E-05
		0.056985	1	0.102421	4.81E-06
		0.153	1	0.62755	2.09E-05
				Total J	4.72637E-05
				Ra * mu	3.12E+08
				Ra/Rm	0.692631778

P (Pa)	Rm*mu	X (m)	# of layers	Ai/A	J(buffer)
50000	4.94E+08	0.007753	0	0.050676	4.05405E-06
		0.008979	1	0.008008	3.76005E-07
		0.153	1	0.941316	3.12782E-05
				Total J	3.57082E-05
				Ra * mu	906237383
				Ra/Rm	1.83448863

P (Pa)	Rm*mu	X (m)	# of layers	Ai/A	J(buffer)
71000	5.6E+08	0.001023	0	0.006689	8.48064E-07
		0.001663	1	0.004181	3.38563E-07
		0.027312	1	0.167642	9.97352E-06
		0.067289	2	0.261288	1.22847E-05
		0.095945	2	0.187291	7.27905E-06
		0.108737	3	0.083609	2.76936E-06
		0.153	3	0.289301	8.34885E-06
				Total J	4.18421E-05
				Ra * mu	1136857268
				Ra/Rm	2.030102264

P (Pa)	Rm*mu	X (m)	# of layers	Ai/A	J(buffer)
100000	6.9E+08	0.00030661	0	0.002004	2.90436E-07
		0.00090068	1	0.003883	3.85689E-07
		0.0061131	1	0.034068	2.57425E-06
		0.0288025	3	0.148297	7.57838E-06
		0.0729548	5	0.288577	8.95179E-06
		0.153	5	0.523171	1.35639E-05
				Total J	3.33444E-05
				Ra * mu	2309004125
				Ra/Rm	3.34638279

APPENDIX VII:
EXPERIMENTS ON BSA FILTRATION WITH H1P30-20 CARTRIDGE

Ionic strength (M)	0.022		μ (Pa.s)=	0.001	buffer		Notation: as in Appendix VI				
A (m2) =	0.06		μ (Pa.s)=	0.001	BSA 1g/L		TMPs are in psi				
Experiment with	Buffer through clean membrane			Buffer through fouled membrane			BSA 1 g/L				
BSA at TMP=	TMP (psi)	J (ml/min)	Rm (m-1)	TMP (psi)	J (ml/min)	Ra (m-1)	TMP (psi)	J (ml/min)	Rc (m-1)	Ra/Rm	Rc/Rm
0.73	0.59	68	2.16E+11	0.69	48	1.42E+11	0.73	48	2.07E+10	0.66	0.10
	13.4	546	6.1E+11	13.58	388	2.6E+11					
4.5	4.56	252	4.5E+11	4.39	130	3.9E+11	4.5	95	3.38E+11	0.87	0.75
	13.33	572	5.79E+11	13.22	317	4.57E+11					
9.5	9.44	419	5.6E+11	9.62	219	5.32E+11	9.5	120	8.76E+11	0.95	1.56
	13.4	546	6.1E+11	13.54	300	5.12E+11					
13.78	13.93	540	6.41E+11	14.02	283	5.9E+11	13.78	129	1.42E+12	0.92	2.22
Ionic strength (M)	0.22										
Experiment with	Buffer through clean membrane			Buffer through fouled membrane			BSA 1 g/L				
BSA at TMP=	TMP (psi)	J (ml/min)	Rm (m-1)	TMP (psi)	J (ml/min)	Ra (m-1)	TMP (psi)	J (ml/min)	Rc (m-1)	Ra/Rm	Rc/Rm
0.64	0.6	38	3.92E+11	0.65	27	2.06E+11	0.64	24.5	5.09E+10	0.52	0.13
	13.69	476	7.15E+11	13.96	318	3.76E+11					
4.69	4.55	224	5.05E+11	4.61	101	6.3E+11	4.69	68	5.8E+11	1.25	1.15
	13.6	502	6.73E+11	13.85	256	6.71E+11					
9.95	9.74	380	6.37E+11	9.71	171	7.74E+11	9.95	89	1.37E+12	1.22	2.15
	13.4	588	5.66E+11	13.86	216	1.03E+12					
13.5	13.82	528	6.5E+11	13.74	196	1.09E+12	13.5	88	2.07E+12	1.68	3.18
Ionic strength (M)	2.2										
Experiment with	Buffer through clean membrane			Buffer through fouled membrane			BSA 1 g/L				
BSA at TMP=	TMP (psi)	J (ml/min)	Rm (m-1)	TMP (psi)	J (ml/min)	Ra (m-1)	TMP (psi)	J (ml/min)	Rc/Rm	Ra/Rm	Rc/Rm
0.8	0.84	66	3.16E+11	0.825	42	1.72E+11	0.8	36	6.41E+10	0.54	0.20
	13.83	495	6.94E+11	13.73	333	3.3E+11					
4.99	4.84	231	5.21E+11	4.89	117	5.18E+11	4.99	70	7.33E+11	0.99	1.41
	13.83	495	6.94E+11	13.77	214	9.05E+11					
9.67	9.85	389	6.29E+11	9.94	137	1.17E+12	9.67	82	1.13E+12	1.87	1.79
	13.83	495	6.94E+11	13.9	160	1.46E+12					
13.73	13.91	494	7E+11	13.93	199	1.04E+12	13.73	85	2.27E+12	1.49	3.25

APPENDIX VII *(Continued)* : EXPERIMENTS AT DIFFERENT pH'S

Ionic strength (M)	0.1		μ (Pa.s)=	0.001	buffer						
A (m2) =	0.06		μ (Pa.s)=	0.001	BSA 1g/L						
Experiment at	Buffer through clean membrane			Buffer through fouled membrane			BSA 1 g/L				
pH = 5 (1)	TMP (Psi)	J (ml/min)	Rm (m-1)	TMP (Psi)	J (ml/min)	Ra (m-1)	TMP (Psi)	J (ml/min)	Rc (m-1)	Ra/Rm	Rc/Rm
	0.76	80	2.36E+11	0.81	15	1.11E+12				4.68	
	4.94	273	4.5E+11	4.74	57	1.62E+12				3.60	
	9.78	456	5.33E+11	9.82	108	1.73E+12	9.87	65	1.51E+12	3.24	2.84
	13.74	554	6.16E+11	14.07	146	1.78E+12				2.89	
Experiment at	Buffer through clean membrane			Buffer through fouled membrane			BSA 1 g/L				
pH = 5 (2)	TMP (Psi)	J (ml/min)	Rm (m-1)	TMP (Psi)	J (ml/min)	Ra (m-1)	TMP (Psi)	J (ml/min)	Rc (m-1)	Ra/Rm	Rc/Rm
	1.06	82	3.21E+11	0.78	15	9.71E+11				3.02	
	4.94	286	4.29E+11	4.76	58	1.61E+12				3.75	
	9.88	430	5.71E+11	9.61	104	1.73E+12	10.01	66	1.47E+12	3.02	2.58
	13.97	560	6.2E+11	13.7	134	1.92E+12				3.10	
Experiment at	Buffer through clean membrane			Buffer through fouled membrane			BSA 1 g/L				
pH = 7	TMP (Psi)	J (ml/min)	Rm (m-1)	TMP (Psi)	J (ml/min)	Ra (m-1)	TMP (Psi)	J (ml/min)	Rc (m-1)	Ra/Rm	Rc/Rm
	0.85	73	2.89E+11	0.835	28	4.52E+11				1.56	
	5.09	254	4.98E+11	4.85	105	6.5E+11				1.30	
	10.1	401	6.26E+11	9.88	180	7.38E+11	9.87	91	1.33E+12	1.18	2.13
	13.94	504	6.87E+11	13.68	251	6.67E+11				0.97	
Experiment at	Buffer through clean membrane			Buffer through fouled membrane			BSA 1 g/L				
pH = 7	TMP (Psi)	J (ml/min)	Rm (m-1)	TMP (Psi)	J (ml/min)	Ra (m-1)	TMP (Psi)	J (ml/min)	Rc (m-1)	Ra/Rm	Rc/Rm
	0.6	38	3.92E+11	0.67	22	3.64E+11				0.93	
	4.55	224	5.05E+11	4.65	95	7.12E+11				1.41	
	9.74	380	6.37E+11	9.71	172	7.66E+11	9.95	89	1.38E+12	1.20	2.16
	13.82	528	6.5E+11	13.86	216	9.44E+11				1.45	
Experiment at	Buffer through clean membrane			Buffer through fouled membrane			BSA 1 g/L				
pH = 9	TMP (Psi)	J (ml/min)	Rm (m-1)	TMP (Psi)	J (ml/min)	Ra (m-1)	TMP (Psi)	J (ml/min)	Rc (m-1)	Ra/Rm	Rc/Rm
	0.88	54	4.05E+11	0.54	28	7.43E+10				0.18	
	4.89	180	6.75E+11	4.675	122	2.77E+11				0.41	
	10.12	302	8.33E+11	9.92	210	3.41E+11	10.01	127	7.85E+11	0.41	0.94
	13.98	395	8.8E+11	13.84	264	4.23E+11				0.48	
Experiment at	Buffer through clean membrane			Buffer through fouled membrane			BSA 1 g/L				
pH = 9	TMP (Psi)	J (ml/min)	Rm (m-1)	TMP (Psi)	J (ml/min)	Ra (m-1)	TMP (Psi)	J (ml/min)	Rc (m-1)	Ra/Rm	Rc/Rm
	0.79	76	2.58E+11	0.84	42	2.39E+11				0.92	
	5.05	245	5.12E+11	5.11	139	4.01E+11				0.78	
	10.07	382	6.55E+11	9.98	232	4.14E+11	9.82	137	7.12E+11	0.63	1.09
	13.92	499	6.93E+11	13.96	289	5.07E+11				0.73	

			Ionic stren	0.1		μ (Pa.s)=	0.001	buffer	
			A (m2) =	0.06		μ (Pa.s)=	0.001	BSA 1g/L	
		STATIC	Buffer through clean membrane			Buffer through fouled membrane			
		pH = 7	TMP (Psi)	J (ml/min)	Rm (m-1)	TMP (Psi)	J (ml/min)	Ra (m-1)	Ra/Rm
			0.87	60	3.6E+11	0.78	50	2.73E+10	0.08
			4.91	230	5.31E+11	4.89	184	1.3E+11	0.24
			9.84	398	6.14E+11	9.87	304	1.92E+11	0.31
			13.87	520	6.63E+11	14	383	2.46E+11	0.37
		Ionic strength (M)	0.01						
		STATIC	Buffer through clean membrane			Buffer through fouled membrane			
		pH = 7	TMP (Psi)	J (ml/min)	Rm (m-1)	TMP (Psi)	J (ml/min)	Ra (m-1)	Ra/Rm
			0.86	55	3.89E+11	0.86	48	5.67E+10	0.15
			4.9	197	6.18E+11	4.85	172	8.26E+10	0.13
			9.9	359	6.85E+11	9.92	290	1.65E+11	0.24
			13.77	469	7.3E+11	13.9	376	1.89E+11	0.26
		STATIC	Buffer through clean membrane			Buffer through fouled membrane			
		pH = 5	TMP (Psi)	J (ml/min)	Rm (m-1)	TMP (Psi)	J (ml/min)	Ra (m-1)	Ra/Rm
			0.82	67	3.04E+11	0.62	37	1.12E+11	0.37
			4.84	225	5.35E+11	4.64	126	3.81E+11	0.71
			9.77	398	6.1E+11	8.85	204	4.68E+11	0.77
			13.8	532	6.45E+11	14.12	267	6.7E+11	1.04
		STATIC	Buffer through clean membrane			Buffer through fouled membrane			
		pH = 9	TMP (Psi)	J (ml/min)	Rm (m-1)	TMP (Psi)	J (ml/min)	Ra (m-1)	Ra/Rm
			0.87	68	3.18E+11	0.8	52	6.44E+10	0.20
			5	204	6.09E+11	4.9	179	7.12E+10	0.12
			9.74	334	7.25E+11	9.78	292	1.08E+11	0.15
			13.97	437	7.94E+11	13.69	358	1.56E+11	0.20
		Ionic strength (M)	1						
		STATIC	Buffer through clean membrane			Buffer through fouled membrane			
		pH = 7	TMP (Psi)	J (ml/min)	Rm (m-1)	TMP (Psi)	J (ml/min)	Ra (m-1)	Ra/Rm
			0.9	75	2.98E+11	0.96	51	1.7E+11	0.57
			4.98	237	5.22E+11	4.87	174	1.73E+11	0.33
			9.84	387	6.32E+11	9.98	300	1.95E+11	0.31
			14.03	474	7.36E+11	13.98	390	1.55E+11	0.21